12-2014

VULNERABILITY FUNCTIONS FOR SEISMIC LOSS ASSESSMENT OF THE MODERN MULTI-STORY BUILDINGS IN DUBAI

Abdul Rahman Abdul Aziz Ashri Hassan

United Arab Emirates University

College of Engineering

Department of Civil and Environmental Engineering

VULNERABILITY FUNCTIONS FOR SEISMIC LOSS ASSESSMENT OF THE MODERN MULTI-STORY BUILDINGS IN DUBAI

Abdel Rahman Abdel Aziz Ashri Hassan

This thesis is submitted in partial fulfillment of the requirements for the degree of Master of Science in Civil Engineering

Under the Supervision of Dr. Aman Mwafy

December 2014

Declaration of Original Work

I, Abdel Rahman Abdel Aziz Ashri Hassan, the undersigned, a graduate student at the United Arab Emirates University (UAEU), and the author of the thesis entitled "Vulnerability Functions for Seismic Loss Assessment of the Modern Multi-story Buildings in Dubai". Hereby, solemnly declare that this thesis is an original research work done and prepared by myself under the supervision of Dr. Aman Mwafy, in the College of Engineering at UAEU. This work has not been previously formed as the basis for the award of any academic degree, diploma or similar title at this or any other university. The materials borrowed from other sources and included in my thesis have been properly cited and acknowledged.

Student's Signature …….. Date ……...

This Master Thesis is approved by the following Examining Committee Members:

1) Advisor (Committee Chair): Dr. Aman Mwafy
   Title: Associate Professor
   Department of Civil and Environmental Engineering
   College of Engineering
   Signature _____ Date _____

2) Member: Dr. Bilal El-Ariss
   Title: Associate Professor
   Department of Civil and Environmental Engineering
   College of Engineering
   Signature _____ Date _____

3) Member (External Examiner): Prof. Abdeldjelil "DJ" Belarbi
   Title: Professor
   Department of Civil and Environmental Engineering
   Institution: University of Houston
   Signature _____ Date _____

This Master Thesis is accepted by:

Dean of the College of Engineering: Prof. Mohsen Sherif

Signature _____Date _____

Dean of the College of Graduate Studies: Prof. Nagi Wakim

Signature _____Date _____

Copy ___ of ___

Abstract

The rapid developments in the United Arab Emirates along with the repeated seismic activity confirm the significance of planning for the possible damage that may hit earthquake-prone areas in order to mitigate earthquake losses. The contemporary buildings are the most important when estimating the potential losses from earthquakes since they represent concentrated economic and human assets. This study aims at developing vulnerability functions for a wide range of modern building inventory in a highly-populated and earthquake-prone area in the UAE. Ten reference buildings with varying heights from 2 to 100 stories and three different lateral force resisting systems are selected to represent the study area. The reference buildings are completely designed and detailed as per the design provisions and construction practice utilized in the UAE. Detailed fiber-based numerical models are developed for the reference structures and forty natural earthquake records are selected to account for the uncertainty in seismic demands. Over 5,000 inelastic analyses are performed to derive three-dimensional vulnerability functions for the investigated structural systems. It is concluded that, unlike the satisfactory performance of the shear wall and tube in tube structural systems, the flat slab-columns system is vulnerable to the severe distant earthquakes. It is suggested to decrease the overstrength factor and increase the deflection amplification factor by 10% for the low-rise flat slab-columns system. For the shear wall and tube in tube systems, the force reduction factors can be increased by at least 10%, with a possibility of further increase after a thorough assessment of the proposed reduction in seismic loads. It is also proposed to adopt an effective stiffness of 0.5EI, 0.8EI and 1.0EI for the vertical elements of the flat slab-columns, shear wall and tube in tube

structural systems, respectively, to arrive at an accurate estimate of the inelastic periods of vibrations. The derived three-dimensional vulnerability relationships in the present study enable the interpolation of results to arrive at the fragilities of a wide range of buildings with different heights and systems. The developed fragility curves are prepared for the direct integration in a comprehensive loss estimation system for the region.

Keywords: fragility functions, seismic design coefficients, modern RC buildings, inelastic dynamic analysis, structural systems, UAE

منحنيات لتقييم خسائر الزلازل للمباني الحديثة متعددة الطوابق بدبي

الملخص

إن معدلات التنمية السريعة بدولة الإمارات العربية المتحدة مع ما تشهده من أنشطة زلزالية متكررة تؤكد على أهمية التنبؤ بالخسائر المحتملة للزلازل وضرورة دراسة أساليب التخفيف من آثارها المتوقعة. تمثل المباني الحديثة أهمية كبرى عند تقدير الخسائر الزلزالية المحتملة نظرا لأنها تمثل أصولا اقتصادية وبشرية كبيرة. تهدف هذه الدراسة إلى إعداد منحنيات للتنبؤ بخسائر الزلازل (vulnerability curves) لمجموعة كبيرة من المبانى المعاصرة في المناطق عالية الكثافة السكانية والأكثر عرضة للزلازل في دولة الإمارات. في هذه الدراسة تم اختيار عشرة مبان بارتفاعات متفاوتة تتراوح بين طابقين و مائة طابق والتي تشمل ثلاثة أنظمة إنشائية مختلفة لمقاومة القوى الجانبية وذلك لتمثيل المباني بمنطقة الدراسة، وقد تم تصميم المباني المختارة وفقا لاعتبارات التصميم (design codes) وممارسات البناء المستخدمة بدولة الإمارات ، وقد اشتملت الدراسة على إعداد نماذج تحليلية مفصلة معتمدة على طريقة النمذجة بالألياف (fiber-based modeling) للمباني المختارة، وكذلك تم اختيار أربعين سجلا لزلازل طبيعية وذلك لمراعاة عدم اليقين في الإجهادات الناتجة من الزلازل، وقد تم إجراء أكثر من خمسة آلاف تحليلا ديناميكيا غير مرنا (inelastic analyses) للحصول على منحنيات ثلاثية الأبعاد للتنبؤ بالخسائر الزلزالية للأنظمة الإنشائية محل الدراسة. وقد خلصت الدراسة إلى أنه خلافا للأداء الجيد لنظام الإنشاء باستخدام جدران القص (shear walls) والنظام المركب (tube in tube)، فإن نظام البلاطات المسطحة مع الأعمدة (flat slab-columns) كان أكثر عرضة لتأثير الزلازل الشديدة المتولدة من مصادر بعيدة ، وقد اقترحت الدراسة تقليل معامل القوة الإضافية (overstrength factor) وزيادة معامل تضخيم التشكلات (deflection amplification factor) بنسبة 10٪ للمباني منخفضة الارتفاع من نظام البلاطات المسطحة مع الأعمدة. بالنسبة لنظام جدران القص والنظام المركب فيمكن زيادة معامل تخفيض قوى التصميم (force reduction factor) بقيمة 10٪ على الأقل، مع إمكانية زيادة معامل تخفيض القوى بدرجة أكبر بعد عمل تقييم شامل للتخفيض المقترح في قوى التصميم للزلازل. وكذلك اقترحت الدراسة استخدام معامل جساءة فعالة يكافئ 50% و 80% و 100% من الجساءة الكلية وذلك للعناصر الإنشائية الرأسية من نظام البلاطات المسطحة مع الأعمدة ونظام جدران القص والنظام المركب على التوالي. وتتيح منحنيات التنبؤ بالخسائر الزلزالية ذات الأبعاد الثلاثية المستنتجة في هذه الدراسة الوصول إلى تقييم فعال للخسائر المحتملة من

الزلازل لمجموعة كبيرة من المباني بارتفاعات متفاوتة وأنظمة إنشائية مختلفة، وقد تم إعداد منحنيات التنبؤ بالخسائر الزلزالية لدمجها مباشرة في نظام شامل لتقييم الخسائر الزلزالية بالمنطقة.

Acknowledgements

I wish to express my sincere gratitude to my supervisor, Dr. Aman Mwafy, Associate Professor of Structural Engineering, for his technical guidance and invaluable suggestions provided throughout the duration of this work. His continuous advice and constant encouragement were a great motivation to complete this study. His esteemed support, both at the academic and the personal levels, has been of paramount importance to my life.

I would like to express my infinite love and thanks to all my family members for their love and support during this study. I deeply appreciate the encouragement given to me by my wife, who made innumerable sacrifices to enable me to concentrate on my studies. The highest appreciation goes to my parents without whom this would have not been possible. All what I have accomplished in life is the result of their love and years of sacrifice.

I would like to thank all faculty members of Civil and Environmental Engineering Department at UAEU for their continuous support. I would also like to thank all of my colleagues for their cooperation. This work was supported by United Arab Emirates University under research grants nos. 31N007 and 31N132.

Dedication

To my beloved mother, dear father, lovely wife and sweet kids

Table of Contents

List of Tables

List of Figures

Abbreviations

2D : two-dimensional

3D : three-dimensional

$(a_g)_y$: peak ground acceleration at first indication of yield

$(a_g)_c$: peak ground acceleration at collapse

a/v : peak ground acceleration/peak ground velocity

C : deflection amplification factor

CP : collapse prevention limit state

D/C : design/capacity

DOF : degree of freedom

ELFP : equivalent lateral force procedure

EQ : earthquake

EVA : eigenvalue analysis

f_c : unconfined concrete strength

f_{cu} : concrete cube strength

f_c' : concrete cylindrical strength

FE : finite element

FSC : flat slab-columns

f_y : yield strength of steel

g : gravitational acceleration

GMI : ground motion intensity

I : moment of inertia

IO : immediate occupancy limit state

ID : inter-story drift

IDA : incremental dynamic analysis

IDR : inter-story drift ratio

IM : intensity measure of input ground motion

IPA : inelastic pushover analysis

LS : life safety limit state

MCE : maximum considered earthquake

MDOF : multi-degree of freedom

MRSA : modal response spectrum analysis

NEHRP : national earthquake hazards reduction program

OP : operational limit state

PGA : peak ground acceleration

PGV : peak ground velocity

PU : uniform load distribution

PT : inverted triangular load distribution

R : force reduction factor

R code : force reduction factor adopted in the design code

R_{μ} : ductility reduction factor

RC : reinforced concrete

S_1 : spectral response acceleration at 1.0 sec.

S_a : spectral acceleration

S_s : spectral response acceleration at 0.2 sec.

SDOF : single degree of freedom

St : story

SW : shear walls

T : period

TIT : tube in tube

THA : time history analysis

T_L : long-period transition period

T_s : transition period

V : shear force

V_d : design base shear

V_e : elastic base shear

V_{fy} : shear force at first indication of yielding

V_y : base shear at ultimate strength

W : total weight

$\beta_{D|GMI}$: demand uncertainty

β_{CL} : drift capacity uncertainty

β_M : modeling uncertainty

Δ : displacement

Δ_y : displacement at first yield

Δ_{max} : maximum deformation

Φ : standard normal cumulative distribution function

λ_{CL} : ln (median of drift capacity for a particular limit state)

$\lambda_{D|GMI}$: ln (calculated median demand drift given the ground motion intensity)

Ω : overstrength factor

Ω_{fy} : overstrength factor at first yield

CHAPTER 1: INTRODUCTION

1.1 PREAMBLE

The building inventory in the UAE has expanded to meet the rapid development and increasing population. The contemporary building stock in this region is the most important when estimating the potential losses from earthquakes. Assessment of the vulnerability of the diverse building inventory, which includes low, medium and high-rise structures, is significant in order to predict and mitigate against possible earthquake losses. The seismic hazard of the UAE is characterized by earthquakes generated from different seismic sources, namely severe long-distance earthquakes and moderate near-source events (e.g. Abdalla and Al-Homoud, 2004; Aldama-Bustos et al., 2009; Khan et al., 2013; Mwafy et al., 2006; Shama, 2011). The special tectonic settings and the repeated seismic activities in the UAE and surrounding regions in recent years have raised concerns regarding the possibility of strong earthquakes to hit this area in future.

Given the special seismological feature and large investments in the construction industry, the Abu Dhabi government has recently enforced unified building codes across the emirate's construction industry, namely the Abu Dhabi international building code, ADIBC (DMA, 2013). The adopted building code is based on the international building code (ICC, 2012) with minimum amendments in the initial implementation phase. The code provisions will be developed in future in order to come up with customized design provisions that address the local construction and seismo-tectonic characteristics. This shows the pressing need for

assessing the seismic vulnerability and important design factors for a wide range of reference structures representing the modern seismic design provisions and structural systems using reliable assessment methodologies and taking into account the local hazard and construction practice in this region. Probabilistic vulnerability assessment of a diverse range of structures representing the inventory is crucial to effectively estimate potential earthquake losses.

The seismic performance of structures is probabilistically assessed through the use of vulnerability relationships. Several methods can be utilized to derive fragility curves for different structural systems (e.g. Calvi et al., 2006b; Cornell and Krawinkler, 2000; Jeong and Elnashai, 2007; Ji et al., 2009; Rossetto and Elnashai, 2003). The analytical method is the most common approach compared with other methods, particularly for regions with limited damage data from previous earthquakes such as the UAE (e.g. Schultz et al., 2010). Therefore, the analytical approach was adopted in several previous studies and in the present study as well (e.g. Jeong et al., 2012; Kwon and Elnashai, 2006; Mwafy, 2012a).

Finally, the seismic design response factors and the actual dynamic characteristics under earthquake loads play a key role in the safety and economy of structures. The seismic design response factors recommended in design codes do not provide a uniform safety margin for different seismic zones to account for the variation of structural systems and construction practices (e.g. FEMA, 2009b; Mwafy and Elnashai, 2002). This confirms the need for verifying the important design factors for a wide range of reference structures representing the UAE using reliable assessment approaches.

1.2 OBJECTIVES

The main objectives of the present study are as follows:

- Review of the current state of knowledge related to the structural systems of multi-story buildings, seismicity of the UAE, and approaches for deriving vulnerability relationships and seismic response factors.
- Select, design and idealize a wide range of reinforced concrete buildings with different heights and structural systems to represent the modern building inventory in a highly-populated and earthquake-prone area in the UAE.
- Develop a diverse range of vulnerability functions representing the modern multi-story building inventory in the UAE using verified analytical models and incremental dynamic analyses under the effect of potential earthquake scenarios.
- Verify the seismic design response factors recommended by the new design provisions adopted in the UAE for different structural systems.

1.3 THESIS OUTLINE

This thesis is organized into seven chapters: The present chapter includes the motivations for and the main objectives of the present study. Chapter 2 presents a literature review of previous studies related to the current research, which includes the common structural systems of multi-story buildings, seismic hazard assessment of the UAE, and approaches for deriving vulnerability functions and seismic design response factors.

Chapter 3 describes the selection and design of the ten reference buildings with different structural systems and building heights. The design approach of

different structural elements using modern design tools and the outcomes of the design process are discussed and summarized in this chapter.

Chapter 4 discusses the analytical modeling of the reference structural systems for inelastic analysis. The analysis platform employed in the current study is introduced, and the developed inelastic models are verified. This chapter also discusses the selection of severe distant and moderate close earthquake scenarios to represent the seismicity of the UAE.

Chapter 5 describes the selection of performance criteria through a large number of inelastic pushover and incremental dynamic analyses along with the limit state criteria recommended by code provisions and previous studies.

Chapter 6 discusses in detail the vulnerability assessment of the contemporary multi-story buildings with different structural systems and building heights. The fragility functions of the reference structures, which are developed through a large number of inelastic analyses, are presented. The verification of the seismic design response factors and dynamic characteristics is also discussed.

Chapter 7 summarizes the main findings and conclusions of this study, particularly regarding the performance assessment of the reference structures using vulnerability relationships and the verifications of the seismic design response factors. Finally, recommendations for future work are offered.

CHAPTER 2: LITERATURE REVIEW

2.1 STRUCTURAL SYSTEMS OF MULTI-STORY BUILDINGS

2.1.1 Developments in the Construction of Multi-story Buildings

Multi-story buildings appeared in the nineteenth century to satisfy the increasing demands of urbanization. The large employment in big cities has been one of the important reasons that has led to an increase in the demand on land use in large cities. While in 1950 there were only 7 urban areas in the world with about 5 million inhabitants, this number increased to 34 in 1980, and increased further to 60 in 2000 (Cohen, 2004). The development of building heights shown in Figure 1 clearly illustrates the significant increase in multi-story building construction with time (Laogan and Elnashai, 1999).

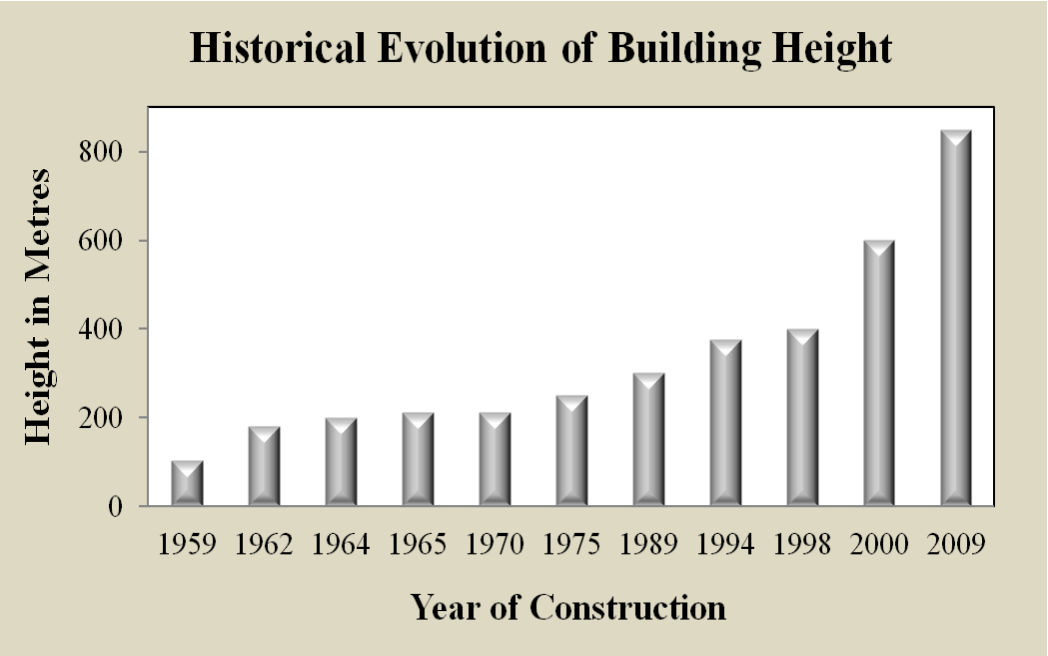

Figure 1. Historical evolution of building height (part of the data was adopted from Laogan and Elnashai, 1999)

The rapid growth of urban population, the high cost of land, a desire to avoid continuous urban spread, and the need to preserve important agricultural production led to an increase in the construction of high-rise buildings. In the UAE, the multi-story buildings have spread widely during the last two decades to meet the needs of a rapidly increasing population. High-rise buildings pose the most significant concerns in the potential consequences from natural hazard events since they represent concentrated economic and human assets. This class of structures represent a priority in design and assessment, particularly with the unprecedented escalation in the number of high-rise buildings in the UAE (Mwafy, 2012a).

2.1.2 Lateral Force Resisting Systems of Multi-story Buildings

The determination of the structural system of a multi-story building involves the selection and arrangement of the main structural members to resist the various combinations of gravity and horizontal loads such as wind and earthquake loads. The factors considered in selecting the structural system include the architectural geometry, material and method of construction, nature and magnitude of lateral loads, and the height of the building. The structure height represents an important factor in choosing the appropriate lateral force resisting system.

Reinforced concrete (RC) provides a wide range of structural systems that can be grouped into different classes according to building height, as shown in Figure 2 (Taranath, 2009). While the structural system must fulfill the architectural requirements that are expected in modern buildings, it should satisfy the required performance under different loads.

No.	System	Number of stories 0 10 20 30 40 50 60 70 80 90 100 110	Ultra-tall buildings 120–200 stories
1	Flat slab and columns		
2	Flat slab and shear walls		
3	Flat slab, shear walls and columns		
4	Coupled shear walls and beams		
5	Rigid frame		
6	Widely spaced perimeter tube		
7	Rigid frame with haunch girders		
8	Core supported structures		
9	Shear wall—frame		
10	Shear wall—Haunch girder frame		
11	Closely spaced perimeter tube		
12	Perimeter tube and interior core walls		
13	Exterior diagonal tube		
14	Modular tubes, and spine wall systems with outrigger and belt walls		

Figure 2. Structural systems of reinforced concrete buildings (Taranath, 2009)

2.1.2.1 Flat Slab-Columns System

The flat slab system is a simple system that consists of floor slabs and supporting columns, as shown in Figure 3. The system is designed to sustain both gravity and lateral loads. Compared with regions of low-to-medium seismicity, the flat slab-columns system is less effective in high seismic regions. Therefore, this system is not recommended in seismic design category (SDC) D, E and F. In areas of low seismicity, this system may be used without limitations. However, lateral drift requirements limit the economical height of this system to about 10 stories, as shown in Figure 2 (Taranath, 2004).

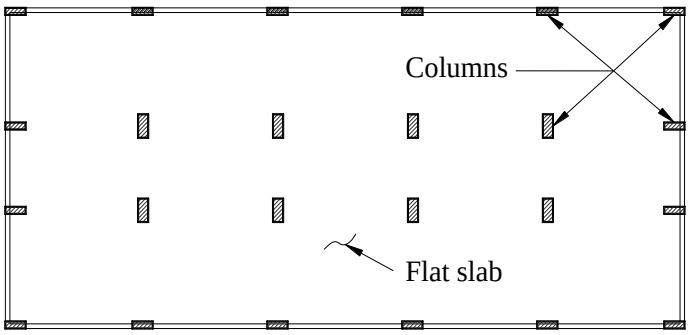

Figure 3. Flat slab framing system

2.1.2.2 Shear Wall / Core Wall System

Core walls, which are typically placed around lifts and stairs, are capable of carrying lateral loads in both directions in addition to gravity loads, as shown in Figure 4. This system can resist shear forces and bending moments in two directions. The shear wall system is normally more effective than the frame system since the lateral deformations of shear wall buildings are relatively small. This system can be used up to about 50 stories, as shown in Figure 2 (Taranath, 2009). The economical height limit can be increased by adding shear walls at the perimeter of the building, as shown in Figure 4.

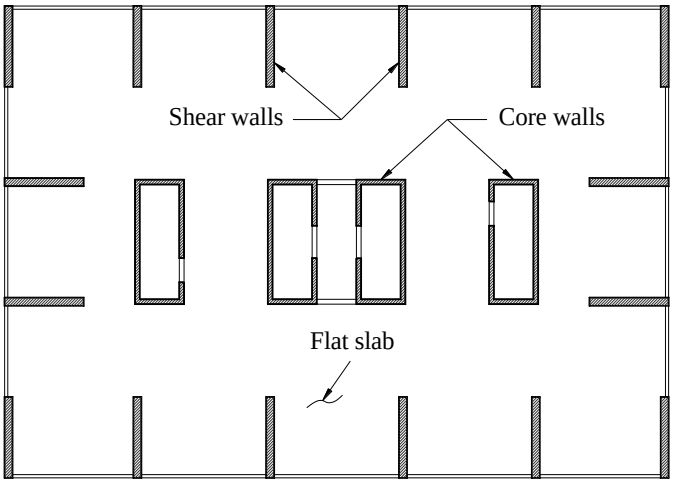

Figure 4. Shear wall structural system

2.1.2.3 Perimeter Tube and Interior Core Wall (Tube in Tube) System

The tube in tube system consists of exterior columns closely placed together and connected with rigid beams to form the outer tube. The interior core walls represent the inner tube, as shown in Figure 5. The floor diaphragm connecting the internal core walls and the external tube transfer the lateral loads to both of them. This structural system can be used up to about 80 stories (Ali and Moon, 2007;

Taranath, 2009). However, the development in construction materials and structural analysis tools enable increasing the height limits of the above-mentioned structural systems beyond the specified limits (Mwafy et al., 2014).

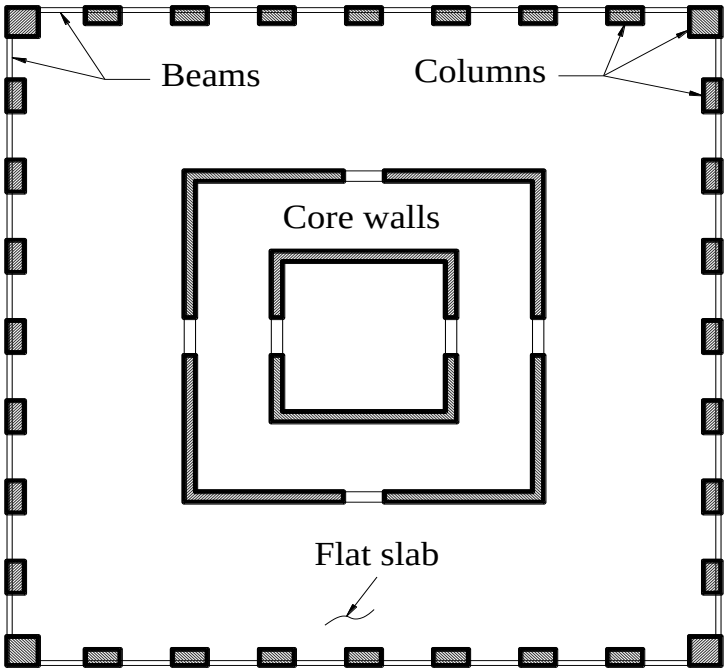

Figure 5. Tube in Tube structural system

2.2 SEISMIC HAZARD ASSESSMENT OF THE UAE

2.2.1 UAE Seismicity

The earthquake hazard in the UAE has traditionally been considered to be negligible. The recent seismic activities however have demonstrated that this viewpoint has no basis since sizable earthquakes can indeed occur in the UAE and surrounding regions (Wyss and Al-Homoud, 2004). Although knowledge about past earthquakes in the UAE is incomplete, recent moderate earthquakes caused considerable concerns in the region and highlighted the fact that damaging earthquakes may occur (e.g. Al Marzooqi et al., 2008).

The UAE is located on the south-eastern part of the Arabian plate. The separation and splitting of the Arabian plate from the African plate along the Red Sea and the Gulf of Aden axes, followed by the drift of the Arabian plate to the north and northeast, lead to a collision with the Eurasian plate that resulted in the formation of the Zagros fold belt and the Thrust belt in Southern Iran, as shown in Figure 6 (Johnson, 1998). The Zagros fold belt is one of the most active fault zones in the world and a major source of earthquakes in the eastern border of the Arabian plate (Abdalla and Al-Homoud, 2004). Moreover, along the northern shore of the Gulf of Oman, this collision is accommodated by subduction of the Arabian plate underneath the Eurasian plate along with the Makran subduction zone. This tectonic setting has a direct impact on the seismicity of the UAE.

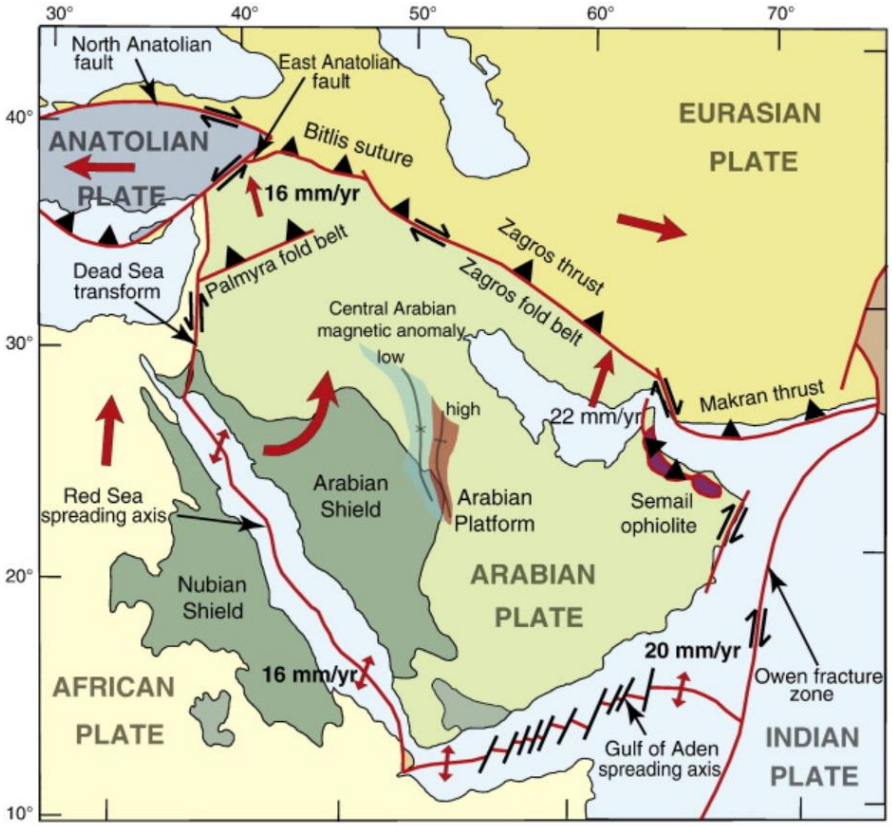

Figure 6. Tectonic setting of the Arabian plate (Johnson, 1998)

2.2.2 Previous Seismic Hazard Studies of the UAE

The rate of earthquakes recorded within or close to the UAE is on the increase. About three earthquakes per year were recorded between 2000 and 2006 compared with 0.65 earthquakes per year from 1924 to 1999 (Aldama-Bustos et al., 2009). The UAE seismic hazard is characterized by earthquakes originating from long distance events and near-source earthquakes (Mwafy et al., 2006). Most seismic activity in the UAE originates from southern Iran and local seismic faults. The probability of generating a large earthquake in southern Iran is substantial (Tavakoli and Ghafory-Ashtiany, 1999). Dubai and the northern emirates are the most prone areas to seismic risk in the UAE.

The Fujairah earthquake of March 11, 2002, which was generated from the local fault of Dibba and measured 5.1 on the Richter scale, was felt in most northern parts of the UAE (Al-Homoud, 2003). The residents of the northern emirates experienced an earthquake of magnitude 6.0 on the Richter scale, which was generated in the Qeshm Island on September 10, 2008 (refer to Figure 7). More recently, an earthquake with a magnitude of 7.8 on the Richter scale hit southern Iran on April 16, 2013, and was strongly felt in most parts of the UAE (Mwafy, 2013a).

Although no significant losses were recorded from these earthquake events, the increasing rate of the seismic activities reflects the potential of a stronger earthquake hitting the region, and emphasizes the significance of adopting reliable seismic assessment strategy in the UAE.

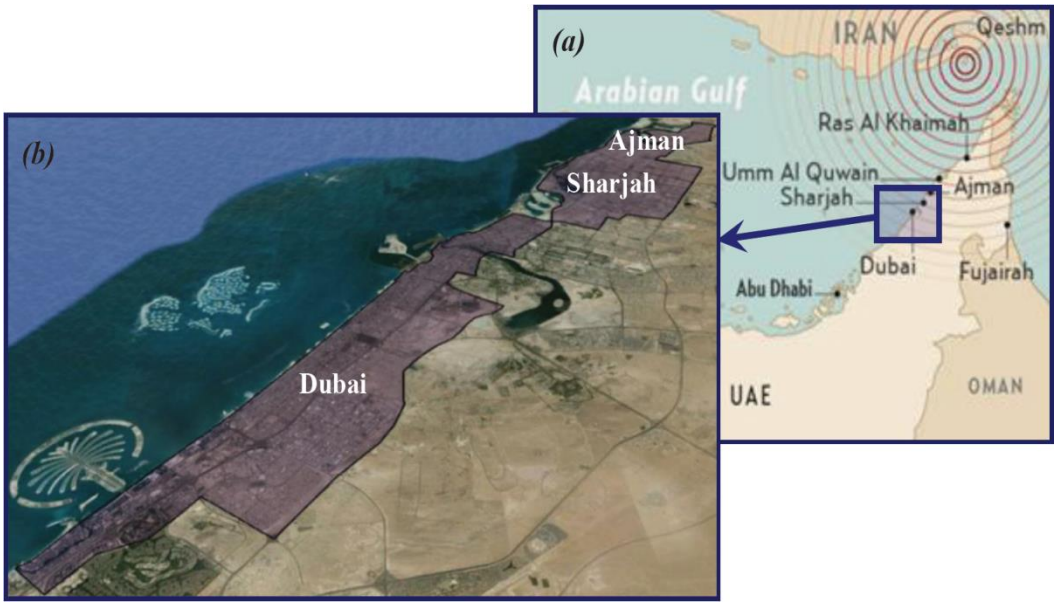

Figure 7. (a) UAE map highlighting the earthquakes generated from southern Iran; and (b) a satellite image of the highly-populated and seismically-active area in the UAE (Mwafy, 2013a)

The seismic risk in the UAE is rapidly increasing because of the accelerated urban development. To overcome potential seismic hazards, several studies have been undertaken to assess the seismicity of the UAE and to verify the currently adopted seismic design criteria. Recent seismic hazard studies are briefly discussed below.

Dubai Municipality has recently established a seismological network in Dubai to monitor the seismic activity for Dubai and surrounding areas (e.g. Al Khatibi et al., 2014). This network consists of four seismic stations installed in 2006, and additional five stations installed in 2012. Despite the low seismic hazard of this area, Al Khatibi et al. (2014) concluded that small-to-moderate earthquakes were recorded in the eastern part of UAE from the active tectonics in the mountainous region of northern Oman.

Khan et al. (2013) conducted a seismic hazard analysis of the UAE. This study was based on an improved seismic source model and next generation attenuation (NGA) equations (PEER, 2013). Low hazard levels and seismic design criteria were proposed for the UAE. For instance, peak ground accelerations **(**PGAs) of 0.047g and 0.118g were adopted for Dubai for return periods of 475 and 2,475 years, respectively, Figure 8.

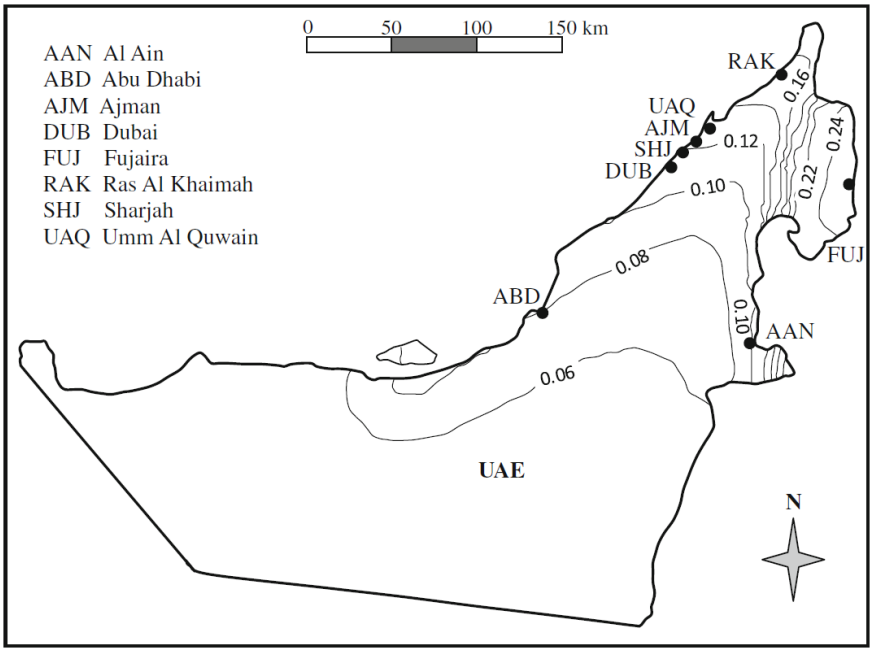

Figure 8. Peak ground accelerations (g) for the UAE for 2,475 years return period (Khan et al., 2013)

A probabilistic seismic hazard analysis (PSHA) was performed by Shama (2011) to obtain the hazard spectra of Dubai Creek on the west coast of the UAE. The conducted PSHA considered all seismic sources that affect the site; including plate boundaries such as the Zagros fold belt, the Makran subduction zone, the transition fault system between them, and the local crustal faults in UAE. The recommended seismic design criteria included those for 475 and 2,475 years return periods. This study concluded that local faults dominate the hazard of the UAE. The

PGA for the 475-year return period is 0.17g, while it is 0.33g for the 2,475-year return period. These results are in line with a number of previous seismic hazard studies for this region (e.g. Abdalla and Al-Homoud, 2004; Mwafy et al., 2006).

A probabilistic seismic hazard assessment, in terms of ground motions in rock, was conducted for three cities in the UAE within a logic-tree framework by Aldama-Bustos et al. (2009). The study accounted for uncertainties in the models for seismic sources and ground motion prediction. The results supported some previous studies regarding the low seismicity of the UAE. It was proposed that seismic design should not be required for structures of normal occupancy except in northerly areas such as Ras Al Khaimah. The seismic hazard calculations and disaggregation presented in this study demonstrated that the hazard is actually dominated by the local seismicity, particularly at longer return periods. It is noted that the study did not consider the effect of surface soil deposits, which could significantly amplify long-period ground motions generated by severe distant earthquakes in the Zagros and Makran regions, and which in turn could affect the high-rise structures in the UAE.

Malkawi et al. (2007) performed seismic hazard assessment for the major cities of the UAE. The seismic source model consisted of a single source, which included the Makran zone, Zagros zone and parts of the Arabian Craton. A PGA of 0.20g was proposed for Dubai for a return period of 475 years.

In the studies of Mwafy el al. (2006) and Sigbjornsson and Elnashai (2006), a site-specific hazard study was accomplished for Dubai. An earthquake catalogue for the study area was extracted from three different sources (Ambraseys and Melville, 2005; Ambraseys et al., 2005; GSHAP, 2014). Figure 9 illustrates the distribution of

earthquake data for the period from 734 to 1996. The dots seen in the figure indicate earthquake epicenters, while their size denotes the earthquake magnitude. It was shown that no earthquakes of a magnitude greater than 6.0 on the Richter scale were closer than 150 km to Dubai. It was also concluded that the epicentral distance of earthquakes of a magnitude 4.5-5.5 on the Richter scale closest to the study area was about 50 km. Figure 9 shows that most of the earthquakes were located on the northern side of the Arabian Gulf, Strait of Hormuz and Gulf of Oman. The results indicated that the Arabian Peninsula is one of the most geologically stable areas in the world (Ambraseys et al., 2005).

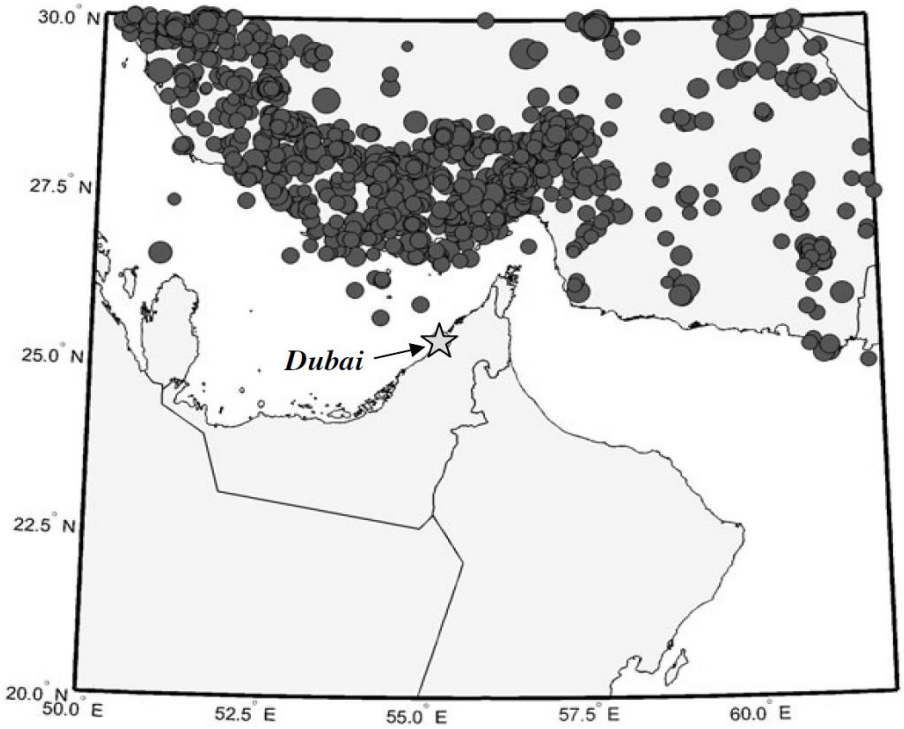

Figure 9. Distribution of earthquake data for the period 734-1996 (Ambraseys and Melville, 2005; Ambraseys et al., 2005; GSHAP, 2014; Mwafy et al., 2006)

The latter studies concluded that the earthquake hazard of Dubai is significantly influenced by the southern Iran seismicity with a possible hazard from local faults. The studies of Mwafy el al. (2006) and Sigbjornsson and Elnashai

(2006) recommended the following two seismic scenarios for Dubai: (i) strong ground motions with long distance (100 km) and a magnitude of 7.0 on the Richter scale, and (ii) moderate earthquakes with relatively short distance (20 km) and a magnitude of 6.0 on the Richter scale. It is worth noting that, despite the limited information available on the seismic activity of the Dibba fault and the fault along the west coast of the UAE, both of these sources were included in the latter two studies. It is concluded that far-field events are likely to have the greatest effect on long period structures while the small-to-moderate earthquakes will have more impact on short period structures or structures responding in their higher modes. The recommended peak ground acceleration in the latter studies for the 475-year return period is 0.16g, while it is 0.22g for the 2,475-year return period.

A probabilistic seismic hazard assessment and seismic zoning study of the UAE and its proximity was accomplished by Abdalla and Al-Homoud (2004). The studied area covered different Gulf countries. This study adopted an earthquake catalogue collected by the International Institute of Earthquake Engineering and Seismology, which included both historical and instrumental events (Vernant et al., 2004). Seismic source regions were modeled and relationships between earthquake magnitude and frequency were established. This study employed a recurrence relation proposed by Gutenberg and Richter (1954) and an attenuation relation for Iran and the surrounding regions developed by the international institute of earthquake engineering and seismology (Vernant et al., 2004; Zare, 2002). Seismic hazard assessment was accomplished for 25 km interval grid points. The seismic hazard maps proposed in this study were based on probable peak ground acceleration for 10% probability of exceedance for 50 and 100 years. PGAs of 0.15g and 0.075g

for a return period of 475 years were proposed in the latter study for Dubai and Abu Dhabi, respectively.

A Global Seismic Hazard Assessment Project (GSHAP) was conducted in 1999 to generate PGA maps for a return period of 475 years for Europe, Africa and Middle East (Grünthal et al., 1999). The results of this study recommended PGAs of 0.32g and 0.24g for Dubai and Abu Dhabi, respectively. The high PGAs recommended in the latter study have been criticized in a number of studies (Abdalla and Al-Homoud, 2004; Aldama-Bustos et al., 2009; Sigbjornsson and Elnashai, 2006). A seismic hazards study was also conducted by Al-Haddad et al. (1994) for the concerned region. Limited earthquake data of the region were collected in this study. The attenuation relationship used in this study was developed for the Western U.S., which may not be appropriate for the Arabian Peninsula. The results of this study suggested a PGA less than 0.05g for a return period of 475 years for Abu Dhabi and Dubai.

The above-mentioned brief review of seismic hazard studies for the Dubai and surrounding areas show that some studies recommended very high PGA (up to 0.32g for a return period of 475-year), while other studies suggested a very low PGA (0.047g for the same return period). A number of studies recommended a moderate design PGA of 0.15g to 0.17g for a return period of 475-year for Dubai (Abdalla and Al-Homoud, 2004; Mwafy et al., 2006; Shama, 2011; Sigbjornsson and Elnashai, 2006). It was thus decided in the present study to adopt the recommendation of the latter four studies, which appear to be between the very high values and the non-conservative design PGA proposed in previous hazard assessment studies.

2.2.3 Seismic Design Maps of the UAE

Abu Dhabi international building code (ADIBC) has been recently adopted by the Emirate of Abu Dhabi (DMA, 2013). The new code provisions are based on the international building code (ICC, 2012). The code provisions will be developed in the future in order to come up with customized design provisions that address the local construction and seismo-tectonic characteristics of the UAE. Three seismic design maps have been recently developed for the UAE, as shown in Figure 10 to Figure 12 (DMA, 2013). Based on these seismic maps, the seismic coefficients "S_S" (0.2 sec spectral response acceleration), "S_1" (1.0 sec spectral response acceleration), and "T_L" (long transition period) are 0.83 g, 0.24 g and 8.0 sec, respectively, for Dubai.

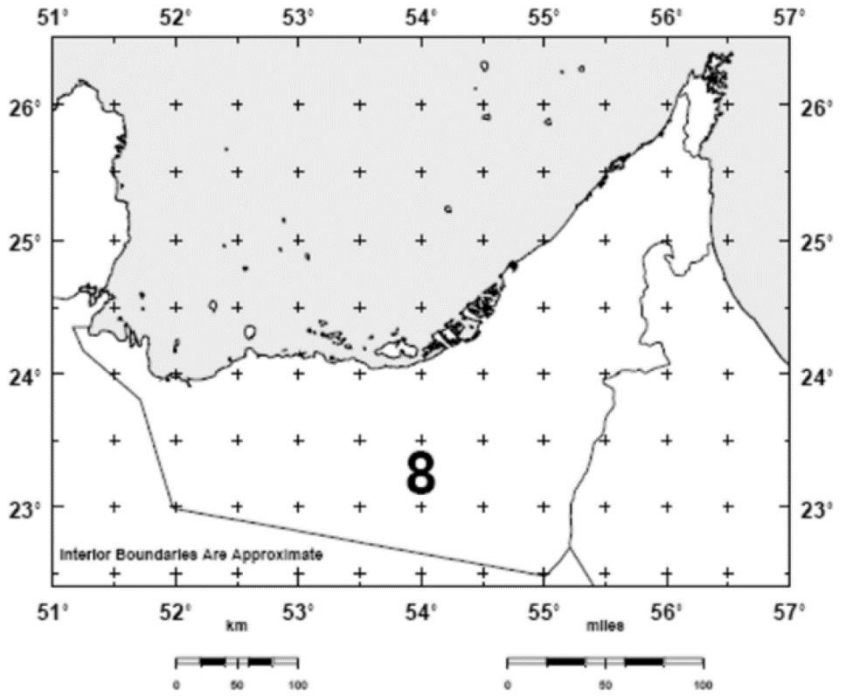

Figure 10. Long-period transition period, T_L (sec), for the UAE (DMA, 2013)

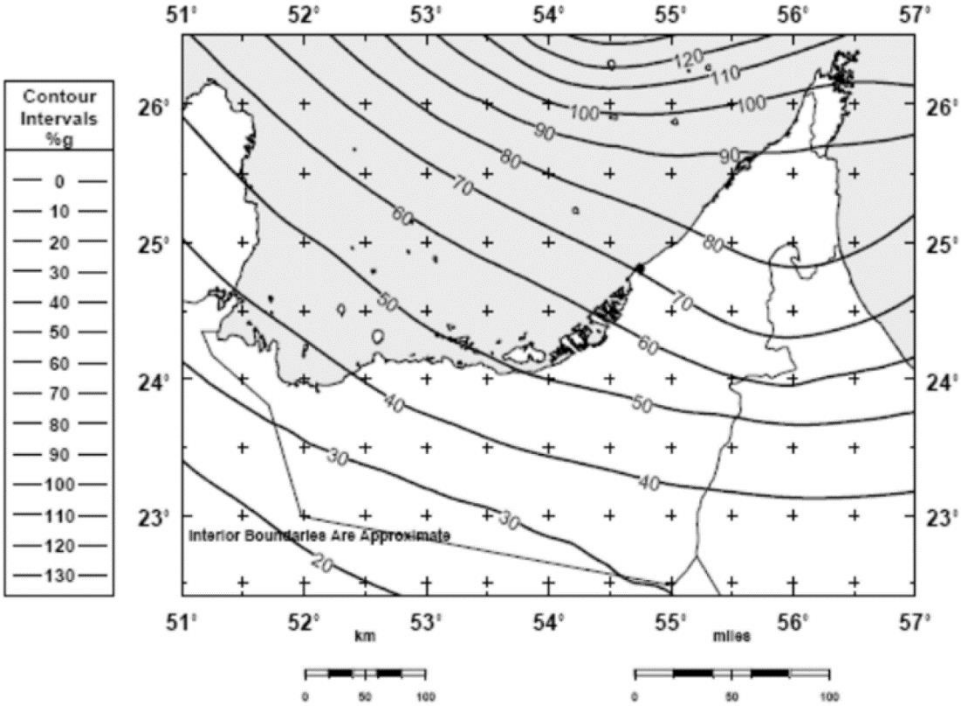

Figure 11. Maximum considered earthquake for the UAE for a 0.2s spectral response acceleration (S_s) - 5% of critical damping, site class B (DMA, 2013)

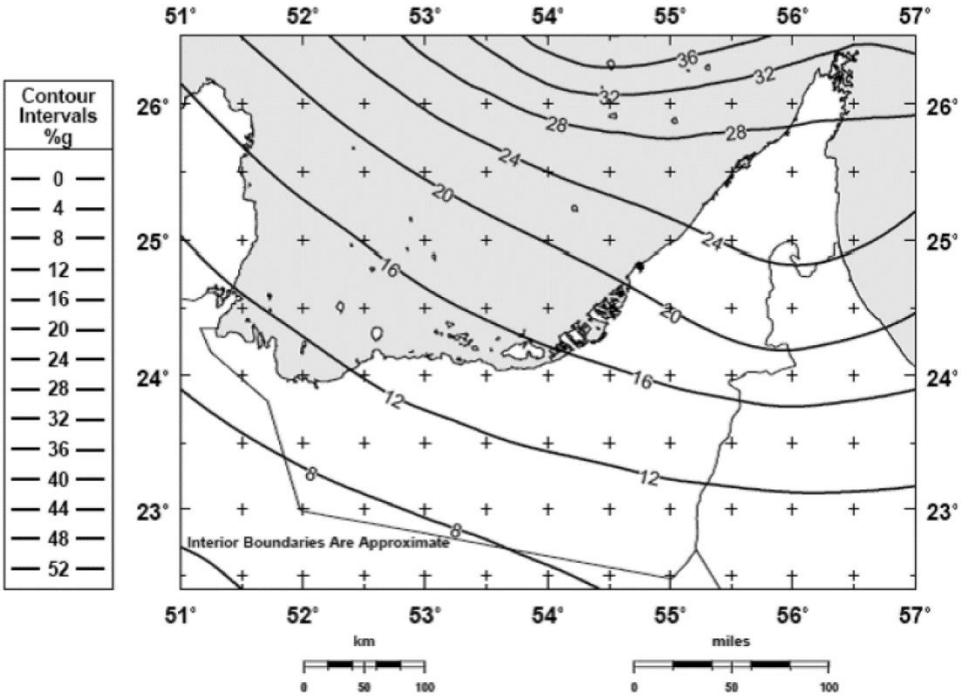

Figure 12. Maximum considered earthquake for the UAE for a 1.0s spectral response acceleration (S_1) - 5% of critical damping, site class B (DMA, 2013)

2.3 VULNERABILITY FUNCTIONS OF MULTI-STORY BUILDINGS

Vulnerability relationships of structures, also termed fragility functions, are related to structural damage and global seismic performance. Structural damage has direct and indirect consequences. For multi-story buildings, damage can cause significant loss to human life and economic assets due to structural collapse. Therefore, to effectively predict and mitigate against the seismic risk, fragility assessment of building inventory is essential not only for new buildings but also for existing structures (Ji et al., 2007b). There are, presently, limited studies related to the seismic vulnerability of high-rise structures, particularly for certain structural systems such as tube in tube. Figure 13 shows typical fragility relationships for different performance limit states.

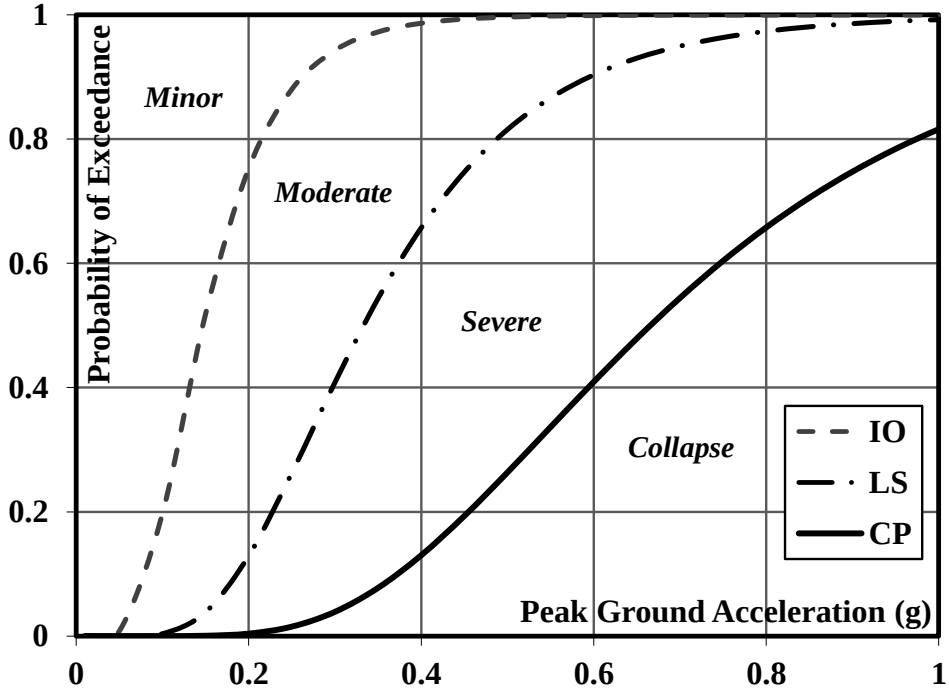

Figure 13. Typical fragility relationships for different performance limit states

2.3.1 Definition of Vulnerability

A vulnerability function is the relationship between the probability of exceeding a specific performance level and the input ground motion intensity, as shown in Eqn. 1 (Ji et al., 2007a).

$$P(\text{fragility}) = P[LS|IM = x], \quad P(LS) = P(C = D) \tag{1}$$

where C and D are the structural capacity and demand, respectively, and IM refers to the intensity measure of input ground motion with intensity level x, and LS represents the limit state.

The derivation of vulnerability relationships for multi-story buildings requires a thorough evaluation of the factors that affect the response of highly variable and complex structural systems as well as the prediction of their seismic response using a wide range of real input ground motions. A realistic performance limit states should also be selected according to the studied structural systems.

2.3.2 Performance Criteria

Four performance limit states are recommended by the NEHRP provisions (FEMA, 2009a). These define the operational (OP), immediate occupancy (IO), life safety (LS) and collapse prevention (CP) limit states. The design of a building to meet the OP performance criterion is not practical since all services required for operation must be ready immediately after the earthquake. This is true for the structures of occupancy category II (FEMA, 2009a). Detailed descriptions of the

expected damage level for the other three performance limit states are provided by NEHRP provisions.

Several previous studies and design guidelines have utilized the interstory drift ratio (IDR) to evaluate the structural damage since it can be related to local or global damage, and it can be calibrated with experimental results (ASCE-41, 2007; Mwafy, 2012a). The IDR is considered in the present study as the primary performance criterion to estimate the damage limits in the reference buildings. ASCE-41 (2007) adopts three performance criteria, which are IO, LS and CP limit states. These are related to minor cracking, extensive damage with a significant margin against collapse, and extensive concrete crushing and buckling of reinforcing steel, respectively. For RC frames, IDRs of 1.0%, 2.0% and 4.0% are adopted by ASCE-41 (2007) for the three limit states, respectively. For RC wall structures, IDRs of 0.5%, 1.0% and 2.0% are adopted for the above-mentioned performance levels, respectively.

The study of Ghobarah (2004) proposed IDRs for frame structures of 0.4%, 1.8% and 3.0%, and for wall structures of 0.4%, 1.5% and 2.5% for the above-mentioned three limit states, respectively. The SEAOC blue book (1999) proposed IDRs of 0.4%, 0.9%, 1.4% and 2.1% for RC shear walls at performance criteria SP1 to SP4, respectively. These performance levels referred to negligible damage, minor to moderate damage, moderate to major damage, and collapse limit states.

The study of Dymiotis et al. (1999), which was based on a wide range of experimental tests, recommended IDR of 4.0% for the CP limit state of RC frames. For RC wall structures, the experimental studies of Lehman et al. (2013), Panagiotou

et al. (2010) and Beyer et al. (2008) proposed IDRs for the IO limit state of 0.30%, 0.35% and 0.50%, respectively. The recommended IDRs were 2.27%, 2.36% and 2.39% for the CP performance level, respectively. The recommendations of the above-mentioned studies along with the large results of the present study are used to select a realistic performance limit states for the wide range of buildings investigated in the current work.

2.3.3 Approaches of Developing Vulnerability Functions

There are several approaches to derive fragility curves for different RC structural systems. These approaches can be classified as belonging to four categories, namely judgmental, empirical, analytical and hybrid. These categories are related to expert opinion, post-earthquake observations, analytical simulations, and combinations of these approaches, respectively (e.g. Calvi et al., 2006b; Jeong and Elnashai, 2007; Ji et al., 2009; Rossetto and Elnashai, 2003). Each method has advantages and disadvantages, as explained hereafter. The analytical approach is the most common approach when compared with other methods, particularly in regions with limited damage data from previous earthquakes (e.g. Schultz et al., 2010).

2.3.3.1 Judgmental Approach

Judgmental fragility curves are based on expert opinion or engineering judgment. Experts in earthquake engineering provide estimates of the potential damage distribution for different types of structures when subjected to various earthquake intensities. This method is not associated with the quality or quantity statistics of building damage. This approach can be applied easily for any structures with limited data (Rossetto and Elnashai, 2003). There are no limits in the methods

that may be used by experts, and this procedure can widely vary in terms of accuracy. This approach is a subjective method and difficult to control since expert opinion may be influenced by individual experience. Therefore, the judgmental approach is often used as a last option or when a high accuracy level is not required (Schultz et al., 2010).

2.3.3.2 Empirical Approach

Empirical fragility relationships are based on the building damage distributions that are recorded in post-earthquake observations. Although it is a realistic and practical method, its application has several limitations. The observational data is related to a certain source and area and may not be applicable for other areas. The experimental verification of observational data is very difficult since laboratory testing is too expensive and time consuming. Hence, the development of accurate fragility curves via this method needs extensive and reliable data collected from a wide range of earthquakes at different locations (Calvi et al., 2006b; Jeong and Elnashai, 2007; Rossetto and Elnashai, 2003; Schultz et al., 2010). The low seismic activities and scarcity of observational data from previous earthquakes in certain regions such as the UAE represent the main challenge for using this approach in such regions.

2.3.3.3 Analytical Approach

Analytical vulnerability relationships are obtained from the numerical analysis of simulated structural models under ground motions with increasing intensity. Detailed modeling approaches and extensive analyses using a wide range of earthquake records typically reduce uncertainty and increase the reliability of the derived fragility curves. This approach has many advantages since it is based on a simulation model of a real structure, and hence it results in a clear relationship between demand and capacity at different levels of input ground motion intensity. It also provides detailed fragility relationships, which not only allow for high sensitivity studies to be conducted, but also lead to calibrate the characteristics of seismic hazard and building stock. Therefore, the fragility curves obtained from this method are verifiable.

The analysis procedure of this method varies from elastic analysis of equivalent single degree of freedom (SDOF) system to inelastic non-linear response history analyses of three-dimensional models of structures (e.g. Mosalam et al., 1997; Singhal and Kiremidjian, 1997). The selection of simplified numerical models exploits the computational power and allows more simulations for different structures to be performed, while the adoption of detailed simulation models increases reliability and decreases uncertainty (Calvi et al., 2006b; Jeong et al., 2012; Ji et al., 2007b; Kwon and Elnashai, 2006; Rossetto and Elnashai, 2003; Schultz et al., 2010).

The main components for analytically deriving fragility curves or damage probabilities are summarized in Figure 14. The analytical fragility curves can be

derived through three different methods, namely non-linear static procedure (ASCE-41, 2007), capacity spectrum method (Freeman, 2004) and incremental dynamic analysis, IDA (Mwafy and Elnashai, 2001; Vamvatsikos and Cornell, 2002). The latter approach is the most accurate procedure for the assessment of the inelastic performance of a structure under seismic loads with increasing severity. It was developed to estimate the physical damage of a given structure by conducting multiple non-linear inelastic response history analyses of a structural model under selected ground motions: Each is scaled to several levels of seismic intensity (Vamvatsikos and Cornell, 2006).

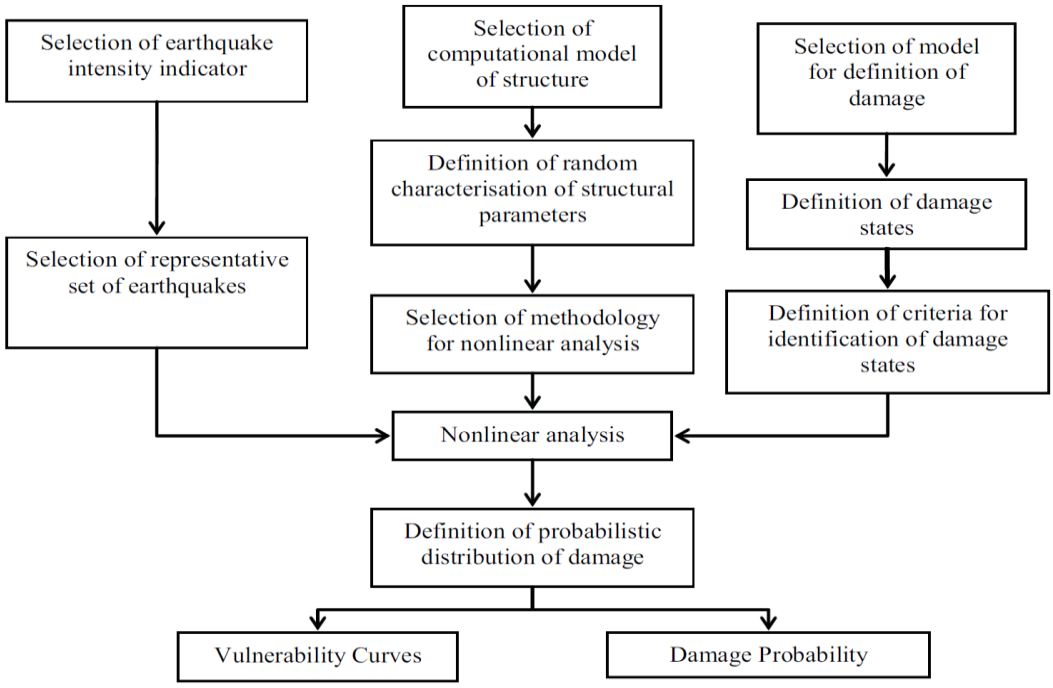

Figure 14. Main components of analytically-derived vulnerability curves (Dumova-Jovanoska, 2004)

2.3.3.4 Hybrid Approach

Hybrid fragility relationships combine two or more of the above-mentioned approaches. This technique attempts to overcome the limitations and disadvantages

associated with each of the previously described methods. The advantages and disadvantages of this method are similar to those of the methods that are combined.

2.3.4 Previous Vulnerability Studies covering RC Multi-story Buildings

Jeong et al. (2012) recently estimated the seismic performance of mid-rise code-complaint RC structures under different ground motion intensities using analytically-derived fragility functions. The reference buildings included regular and irregular structures. This study was conducted to evaluate the seismic safety of contemporary buildings at different limit states since such type of buildings have recorded human and financial losses due to recent earthquake events. A fiber-based modeling approach was used to develop the numerical models of the selected buildings. The analysis involved IDAs for each building using sixty real earthquake records. The records were selected to represent three ground conditions: rock, stiff soil and soft soil. This study adopted three limit states: immediate occupancy (IO), life safety (LS) and collapse prevention (CP). A large number of IDAs were conducted to derive the fragility relationships. It was concluded that the majority of reference buildings satisfied the LS limit state. The study suggests a simple relationship to enable the quantifying of the LS limit state probabilities of mid-rise RC buildings designed to contemporary seismic codes.

Mwafy (2012a) proposed an approach for developing fragility curves, which is an essential component of loss assessment systems. The framework of this study focused on analytically-derived fragility relationships for the contemporary high-rise buildings in the UAE due to the high level of human assets and financial investment of this type of buildings. Only the shear wall structural system was investigated in

this study. The procedure presented in this study for deriving fragility curves was as follows: (i) selection and design of representative structures; (ii) analytical modeling; (iii) uncertainty modeling; (iv) selection and scaling of input ground motions; (v) limit states; and (vi) development of fragility relationships using IDAs. Six RC shear wall buildings, varying in height from 10 to 60 stories, were selected and designed according to the building codes and construction practice adopted in the UAE. Inelastic pushover analyses (IPA) and IDAs were carried out for the reference structures. Twenty natural and artificial earthquake records were selected to represent the seismic hazard.

To derive the fragility curves in the latter study using IDAs, the analytical models of the reference buildings were assessed using the above-mentioned ground motions. The selected ground motions were scaled based on their PGA, which was used as the measure of input ground motion intensity. Following ASCE-41 (2007), three performance criteria were adopted in this study, namely IO, LS, and CP. This study concluded that modern shear wall buildings in the UAE are vulnerable to the severe distant seismic scenario, and recommended expanding the study to cover other classes of buildings and infrastructure in the study region.

Ji et al. (2007a) presented an analytical framework for the seismic vulnerability assessment of RC high-rise structures. The parameters were selected using genetic algorithms, which provided an efficient computational model for performing dynamic response history analysis. The study considered the uncertainty in structural material and seismic demand. Thirty natural and twenty artificial strong input ground motions were selected for the analysis that produced a range in structural response parameters due to the variation in magnitude, distance and site

condition. Fragility relationships were developed for a 54-story building from the UAE for three performance levels: serviceability, damage control, and collapse prevention. The proposed fragility assessment framework by Ji et al (2007a) is depicted in Figure 15.

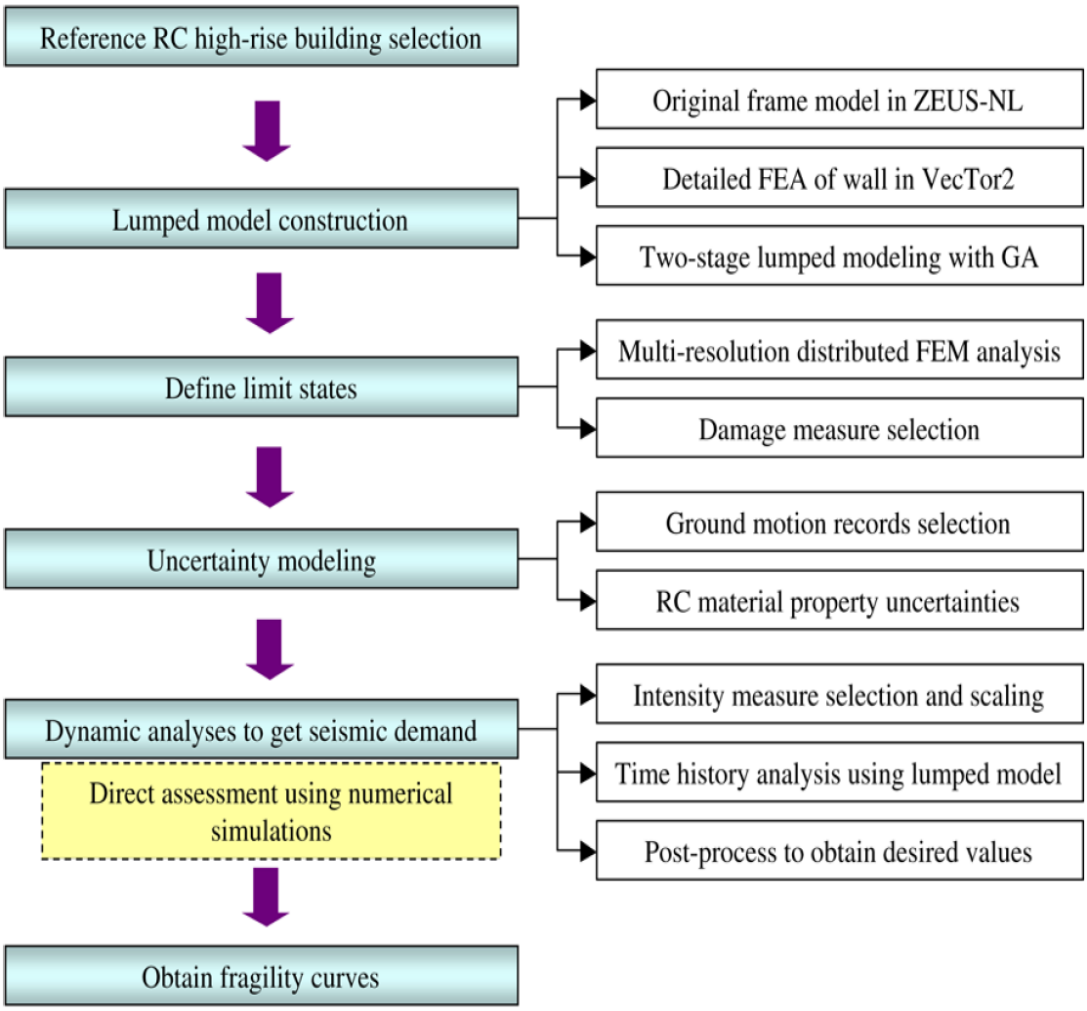

Figure 15. Fragility assessment framework proposed by Ji et al. (2007a)

Several other studies have been conducted to develop analytical fragility functions in different parts of the world. For instance, Kircil and Polat (2006) developed fragility relationships for mid-rise RC frame buildings in Turkey based on analytical simulation with respect to the number of stories of the buildings. Sample 3, 5 and 7-story building models were designed according to the Turkish seismic code.

The models of the buildings were analyzed under the effect of twelve artificial input ground motions. It was concluded that the fragility parameters changed significantly due to the number of stories of the building. Fragility relationships were performed for two performance levels, yielding and collapse. The developed fragility functions were constructed in terms of spectral displacement (S_d), spectral acceleration (S_a) and PGA.

Erberik and Elnashai (2004) derived fragility relationships for the flat slab structural system in order to estimate and mitigate against probable losses under earthquakes. This study was motivated by the poor performance of this type of structures under lateral loads. Due to the absence of deep beams, flat slab system had low lateral stiffness, which caused excessive deformations under earthquake loads. Ten earthquake records matching the code spectrum were used to conduct the dynamic analysis for a five-story flat slab reference building. The IDR was used for determining the limit states since the behavior and the failure modes of such structures are governed by deformation. Inelastic time history analyses were conducted to estimate the seismic response of the reference structure and to derive the vulnerability curves.

2.4 SEISMIC DESIGN RESPONSE FACTORS

The approach of reducing the seismic forces using a reduction factor to reach the design force is commonly used in seismic codes (e.g. ASCE-7, 2010; EC8, 2004). The seismic design factors, namely overstrength (Ω), force reduction (R) and deflection amplification (C) factors, are adopted by design provisions to reduce seismic loads and amplify deformations to arrive at safe structures and economic

designs. Therefore, these seismic design factors play a key role in the seismic design of structures. It was confirmed from previous studies that these design factors depend on several parameters such as the structural system (e.g. Mwafy and Elnashai, 2002; Mwafy, 2011; Tsopelas and Husain, 2004). These important factors can be estimated through two main methodologies based on the idealizations considered in analysis: (i) SDOF models (e.g. Borzi and Elnashai, 2000), and (ii) MDOF models representing real buildings, which is the most realistic approach (e.g. Mwafy and Elnashai, 2002; Mwafy, 2011).

Elnashai and Broderick (1996) and Mwafy and Elnashai (2002) proposed the following definition for estimating the ductility reduction factor (R_μ) of a specific structure under a certain earthquake record:

$$R_\mu = [(a_g)_c / (a_g)_y] \quad (2)$$

where $(a_g)_c$ and $(a_g)_y$ are the PGA of the earthquake that causes collapse and the PGA at the first indication of yield, respectively.

On the other hand, structures designed according to modern seismic codes commonly exhibit a considerable level of overstrength. Therefore, the first indication of yielding is usually observed at high intensity levels compared to the yield level included in the design. FEMA P-750 (FEMA, 2009a) emphasizes that the first significant yield of adequately designed structures may occur at lateral load levels that are higher than the design forces by from 30 to 100%. The above-mentioned definition of R_μ is therefore appropriate for ideal systems. For practically designed

structures, this definition should consider the overstrength. The suggested approach by Mwafy (2011) to estimate the R factor is therefore as follows:

$$R = R_{\mu} \cdot \Omega_{fy} = [(a_g)_c / (a_g)_y] \cdot \Omega_{fy} \quad (3)$$

where Ω_{fy} is the overstrength factor at first yield. For 5% inherent damping and a critical period of vibration greater than the transition period (T_s), the C factor can be assumed equal to R factor (ASCE-7, 2010). This assumption is based on the Newmark's equal displacement rule, which considers approximately equal inelastic and elastic displacements. Figure 16 shows the relationship between seismic design response factors (Mwafy and Elnashai, 2002). The calculations of the R and C factors in the present study are based on the actual capacity of structures using MDOF models representing real buildings since this methodology is more realistic and reliable.

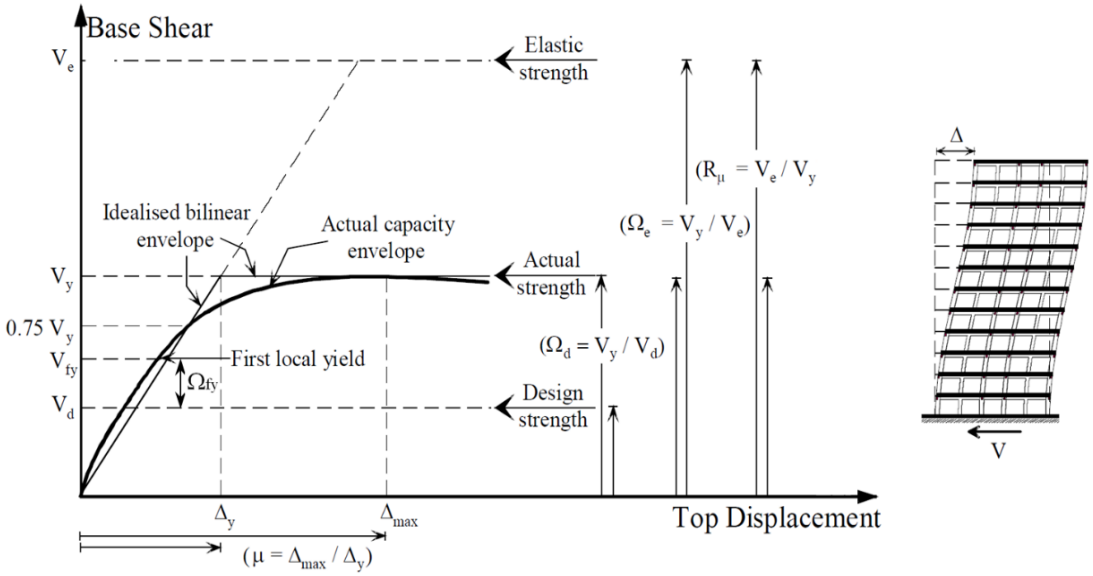

Figure 16. Relationship between seismic design response factors (Mwafy and Elnashai, 2002)

2.5 PERIODS OF VIBRATION

The dynamic characteristics of structures, such as the periods of vibration, are essential for the structural design of buildings under dynamic loading. Therefore, it is essential in seismic design to accurately estimate the time periods of the structure. RC buildings experience deterioration in stiffness and strength during earthquake shaking because of concrete cracking and steel yielding of different structural members. The ability of structural elements to dissipate seismic energy is decreased with the number of load reversals. Therefore, it has been recognized that after the first significant excursion beyond the yield limit, structures soften and respond with higher natural periods (e.g. Elnashai and Mwafy, 2002; Udwadia and Trifunac, 1973).

The elongated fundamental period, as an indicator of the degree of inelasticity of a structure under seismic loading, is a key factor to evaluate the structural performance. One of the fundamental observations from the structural response under earthquake loading is that damage (or inelastic response) and the dynamic characteristics of structures (i.e., periods of vibration and mode shapes) are closely correlated (e.g. Roufaiel and Meyer, 1987). Different damage models based on period elongation were suggested to estimate the global damage of RC structures (e.g. Dipasquale et al., 1990; Massumi and Moshtagh, 2013; Williams and Sexsmith, 1995).

Katsanos et al. (2014) recently investigated the elongation of the fundamental period of RC structures under earthquake loading and its correlation with different intensity measures and engineering demand factors. The study focused on a limited

number of mid-rise structures designed according to the Eurocode. The MDOF systems of the reference structures were transformed to equivalent SDOF systems, which were used to investigate the elongation of periods with increasing the level of earthquake loading. The study concluded that the structures designed according to modern seismic codes are expected to display low-to-moderate period elongation even at twice the design earthquake intensity.

Calvi et al. (2006a) concluded that a significant period elongation occurs for RC structures under strong ground shaking. The results of this study were supported by experimental tests of RC buildings and ground motion measurements observed from damaged RC structures under strong earthquakes. The study concluded that the initial period of vibration was elongated between 1.8 to 2.5 times under strong ground motions, which corresponded to 70 to 85% of stiffness degradation. This period elongation was attributed to the significant damage level of structural members.

2.6 CONCLUDING REMARKS

The requirements for the vulnerability assessment of modern multi-story buildings were reviewed in this chapter. It was shown from the brief literature review that none of the previous studies covered different structural systems and a wide range of building configurations. Moreover, previous studies have not mainly focused on the study region, particularly the UAE. This was due to the general belief that the Arabian Peninsula is a stable seismic zone. However, recent seismic hazard studies have clearly confirmed the pressing need for a comprehensive vulnerability assessment study for the UAE that covers different structural systems and building

configurations. Recent seismic activity in the UAE and surrounding region has also indicated that damaging earthquakes may occur in future. A comprehensive vulnerability assessment for the modern multi-story building inventory in the UAE is thus carried out in the present study by deriving fragility relationships and evaluating the seismic response factors.

CHAPTER 3: SELECTION AND DESIGN OF REPRESENTATIVE STRUCTURAL SYSTEMS

3.1 BUILDING STOCK AND CLASSIFICATION

3.1.1 Building Inventory

The focus of this study is on the seismic fragility of the modern building inventory in a seismically active area in the UAE. While this area extends from Dubai to Ajman, more emphasis is given in the present study to the highly populated area of Dubai. Collecting information for the existing building stock in the studied area is a great challenge due to the lack of census surveys and the rapid developments of the building inventory. The modern building inventory in the reference area selected in the present study was collected in another study based on the twelve zones shown in Figure 17 (Mwafy, 2012b; Mwafy, 2013b). Zones 1 to 7 are for Dubai, while zones 8 to 12 are for Sharjah and Ajman. The studied area was divided into these zones based on the common building characteristics. Each of the 12 zones shown in Figure 17 was divided into a number sub-zones to facilitate collecting the required data from satellite images and site visits. Figure 18 shows the percentage of buildings in different zones (Mwafy, 2012b; Mwafy, 2013b).

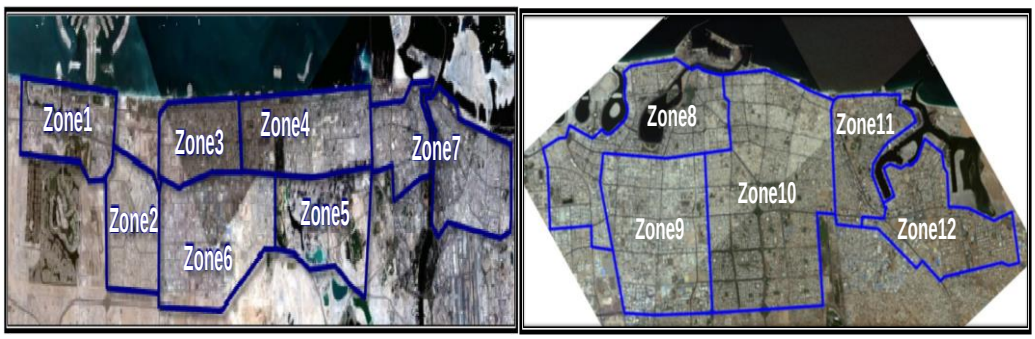

Figure 17. Zones of the studied area - Zones 1 to 7 are for Dubai, while Zones 8 to 12 are for Sharjah and Ajman (Mwafy, 2012b; Mwafy, 2013b)

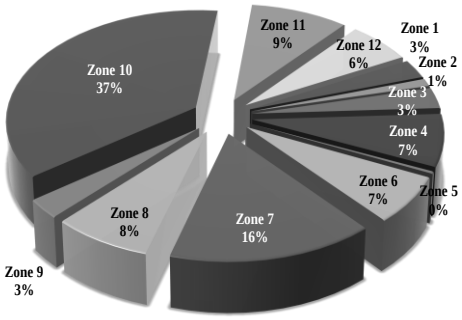

Figure 18. Percentage of buildings in different zones (Mwafy, 2012b; Mwafy, 2013b)

3.1.2 Building Classification

Although the building inventory was classified according to a number of criteria, the most significant classification criterion for contemporary multi-story buildings was the structure height. The building inventory in the studied area was therefore classified to ten categories according to the number of stories, namely 1-4, 5-10, 11-20, 21-30, 31-40, 41-50, 51-60, 61-70, 71-90 and 91-100 stories. Figure 19 shows the distribution of buildings in the twelve zones in the studied area according to their height (Mwafy, 2012b; Mwafy, 2013b).

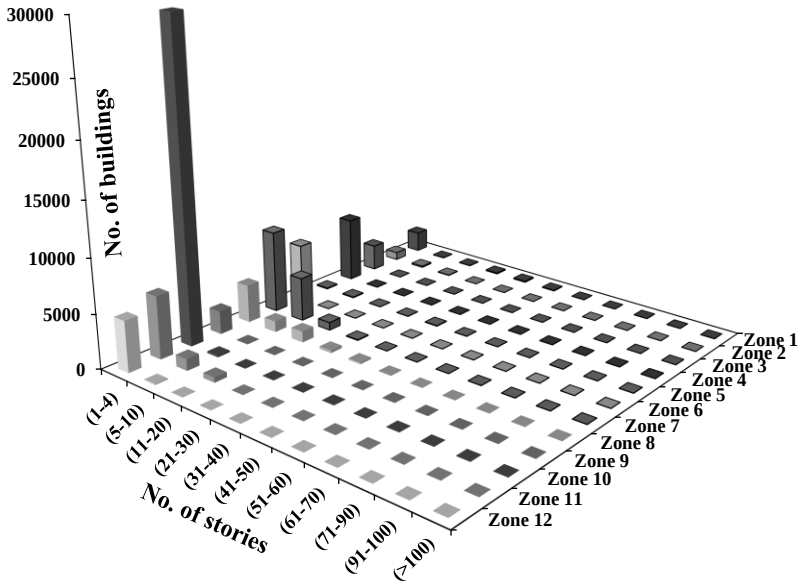

Figure 19. Building classification in different zones according to height (Mwafy, 2012b; Mwafy, 2013b)

3.2 SELECTION OF REPRESENTATIVE STRUCTURAL SYSTEMS

Ten reference structures of low, medium and high-rise buildings are selected based on the previously collected inventory to represent the contemporary buildings in the studied area. The selected structures are for RC buildings of 2, 8, 18, 26, 40, 50, 56, 66, 80 and 100-story. The ten buildings have six different layouts shown in Figure 20 to Figure 25, which represent common building layouts in the studied area. Each of the selected buildings consists of substructure (with the exception of 2 and 8-story structures), a ground floor and a number of typical floors. The total height of the ten reference buildings are 8.0, 28.5, 58.9, 84.5, 129.3, 161.3, 180.5, 212.5, 257.3 and 321.3 meters, respectively.

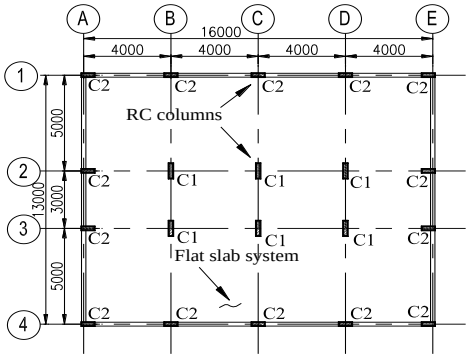

Figure 20. Layout of the 2-story building including a description of different structural members

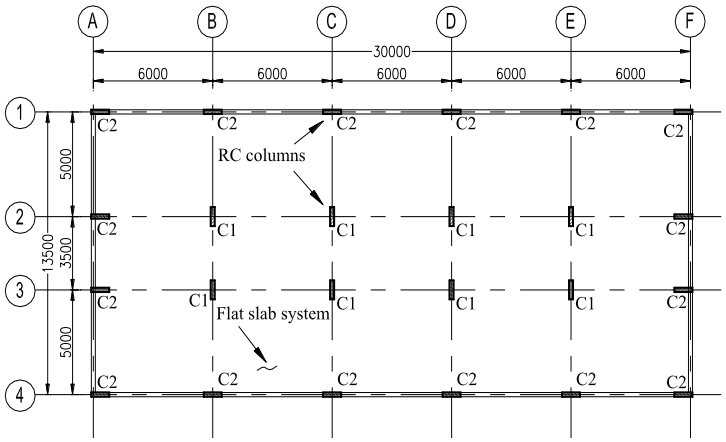

Figure 21. Layout of the 8-story building including a description of different structural members

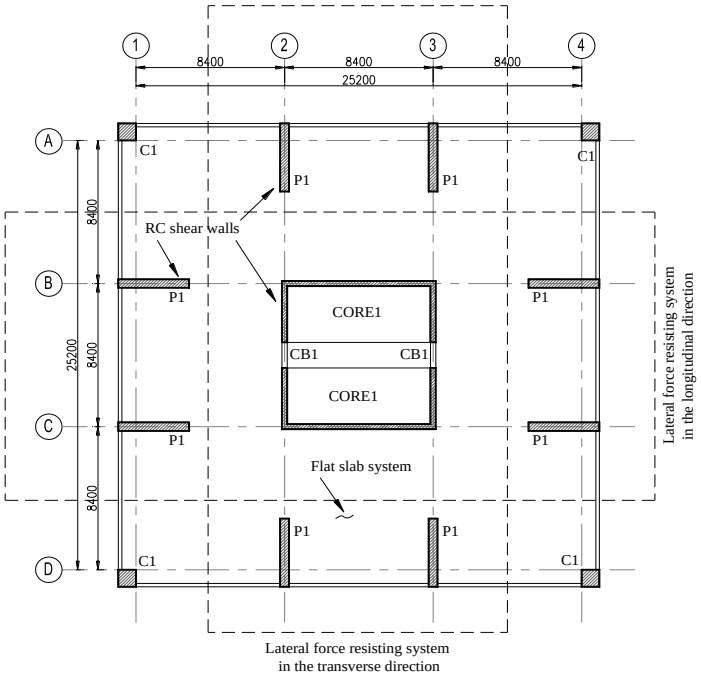

Figure 22. Layout of the 18- and 26-story buildings including a description of different structural members

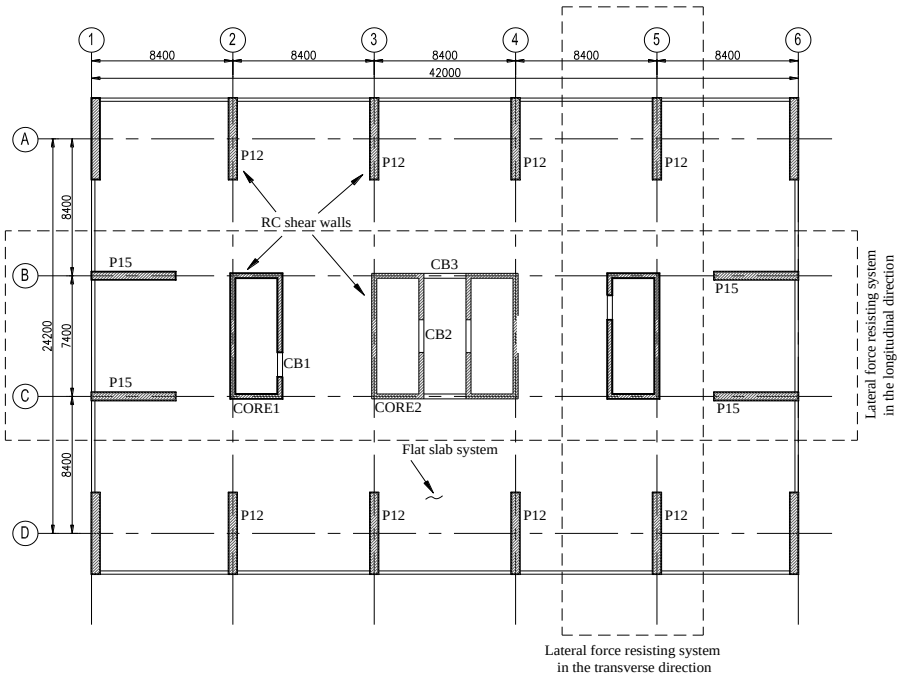

Figure 23. Layout of the 40- and 50-story buildings including a description of different structural members

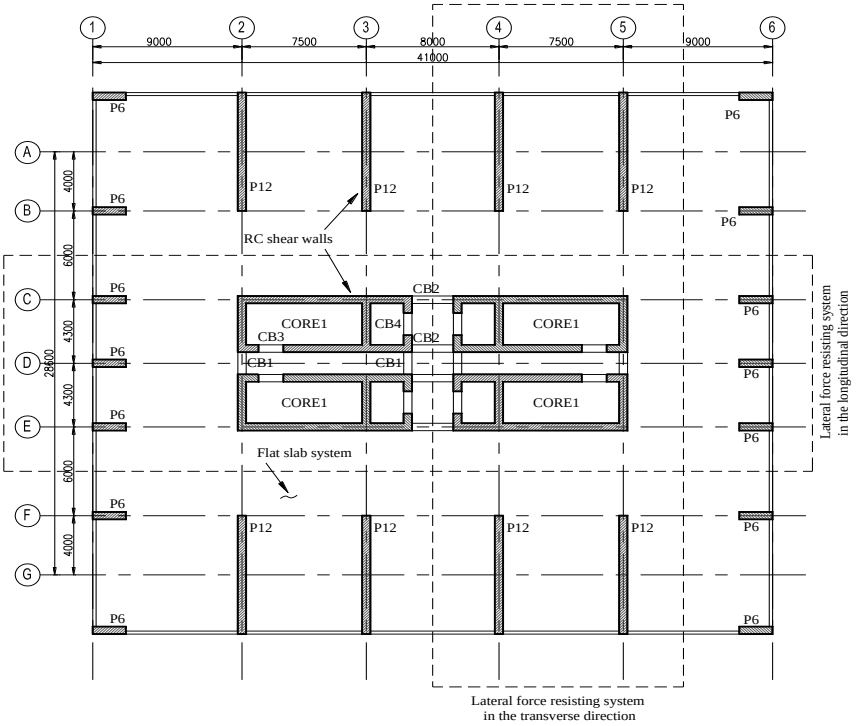

Figure 24. Layout of the 56- and 66-story buildings including a description of different structural members

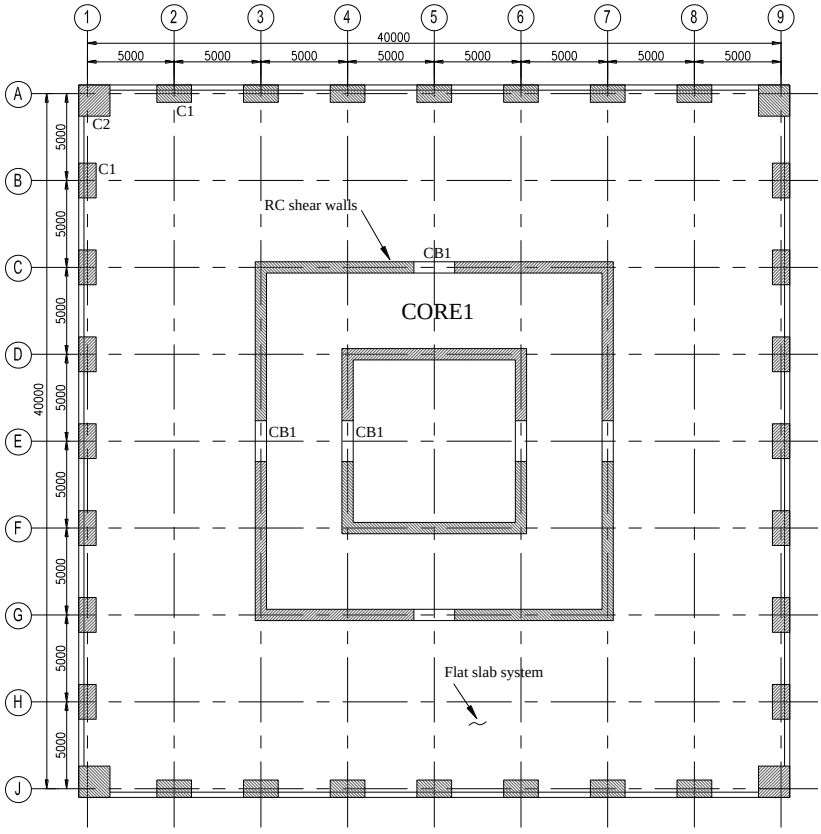

Figure 25. Layout of the 80- and 100-story buildings including a description of different structural members

The following three lateral force resisting systems are considered in the present study: (i) flat slab-columns (FSC); (ii) shear walls (SW); and (iii) tube in tube (TIT). These structural systems are selected to suit each building height and to represent the commonly used lateral force resisting systems for contemporary buildings in the studied area (e.g. Ali and Moon, 2007; Taranath, 2009). The FSC system is used for the 2 and 8-story buildings, while the SW system is employed for the 18, 26, 40, 50, 56 and 66-story buildings. The TIT system is finally considered for the 80 and 100-story buildings. Table 1 shows the selected reference structures with their lateral force resisting systems to represent the modern building inventory in the studied area. The selected wide range of buildings with different layouts, heights and structural systems in this comprehensive study ensure the reliable representation of the diverse contemporary buildings in the studied area.

Table 1. Selected reference structures to represent the modern RC building inventory in the studied area

Ser.	System	Ref.	Building classification based on the number of stories	Reference building	Lateral force resisting system
1	i	2St	1 to 4	2-story	flat slab-columns (FSC)
2		8St	5 to 10	8-story	
3	ii	18St	11 to 20	18-story	shear walls (SW)
4		26St	21 to 30	26-story	
5		40St	31 to 40	40-story	
6		50St	41 to 50	50-story	
7		56St	51 to 60	56-story	
8		66St	61 to 70	66-story	
9	iii	80St	71 to 90	80-story	tube in tube (TIT)
10		100St	91 to 100	100-story	

3.3 DESIGN PROCESS

The ten reference buildings are completely designed and detailed as per the latest international building codes and construction practice adopted in the UAE in order to arrive at the optimum concrete cross-sections and steel reinforcement for all structural members (ACI-318, 2011; ASCE-7, 2010; DMA, 2013; ICC, 2012). The

dead loads used in the design include the own-weight of structural elements in addition to a uniformly distributed superimposed dead load of 4.0 kN/m^2 on slabs. Following the ASCE-7 (2010), the considered live load for residential buildings is 2.0 kN/m^2, except for staircases and exit ways, which is 4.8 kN/m^2. Wind loads are calculated using the ASCE-7 provisions (2010) based on a basic wind speed of 45 m/s and an exposure category "C".

Seismic loads of the reference structures are estimated as per the ASCE-7 (2010) design provisions. The seismic action is estimated using both the Equivalent lateral force procedure (ELFP) and modal response spectrum analysis (MRSA). For the latter procedure, the code spectrum is used with twelve modes of vibration, which account for more than 90% of the mass in each of the orthogonal horizontal directions of the investigated buildings. According to the design code, the modal base shear from MRSA used in design should be at least 85% of the value obtained from ELFP.

The site class "C" and seismic design category "C" are adopted based on the common soil conditions and seismicity of the studied area (DMA, 2013; Irfan et al., 2012). The adopted seismic design category follows the recommendations of recent hazard assessment studies and currently implemented regulations for the studied area (e.g. Abdalla and Al-Homoud, 2004; DMA, 2013; Mwafy et al., 2006). It is worth noting that ASCE-7 (2010) recommends the use of spectral seismic design maps to quantify seismic hazards on the basis of contour lines. These maps have been recently prepared for the UAE and implemented in the Abu Dhabi international building code (DMA, 2013). Based on the seismic maps of the reference site, the coefficients "S_S" (0.2 sec spectral response acceleration) and "S_1" (1.0 sec spectral

response acceleration) are 0.83 and 0.24, respectively, while the long transition period "T_L" is 8 sec.

Detailed three-dimensional (3D) finite element (FE) models are developed for the design of the reference buildings using the structural analysis and design software ETABS (CSI, 2012a). This software is predominately used by structural design engineers for the analysis and design of buildings. Frame elements are used to model columns and beams, while shell elements are used to model floor slabs, shear walls and core walls. The frame and shell elements are designed using the recommended cracked sections (ACI-318, 2011). Figure 26 depicts the developed ETABS models of the selected buildings with samples of the cross-sections used in the design of each building.

The ten investigated buildings are designed and detailed according to different load combinations and the design provisions recommended by ACI-318 (2011). The yield strength of the reinforcing steel is 460 MPa. The cylinder concrete strength of vertical structural members decreases along the building height from 64 to 32 MPa (cube strength of 80 to 40 MPa). Floor slabs are designed using a constant cylinder concrete strength of 32 MPa throughout the building height. The cross-sections of shear walls and the associated reinforcing steel vary throughout the building height. The floor slab consists of a cast-in-place flat slab system with varied thickness according to spans of building layout. Different material strength values, cross-sectional dimensions and reinforcement are adopted to obtain the most efficient and economical design for the reference buildings.

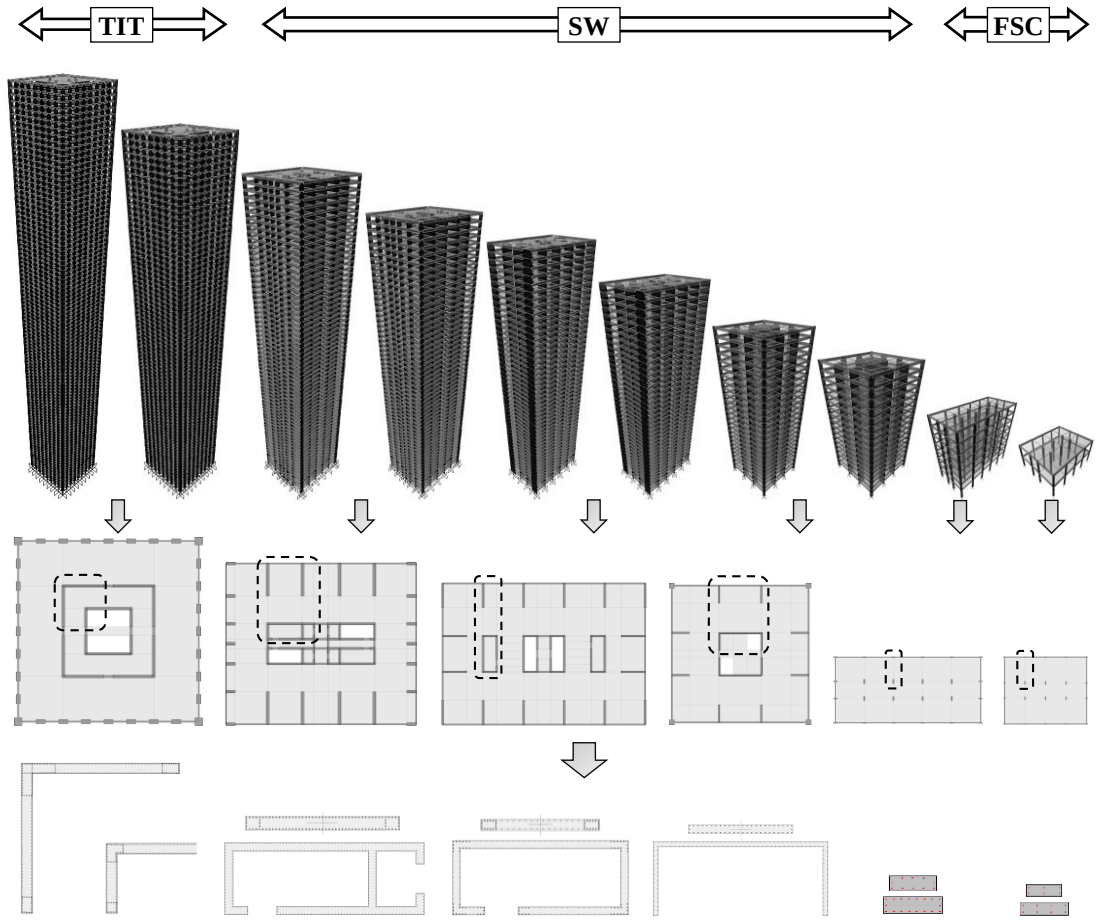

Figure 26. Analytical models of the reference buildings and samples of different cross-sections used in design

3.4 BOUNDARY ELEMENTS IMPACT ON SHEAR WALL DESIGN

The impacts of boundary elements on the design of shear wall structures was investigated by Ashri (2013) before conducting the design of the ten reference structures. Three buildings with different heights ranging from 20 to 60-story were studied. The layout of the investigated buildings is similar to the layout shown in Figure 23. Shear walls were designed with and without boundary elements, and the cost and performance of the two design cases were compared. The design summary of the shear walls with and without boundary elements is presented in Table 2. Based on the design results, it was concluded that the use of boundary elements results in a significant saving in the steel reinforcement of structural walls, particularly at the

lower stories of high-rise buildings. In addition, the lateral capacity was improved by using boundary elements. The shear walls and the core walls of the ten high-rise buildings investigated in the present study are therefore designed based on the boundary elements requirements recommended by the ACI-318 provisions (2011).

Table 2. Design summary of the shear walls at lower stories of the 20-, 30- and 60-story buildings with and without boundary elements (Ashri, 2013)

20-story building, Pier P12				
Location of section	Base	Floor no.4	Floor no.9	Floor no.14
Pier section (mm x mm)	350x3000	350x3000	300x3000	300x3000
Concrete strength (fc') MPa	36	36	36	36
Vertical steel ratio (μ%) with boundary elements	2.70%	1.76%	1.00%	1.00%
Vertical steel ratio (μ%) without boundary elements	2.76%	1.78%	1.00%	1.00%
Vertical steel saving (%) by using boundary elements	2.17%	1.12%	0.00%	0.00%
30-story building, Pier P12				
Location of section	Base	Floor no.4	Floor no.9	Floor no.14
Pier section (mm x mm)	350x4000	350x4000	300x4000	300x4000
Concrete strength (fc') MPa	40	40	36	36
Vertical steel ratio (μ%) with boundary elements	3.85%	2.15%	2.00%	1.20%
Vertical steel ratio (μ%) without boundary elements	4.13%	2.24%	2.05%	1.20%
Vertical steel saving (%) by using boundary elements	6.78%	4.02%	2.44%	0.00%
60-story building, Pier P12				
Location of section	Base	Floor no.4	Floor no.9	Floor no.14
Pier section (mm x mm)	500x5000	500x5000	450x5000	450x5000
Concrete strength (fc') MPa	56	56	48	48
Vertical steel ratio (μ%) with boundary elements	3.67%	2.54%	3.87%	2.33%
Vertical steel ratio (μ%) without boundary elements	5.33%	4.02%	4.13%	2.43%
Vertical steel saving (%) by using boundary elements	31.14%	36.82%	6.30%	4.12%

3.5 DESIGN RESULTS

The automated design process are carried out using ETABS (CSI, 2012a) for all investigated buildings under all load combinations recommended by ACI-318 (2011). Floor slabs are designed using the design software SAFE (CSI, 2012b). Lateral actions due to seismic forces are considered in the design of floor slabs by exporting the straining actions from ETABS to SAFE. Moreover, to verify the results obtained from the design software, selected cross-sections are designed using Excel spreadsheets based on the straining actions obtained from ETABS and SAFE.

All design information of the ten reference buildings obtained from this comprehensive task is stored in spreadsheets and AutoCAD drawings. Figure 27 to Figure 32 depict the reinforcement details of the floor slabs used in the ten reference buildings. Table 3 to Table 26 summarize the design information of vertical structural members, reinforcement details of slabs and reinforcement schedules of coupling beams. The design results are used to idealize the reference buildings for multi-degree-of-freedom inelastic simulations, as discussed in the next chapter.

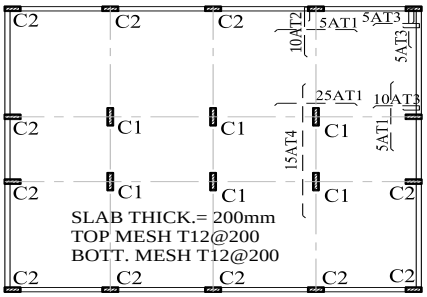

Figure 27. Typical reinforcement details of floor slabs - 2St building

Table 3. Schedule of extra top rebars of floor slabs - 2St building

Model	Reinforcement	Shape	Length (mm)
AT1	T12@200		3000
AT2	T12@200		3000
AT3	T12@200		2500
AT4	T12@200		6000

Table 4. Design summary of vertical structural members of the 2St building

Column C1	
Location of section	Base
Vertical steel ratio (μ%)	1.67 %
VL. Reinforcement	10T16
HL. Reinforcement	T10-100mm
Design/Capacity (D/C) Ratio	0.97
Column section (mm x mm)	200x600
Concrete strength (fc') MPa	32
Column C2	
Location of section	Base
Vertical steel ratio (μ%)	1.50 %
VL. Reinforcement	6T16
HL. Reinforcement	T10-100mm
Design/Capacity (D/C) Ratio	0.99
Column section (mm x mm)	200x400
Concrete strength (fc') MPa	32

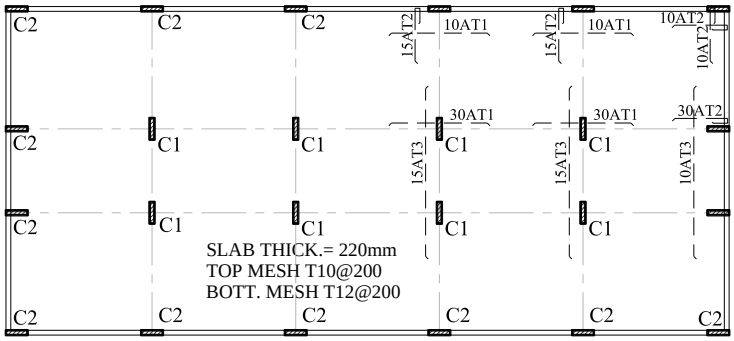

Figure 28. Typical reinforcement details of floor slabs - 8St building

Table 5. Schedule of extra top rebars of floor slabs - 8St building

Model	Reinforcement	Shape	Length (mm)
AT1	T16@200		4000
AT2	T16@200		3000
AT3	T16@200		7000

Table 6. Design summary of vertical structural members of the 8St building

Column C1		
Location of section	Base	Floor no.5
Vertical steel ratio (μ%)	2.50 %	1.0%
VL. Reinforcement	24T20	12T16
HL. Reinforcement	T10-150mm	T10-125mm
Design/Capacity (D/C) Ratio	1.00	0.57
Column section (mm x mm)	300x1000	250x1000
Concrete strength (fc') MPa	32	32
Column C2		
Location of section	Base	Floor no.5
Vertical steel ratio (μ%)	1.20 %	1.0%
VL. Reinforcement	12T16	8T16
HL. Reinforcement	T10-125mm	T10-100mm
Design/Capacity (D/C) Ratio	0.99	0.92
Column section (mm x mm)	250x800	200x800
Concrete strength (fc') MPa	32	32

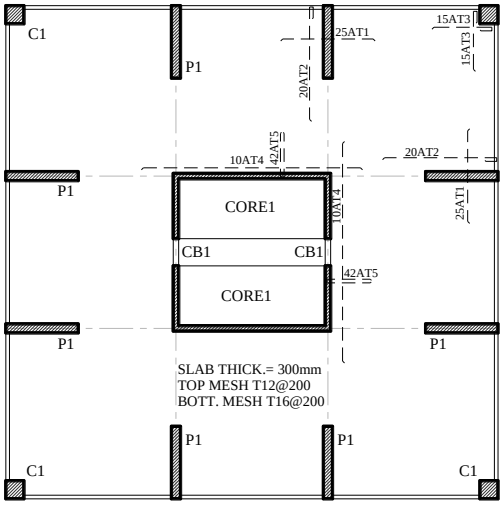

Figure 29. Typical reinforcement details of floor slabs - 18 and 26St buildings

Table 7. Schedule of extra top rebars of floor slabs - 18 and 26St buildings

Model	From base 1 to floor 7	From floor 8 to roof	Shape	Length (mm)
AT1	T16@200	T12@200		5000
AT2	T16@200	T12@200		6000
AT3	T16@200	T12@200		4000
AT4	T20@200	T16@200		12000
AT5	T20@200	T16@200		5000

Table 8. Schedule of reinforcement for coupling beams - 18St building

Model	Location	Dimensions (mm)		Reinforcement		Side bars	Stirrups
		Width	Depth	Bottom	Top		
CB1	Base 1	250	1000	6T25	6T25	4T12	1T10@150
CB1	Floor 8	200	1000	4T25	4T25	4T12	1T10@200

Table 9. Schedule of reinforcement for coupling beams - 26St building

Model	Location	Dimensions (mm)		Reinforcement		Side bars	Stirrups
		Width	Depth	Bottom	Top		
CB1	Base 1	300	1000	8T25	8T25	4T12	2T10@150
CB1	Floor 8	250	1000	6T25	6T25	4T12	1T10@150
CB1	Floor 17	200	1000	4T25	4T25	4T12	1T10@200

Table 10. Design summary of vertical structural members - 18St building

Pier P1			
Location of section	Base	Floor no.3	Floor no.8
Vertical steel ratio (μ%)	2.70 %	1.00%	1.00%
HL. Reinforcement	T12-200	T12-200	T12-200
Design/Capacity (D/C) Ratio	1.00	0.92	0.71
Pier section (mm x mm)	300x3500	300x3500	250x3500
Concrete strength (fc') MPa	32	32	32
CORE 1			
Location of section	Base		Floor no.8
Vertical steel ratio (μ%)	0.60%		0.60%
HL. Reinforcement	T12-200		T12-200
Design/Capacity (D/C) Ratio	0.77		0.46
Core thickness (mm)	250		200
Concrete strength (fc') MPa	32		32

Table 11. Design summary of vertical structural members - 26St building

Pier P1					
Location of section	Base	Floor no.3	Floor no.8	Floor no.12	Floor no.17
Vertical steel ratio (μ%)	3.80%	2.00%	1.80%	1.00%	1.00%
HL. Reinforcement	T12-200	T12-200	T12-200	T12-200	T12-200
Design/Capacity (D/C) Ratio	1.00	1.00	1.00	0.84	0.62
Pier section (mm x mm)	350x3500	350x3500	300x3500	300x3500	250x3500
Concrete strength (fc') MPa	36	36	32	32	32
CORE 1					
Location of section	Base		Floor no.8		Floor no.17
Vertical steel ratio (μ%)	0.60%		0.60%		0.60%
HL. Reinforcement	T12-200		T12-200		T12-200
Design/Capacity (D/C) Ratio	0.85		0.71		0.43
Core thickness (mm)	300		250		200
Concrete strength (fc') MPa	36		32		32

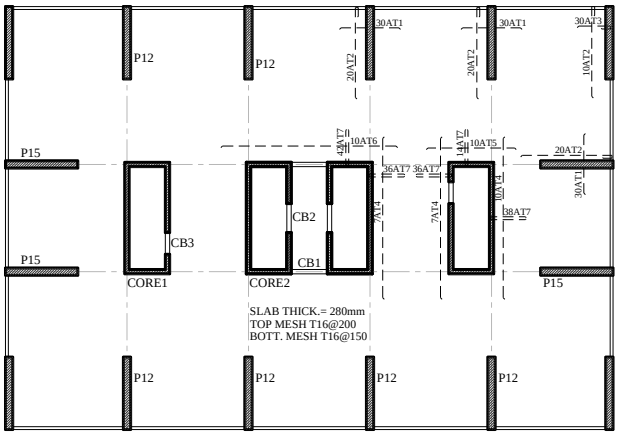

Figure 30. Typical reinforcement details of floor slabs - 40 and 50St buildings

Table 12. Schedule of extra top rebars of floor slabs - 40 and 50St buildings

Model	From base 1 to floor 7	From floor 8 to roof	Shape	Length (mm)
AT1	T20@200	T16@200		5000
AT2	T20@200	T16@200		7000
AT3	T20@200	T16@200		3000
AT4	T25@200	T20@200		11000
AT5	T25@200	T20@200		6000
AT6	T25@200	T20@200		12000
AT7	T25@200	T20@200		5000

Table 13. Schedule of reinforcement for coupling beams - 40St building

Model	Location	Dimensions (mm)		Reinforcement		Side bars	Stirrups
		Width	Depth	Bottom	Top		
CB1	Base 1	350	1000	8T25	8T25	4T12	2T10@100
CB1	Floor 9	300	1000	7T25	7T25	4T12	2T10@150
CB1	Floor 19	250	1000	5T25	5T25	4T12	1T10@150
CB1	Floor 29	200	1000	3T25	3T25	4T12	1T10@200

Table 14. Schedule of reinforcement for coupling beams - 50St building

Model	Location	Dimensions (mm)		Reinforcement		Side bars	Stirrups
		Width	Depth	Bottom	Top		
CB1	Base 1	400	1000	9T25	9T25	4T12	2T10@100
CB1	Floor 9	350	1000	7T25	7T25	4T12	2T10@100
CB1	Floor 19	300	1000	6T25	6T25	4T12	2T10@150
CB1	Floor 29	250	1000	4T25	4T25	4T12	1T10@150
CB1	Floor 39	200	1000	2T25	2T25	4T12	1T10@200

Table 15. Design summary of vertical structural members - 40St building

Pier P12								
Location of section	Base	Floor no.4	Floor no.9	Floor no.14	Floor no.19	Floor no.24	Floor no.29	Floor no.34
Vertical steel ratio (μ%)	2.82%	1.77%	2.32%	1.00%	1.00%	1.00%	1.00%	1.00%
HL. Reinforcement	T12-200	T12-200	T12-200	T12-200	T12-200	T12-200	T12-200	T12-200
Design/Capacity (D/C) Ratio	0.98	0.93	0.98	0.92	0.92	0.67	0.52	0.26
Pier section (mm x mm)	400x5000	400x5000	350x5000	350x5000	300x5000	300x5000	250x5000	250x5000
Concrete strength (fc') MPa	48	48	40	40	36	36	36	36
CORE 1								
Location of section	Base		Floor no.9		Floor no.19		Floor no.29	
Vertical steel ratio (μ%)	1.00%		1.00%		1.00%		1.00%	
HL. Reinforcement	T12-200		T12-200		T12-200		T12-200	
Design/Capacity (D/C) Ratio	0.66		0.66		0.59		0.39	
Core thickness (mm)	350		300		250		200	
Concrete strength (fc') MPa	48		40		36		36	
CORE 2								
Location of section	Base		Floor no.9		Floor no.19		Floor no.29	
Vertical steel ratio (μ%)	1.00%		1.00%		1.00%		1.00%	
HL. Reinforcement	T12-200		T12-200		T12-200		T12-200	
Design/Capacity (D/C) Ratio	0.78		0.70		0.55		0.38	
Core thickness (mm)	350		300		250		200	
Concrete strength (fc') MPa	48		40		36		36	

Table 16. Design summary of vertical structural members - 50St building

Pier P12										
Location of section	Base	Floor no.4	Floor no.9	Floor no.14	Floor no.19	Floor no.24	Floor no.29	Floor no.34	Floor no.39	Floor no.44
Vertical steel ratio (μ%)	3.62%	2.31%	3.88%	2.25%	1.85%	1.06%	1.00%	1.00%	1.00%	1.00%
HL. Reinforcement	T12-150	T12-150	T12-200	T12-200	T12-200	T12-200	T12-200	T12-200	T12-200	T12-200
Design/Capacity (D/C) Ratio	1.00	0.988	0.994	0.988	0.988	0.872	0.874	0.638	0.498	0.24
Pier section (mm x mm)	450x5000	450x5000	400x5000	400x5000	350x5000	350x5000	300x5000	300x5000	250x5000	250x5000
Concrete strength (fc') MPa	48	48	40	40	40	40	36	36	36	36
CORE 1										
Location of section	Base		Floor no.9		Floor no.19		Floor no.29		Floor no.39	
Vertical steel ratio (μ%)	1.00%		1.00%		1.00%		1.00%		1.00%	
HL. Reinforcement	T12-150		T12-200		T12-200		T12-200		T12-200	
Design/Capacity (D/C) Ratio	0.77		0.78		0.70		0.63		0.40	
Core thickness (mm)	400		350		300		250		200	
Concrete strength (fc') MPa	48		40		40		36		36	
CORE 2										
Location of section	Base		Floor no.9		Floor no.19		Floor no.29		Floor no.39	
Vertical steel ratio (μ%)	1.00%		1.00%		1.00%		1.00%		1.00%	
HL. Reinforcement	T12-150		T12-200		T12-200		T12-200		T12-200	
Design/Capacity (D/C) Ratio	0.87		0.83		0.67		0.58		0.40	
Core thickness (mm)	400		350		300		250		200	
Concrete strength (fc') MPa	48		40		40		36		36	

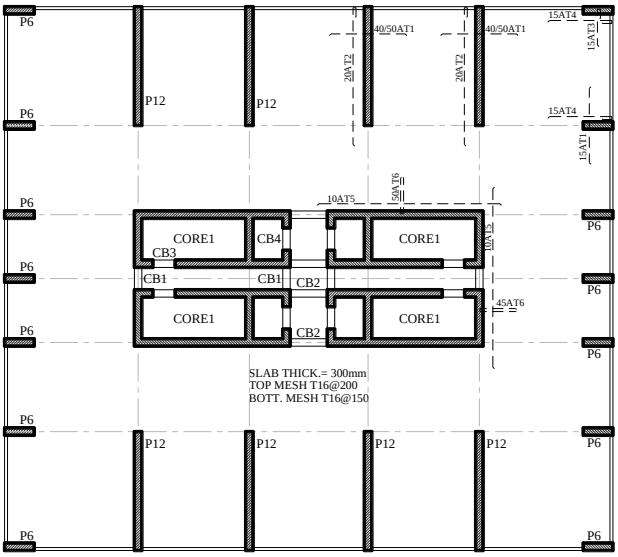

Figure 31. Typical reinforcement details of floor slabs - 56 and 66St buildings

Table 17. Schedule of extra top rebars of floor slabs - 56 and 66St buildings

Model	From base 1 to floor 7	From floor 8 to roof	Shape	Length (mm)
AT1	T20@200	T16@200		5000
AT2	T20@200	T16@200		11000
AT3	T20@200	T16@200		3000
AT4	T20@200	T16@200		5000
AT5	T25@200	T20@200		12000
AT6	T25@200	T20@200		5000

Table 18. Schedule of reinforcement for coupling beams - 56St building

Model	Location	Dimensions (mm)		Reinforcement		Side bars	Stirrups
		Width	Depth	Bottom	Top		
CB1	Base 1	450	1000	10T25	10T25	4T12	2T10@100
CB1	Floor 9	400	1000	8T25	8T25	4T12	2T10@100
CB1	Floor 20	350	1000	6T25	6T25	4T12	2T10@150
CB1	Floor 31	300	1000	4T25	4T25	4T12	2T10@150
CB1	Floor 42	250	1000	2T25	2T25	4T12	1T10@200

Table 19. Schedule of reinforcement for coupling beams - 66St building

Model	Location	Dimensions (mm)		Reinforcement		Side bars	Stirrups
		Width	Depth	Bottom	Top		
CB1	Base 1	600	1000	12T25	12T25	4T12	2T10@100
CB1	Floor 9	500	1000	10T25	10T25	4T12	2T10@100
CB1	Floor 20	400	1000	8T25	8T25	4T12	2T10@150
CB1	Floor 31	350	1000	6T25	6T25	4T12	2T10@150
CB1	Floor 42	300	1000	4T25	4T25	4T12	2T10@200
CB1	Floor 53	250	1000	2T25	2T25	4T12	1T10@200

Table 20. Design summary of vertical structural members - 56St building

Pier P12									
Location of section	Base	Floor no.3	Floor no.9	Floor no.14	Floor no.20	Floor no.25	Floor no.31	Floor no.36	Floor no.42
Vertical steel ratio (μ%)	3.2%	1.50%	3.60%	2.30%	2.70%	1.00%	2.00%	1.00%	1.00%
HL. Reinforcement	T12-150	T12-150	T12-200	T12-200	T12-200	T12-200	T12-200	T12-200	T12-200
Design/Capacity (D/C) Ratio	1.00	0.99	1.00	0.99	1.00	0.99	0.99	0.80	0.67
Pier section (mm x mm)	600x7000	600x7000	500x7000	500x7000	400x7000	400x7000	300x7000	300x7000	250x7000
Concrete strength (fc') MPa	48	48	40	40	40	40	36	36	36
CORE 1									
Location of section	Base		Floor no.9		Floor no.20		Floor no.31		Floor no.42
Vertical steel ratio (μ%)	1.36%		1.25%		1.00%		1.00%		1.00%
HL. Reinforcement	T12-150		T12-200		T12-200		T12-200		T12-200
Design/Capacity (D/C) Ratio	0.99		0.98		0.88		0.74		0.42
Core thickness (mm)	450		400		350		300		250
Concrete strength (fc') MPa	48		40		40		36		36

Table 21. Design summary of vertical structural members - 66St building

Pier P12									
Location of section	Base	Floor no.3	Floor no.9	Floor no.14	Floor no.20	Floor no.25	Floor no.31	Floor no.42	Floor no.53
Vertical steel ratio (μ%)	3.00%	1.00%	1.20%	1.00%	2.00%	1.00%	1.00%	1.00%	1.00%
HL. Reinforcement	T12-150	T12-150	T12-150	T12-150	T12-200	T12-200	T12-200	T12-200	T12-200
Design/Capacity (D/C) Ratio	0.98	1.00	1.00	0.92	0.99	0.97	0.97	0.85	0.62
Pier section (mm x mm)	800x9000	800x9000	700x9000	700x9000	600x9000	600x9000	500x9000	400x9000	300x9000
Concrete strength (fc') MPa	48	48	48	48	40	40	40	36	36
CORE 1									
Location of section	Base		Floor no.9		Floor no.20		Floor no.31		Floor no.42
Vertical steel ratio (μ%)	1.50%		1.00%		1.00%		1.00%	1.00%	1.00%
HL. Reinforcement	T12-150		T12-150		T12-200		T12-200	T12-200	T12-200
Design/Capacity (D/C) Ratio	0.98		0.92		0.95		0.71	0.59	0.38
Core thickness (mm)	600		500		400		350	300	250
Concrete strength (fc') MPa	48		48		40		40	36	36

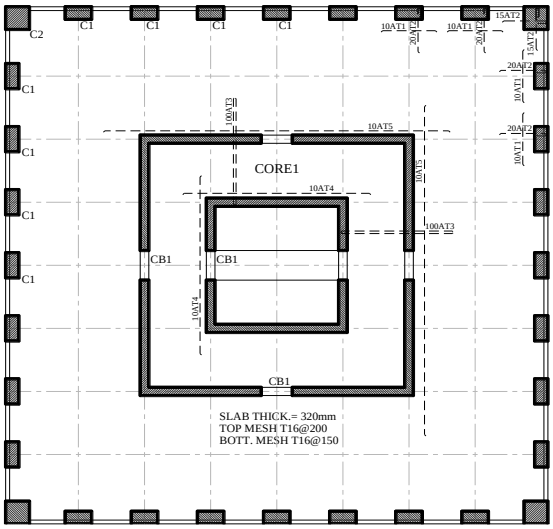

Figure 32. Typical reinforcement details of floor slabs - 80 and 100St buildings

Table 22. Schedule of extra top rebars of floor slabs - 80 and 100St buildings

Model	From base 1 to floor 7	From floor 8 to roof	Shape	Length (mm)
AT1	T20@200	T16@200		4000
AT2	T20@200	T16@200		4000
AT3	T25@200	T20@200		17000
AT4	T25@200	T20@200		14000
AT5	T25@200	T20@200		26000

Table 23. Schedule of reinforcement for coupling beams - 80St building

Model	Location	Dimensions (mm)		Reinforcement		Side bars	Stirrups
		Width	Depth	Bottom	Top		
CB1	Base 1	550	1200	12T32	12T32	6T12	2T12@100
CB1	Floor 7	500	1200	16T25	16T25	6T12	2T12@100
CB1	Floor 17	450	1200	12T25	12T25	6T12	2T10@100
CB1	Floor 27	400	1200	10T25	10T25	6T12	2T10@100
CB1	Floor 37	350	1200	8T25	8T25	6T12	2T10@150
CB1	Floor 47	300	1200	6T25	6T25	6T12	2T10@150
CB1	Floor 57	300	1200	4T25	4T25	6T12	2T10@200
CB1	Floor 67	250	1200	2T25	2T25	6T12	1T10@200

Table 24. Schedule of reinforcement for coupling beams - 100St building

Model	Location	Dimensions (mm)		Reinforcement		Side bars	Stirrups
		Width	Depth	Bottom	Top		
CB1	Base 1	650	1200	12T40	12T40	6T12	2T12@100
CB1	Floor 7	600	1200	16T32	16T32	6T12	2T12@100
CB1	Floor 17	550	1200	12T32	12T32	6T12	2T12@100
CB1	Floor 27	500	1200	16T25	16T25	6T12	2T10@100
CB1	Floor 37	450	1200	12T25	12T25	6T12	2T10@100
CB1	Floor 47	400	1200	10T25	10T25	6T12	2T10@100
CB1	Floor 57	400	1200	8T25	8T25	6T12	2T10@150
CB1	Floor 67	350	1200	6T25	6T25	6T12	2T10@150
CB1	Floor 77	350	1200	4T25	4T25	6T12	2T10@200
CB1	Floor 87	300	1200	2T25	2T25	6T12	1T10@200

Table 25. Design summary of vertical structural members - 80St building

Column C1								
Location of section	Base	Floor no.7	Floor no.17	Floor no.27	Floor no.37	Floor no.47	Floor no.57	Floor no.67
Vertical steel ratio (μ%)	3.4%	3.00%	2.60%	1.70%	1.33%	1.00%	1.00%	1.00%
HL. Reinforcement	T12-150	T12-150	T12-200	T12-200	T10-200	T10-200	T10-200	T10-200
Design/Capacity (D/C) Ratio	0.94	0.91	0.95	0.91	0.94	0.78	0.62	0.36
Column section (mm x mm)	900x2000	850x2000	800x2000	750x2000	700x2000	650x2000	600x2000	550x2000
Concrete strength (fc') MPa	56	56	48	48	40	40	36	36
Column C2								
Location of section	Base		Floor no.17		Floor no.37		Floor no.57	
Vertical steel ratio (μ%)	2.50%		2.50%		1.00%		1.00%	
HL. Reinforcement	T12-150		T12-200		T10-200		T10-200	
Design/Capacity (D/C) Ratio	0.89		0.89		0.91		0.58	
Column section (mm x mm)	1700x1700		1600x1600		1500x1500		1500x1500	
Concrete strength (fc') MPa	56		48		40		36	
CORE 1								
Location of section	Base	Floor no.7	Floor no.17	Floor no.27	Floor no.37	Floor no.47	Floor no.57	Floor no.67
Vertical steel ratio (μ%)	1.00%	1.00%	1.00%	1.00%	1.00%	1.00%	1.00%	1.00%
HL. Reinforcement	T12-100	T12-100	T12-15	T12-150	T12-200	T12-200	T12-200	T12-200
Design/Capacity (D/C) Ratio	0.98	0.93	1.00	0.92	0.97	0.83	0.72	0.44
Core thickness (mm)	550	500	450	400	350	300	300	250
Concrete strength (fc') MPa	56	56	48	48	40	40	36	36

Table 26. Design summary of vertical structural members - 100St building

Column C1										
Location of section	Base	Floor no.7	Floor no.17	Floor no.27	Floor no.37	Floor no.47	Floor no.57	Floor no.67	Floor no.77	Floor no.87
Vertical steel ratio (μ%)	4.00%	3.40%	3.9%	3.00%	2.60%	1.70%	1.33%	1.00%	1.00%	1.00%
HL. Reinforcement	T12-150	T12-150	T12-150	T12-150	T12-200	T12-200	T10-200	T10-200	T10-200	T10-200
Design/Capacity (D/C) Ratio	0.95	0.93	0.93	0.91	0.95	0.91	0.94	0.77	0.62	0.34
Column section (mm x mm)	1000x2000	950x2000	900x2000	850x2000	800x2000	750x2000	700x2000	650x2000	600x2000	550x2000
Concrete strength (fc') MPa	64	64	56	56	48	48	40	40	36	36
Column C2										
Location of section	Base	Floor no.17	Floor no.37	Floor no.57	Floor no.77					
Vertical steel ratio (μ%)	3.6%	3.6%	3.00%	1.00%	1.00%					
HL. Reinforcement	T12-150	T12-150	T12-200	T10-200	T10-200					
Design/Capacity (D/C) Ratio	0.93	0.95	0.93	0.94	0.60					
Column section (mm x mm)	1800x1800	1700x1700	1600x1600	1600x1600	1600x1600					
Concrete strength (fc') MPa	64	56	48	40	36					
CORE 1										
Location of section	Base	Floor no.7	Floor no.17	Floor no.27	Floor no.37	Floor no.47	Floor no.57	Floor no.67	Floor no.77	Floor no.87
Vertical steel ratio (μ%)	1.00%	1.00%	1.00%	1.00%	1.00%	1.00%	1.00%	1.00%	1.00%	1.00%
HL. Reinforcement	T12-100	T12-100	T12-100	T12-150	T12-150	T12-150	T12-200	T12-200	T12-200	T12-200
Design/Capacity (D/C) Ratio	0.96	0.92	0.99	0.93	1.00	0.93	0.98	0.84	0.73	0.45
Core thickness (mm)	650	600	550	500	450	400	400	350	350	300
Concrete strength (fc') MPa	64	64	56	56	48	48	40	40	36	36

3.6 CONCLUDING REMARKS

The selection and design of a wide range of multi-story buildings with different structural systems and building heights to represent the modern building inventory in a seismically active area in the UAE was discussed in this chapter. Several observations were noted during the design process. The design of floor slabs was strongly affected by considering the seismic loads in design due to the stress concentration at the connections between floor slabs and vertical elements, particularly the stiff shear walls. The results indicated that the slab reinforcing steel was highly increased at the slab connection with shear walls and core walls when seismic loads were considered. This confirms the significance of lateral loads in the design of floor slabs.

The use of boundary elements resulted in a significant saving in the steel reinforcement of structural walls, particularly at the lower stories of high-rise buildings. The lateral strength was also improved by using boundary elements. The shear walls and core walls of the reference high-rise buildings were therefore designed based on the boundary elements requirements recommended by the ACI-318 provisions. Although the design provisions recommended by the design codes were fully implemented in the design of high-rise buildings, the design results confirmed that the design should be verified using inelastic dynamic analysis, particularly for the TIT system. The latter observation is consistent with the recent recommendations for the performance based seismic design of high-rise buildings.

CHAPTER 4: ANALYTICAL MODELING AND SELECTION OF INPUT GROUND MOTIONS

4.1 FIBER-BASED ANALYTICAL MODELING

Detailed fiber-based analytical models are developed for the ten reference buildings. The developed models are used to conduct a large number of eigenvalue analyses (EVAs), inelastic pushover analyses (IPAs), dynamic time history analyses (THAs) and incremental dynamic analyses (IDAs). The above-mentioned analyses are conducted using ZEUS-NL (Elnashai et al., 2012), which is a contemporary platform for inelastic analysis using the fiber modeling approach. ZEUS-NL was originally developed at Imperial College London, and has been improved at the University of Illinois at Urbana-Champaign. This inelastic analysis platform has been extensively verified through experimental tests carried out in Europe and the U.S., and hence has been adopted in several research projects covering complex structures (e.g. Jeong and Elnashai, 2005; Kwon and Elnashai, 2006; Mwafy, 2012a). The adopted idealization effectively accounts for reinforcing steel, unconfined concrete and confined concrete. This idealization enables tracing the stress-strain response at Gauss sections through the integration of the non-linear stress-strain response of different fibers in which the section is subdivided, as illustrated in Figure 33.

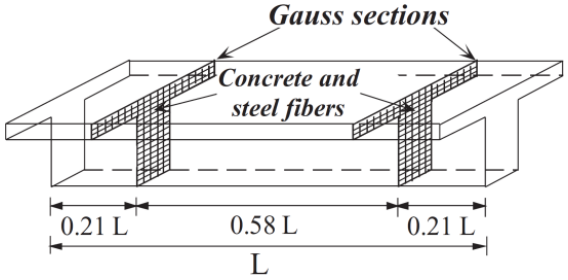

Figure 33. Modeling structures using elasto-plastic frame element (Mwafy, 2012a)

The modeling uncertainty is reduced by utilizing the fiber modeling approach since assumptions such as the moment–curvature relationships needed by other idealization approaches are avoided. Each of the structural elements in the current study is modeled using a number of elasto-plastic frame elements capable of representing the spread of inelasticity within the element cross-section and along the member length through the fiber modeling idealization. This approach enables modeling different arrangements of reinforcing steel along the element length as specified in design (at the two edges and at the mid-span). The slab/beam ends are connected with shear wall/core wall (the length between the centerline and the edge of the vertical element representing the shear wall/core wall) by rigid arms.

The following cross-sections are used from the ZEUS-NL library to model different structural elements: (i) RC rectangular section for slabs, (ii) RC T-section for beams, (iii) RC flexural wall section for shear walls, (iv) RC hollow rectangular section for cores, and (v) rectangular solid section for rigid arms. The appropriate material stress-strain relationships are applied to different fibers, and their strains and stresses are monitored. The response of cross-sections is assembled from the response of different fibers. The reinforcing steel is represented by a bilinear elasto-plastic model, while the concrete response is represented by a uniaxial constant confinement concrete model (Elnashai et al., 2012). The actual (mean) material strength values are used in the inelastic analysis (e.g. Rossetto and Elnashai, 2005). Columns and shear walls are considered to be fixed at the foundation level (ASCE-7, 2010).

The damping parameters were investigated prior to conducting the ZEUS-NL inelastic analysis. Hysteretic damping is accounted for in the fiber formulation of the

inelastic frame elements. A relatively small quantity of the non-hysteretic type of damping is also added to the inelastic models through stiffness-proportional damping (e.g. Priestley and Grant, 2005). In addition to the hysteretic damping due to inelastic energy absorption, an initial stiffness-proportional viscous damping of 0.5% is used. The stiffness-proportional damping coefficient is calculated based on a weighted period, which represents the mean cracked period of the first three translational modes in the direction of excitation weighted based on the mass participation factor and the corresponding spectral acceleration (Alwaeli et al., 2014). Gravity loads are applied as point loads at horizontal frame member nodes. Mass is represented by lumped mass elements and distributed in the same pattern employed for gravity loads.

4.1.1 Analytical Modeling of Flat Slab-Column (FSC) Structures

Three-dimensional (3D) inelastic analytical models are developed using ZEUS-NL for the 2 and 8-story buildings, which represent the FSC system in the present study. The transverse direction is considered in the present study since the lateral force resisting systems in this direction are more critical compared with the longitudinal counterparts. The framing systems in the transverse direction consist of a number of frames (columns with slabs/beams). Figure 34 depicts the ZEUS-NL fiber-based 3D analytical models developed for the 2 and 8-story buildings for inelastic analyses.

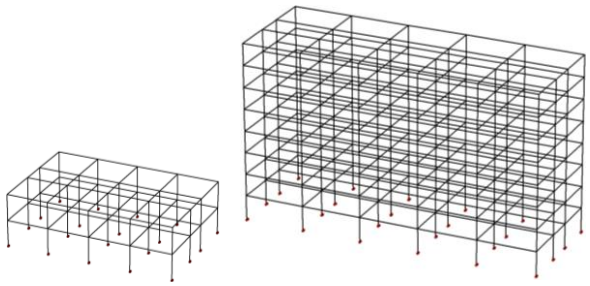

Figure 34. 3D fiber-based models for the 2 and 8-story buildings for inelastic analysis

4.1.2 Analytical Modeling of Shear Wall (SW) Structures

The layouts of the SW buildings shown in Figures 22 to 24 clearly confirmed the symmetry of the lateral force resisting systems in the two orthogonal directions. Two-dimensional (2D) fiber-based analytical models are therefore developed using ZEUS-NL for the 18, 26, 40, 50, 56 and 66-story buildings, which represent the SW structural system in the present study.

For the 18 and 26-story buildings, it is assumed that a single lateral force resisting system is in each of the longitudinal and transverse directions because the layout is square and symmetric. Each framing system of the above-mentioned structures consists of four external shear walls and an internal core, which are loaded with 100% of the total mass of the structure. The other vertical elements at the edges are assumed to resist gravity loads only. Figure 35 describes the adopted modeling approach used to idealize the 18 and 26-story buildings in the transverse direction for inelastic analyses.

For the 40 and 50-story buildings, only the framing systems in the transverse direction are considered in the analysis. The lateral force resisting system in this direction is noticed as the critical framing system as compared with the longitudinal

counterpart. It is considered that four framing systems are in the transverse direction of each building. Each framing system of above-mentioned structures consists of two external structural walls and an internal core wall, which are loaded with 25% of the total mass of the structure. The other vertical elements at the left and right edges are supposed to resist gravity loads only. Figure 36 describes the adopted modeling approach used to idealize the 40 and 50-story buildings in the transverse direction for inelastic analyses.

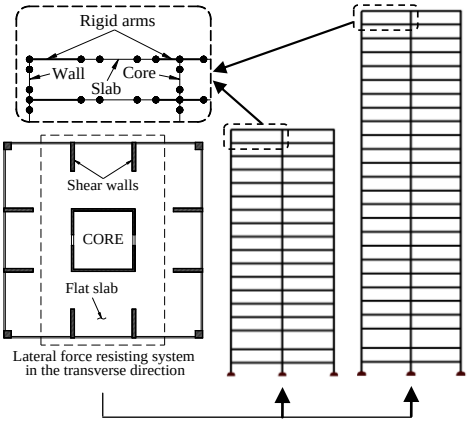

Figure 35. Modeling approach of the 18 and 26-story buildings

For the 56 and 66-story buildings, only the framing system in the transverse direction is considered in analysis since the lateral force resisting system in this direction is more critical as compared with the longitudinal counterpart. It is assumed that two framing systems are in the transverse direction of each building. Each framing system of above-mentioned structures consists of four external shear walls and two internal core walls, which are loaded with 50% of the total mass of the building. The other vertical elements at the left and right margins are considered to resist gravity loads only. Figure 37 describes the adopted modeling approach used to idealize the 56 and 66-story buildings in the transverse direction for inelastic analysis.

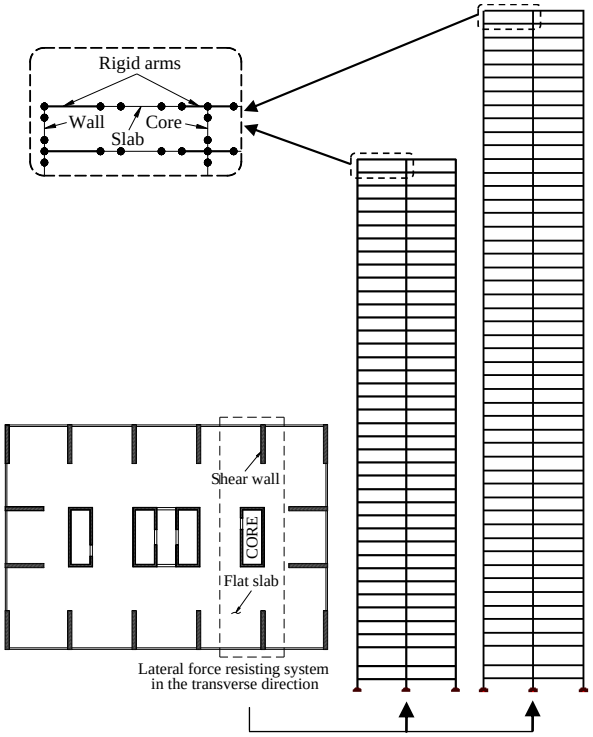

Figure 36. Modeling approach of the 40 and 50-story buildings

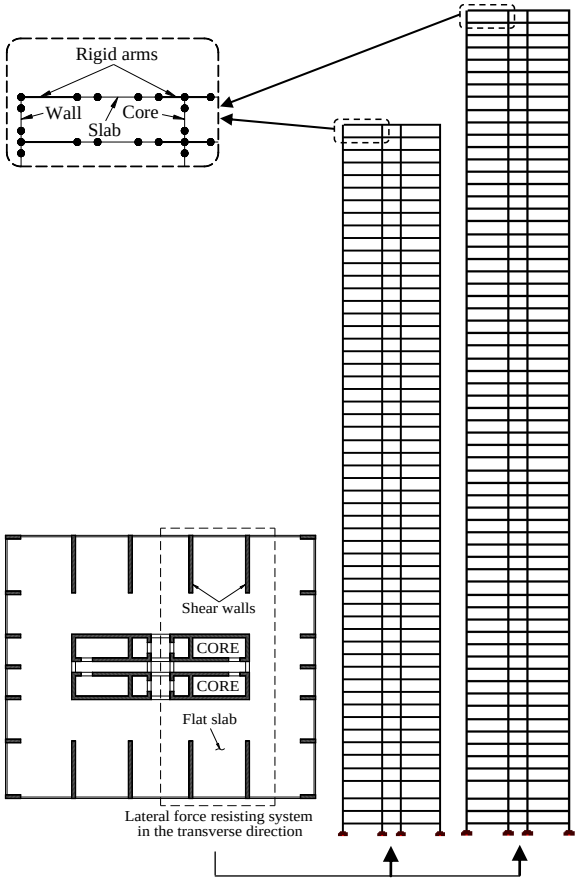

Figure 37. Modeling approach of the 56 and 66-story buildings

4.1.3 Analytical Modeling of Tube in Tube (TIT) Structures

Although the development of three-dimensional (3D) fiber-based models of the 80 and 100-story buildings is a challenging task, it is essential for such structures to accurately idealize the internal and external tubes and their seismic response. ZEUS-NL is therefore utilized to develop 3D fiber-based analytical models for the 80 and 100-story buildings, which represent the TIT system in the present study. The TIT system consists of an external tube (columns with beams) and internal tubes (core walls). Figure 38 describes the adopted modeling approach used to develop the 3D fiber-based models of the 80 and 100-story buildings for inelastic analysis. The 3D modeling procedure of the TIT system involves the following:

1- Develop of full 3D ETABS models (CSI, 2012a), as shown in Figure 38 (a). Shear walls, core walls and floor slabs are modeled using shell elements, while columns and beams are idealized using frame elements.

2- Develop of simplified 3D SAP2000 models (CSI, 2012c) as shown in Figure 38 (b). Shear walls, core walls and floor slabs are modeled using frame elements with equivalent cross-sections.

3- Verify the simplified 3D models by comparing their dynamic characteristics with the full 3D models. Figure 39 clearly confirms the correlation between the dynamic characteristics of the above-mentioned two modeling approaches.

4- Transfer the simplified 3D model to ZEUS-NL and model structural members using cubic elasto-plastic frame elements.

5- Verify the ZEUS-NL models by comparing their results with the full 3D ETABS models, as discussed in the following section.

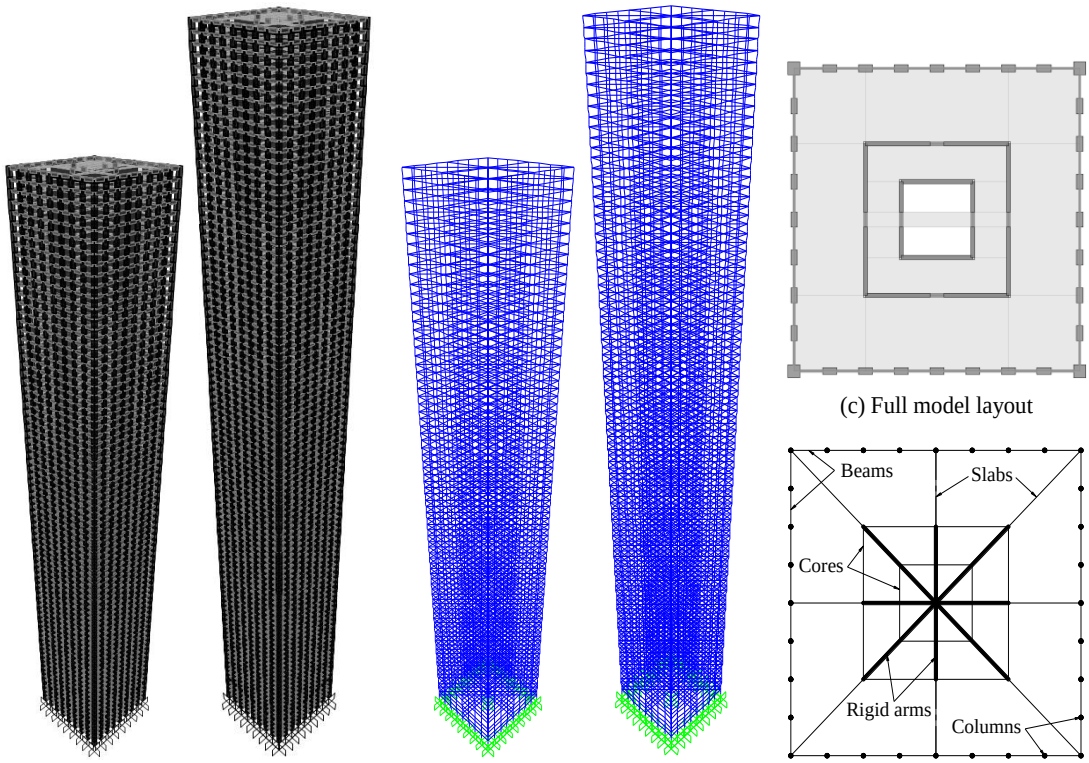

(a) Full 3D models (b) Simplified 3D models (c) Full model layout (d) Simplified model layout

Figure 38. Modeling approach used to develop the 3D fiber-based models of the 80 and 100-story buildings

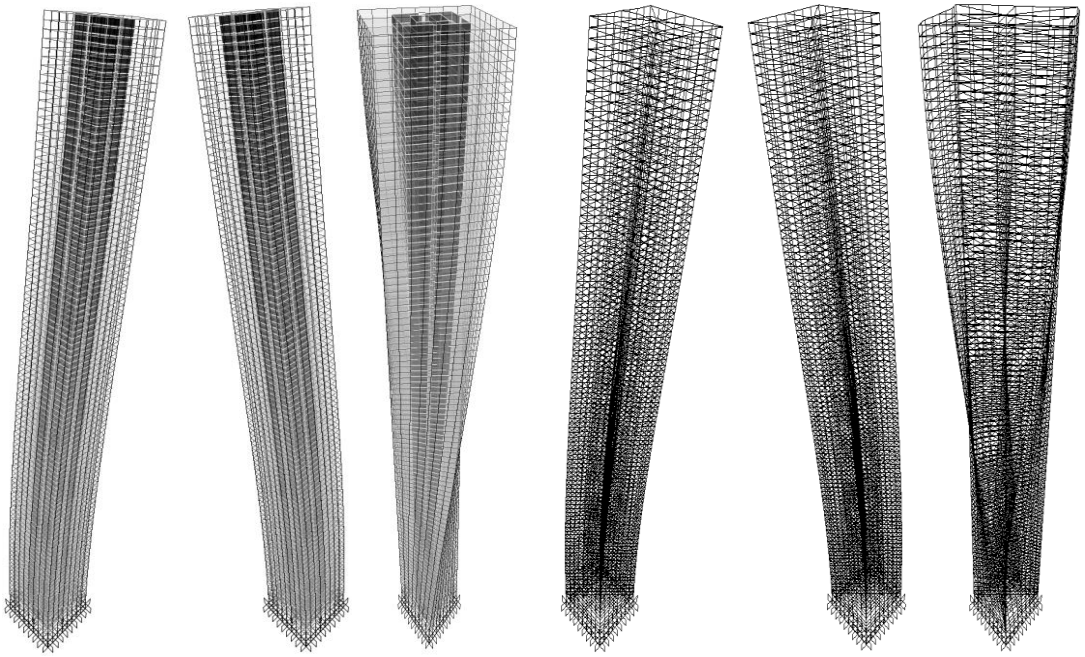

T1=8.98 sec. T2=8.94 sec. T3=3.03 sec. T1=8.87 sec. T2=8.87 sec. T3=2.43 sec.

(a) First three mode shapes of the full 3D model (b) First three mode shapes of the simplified 3D model

Figure 39. Comparison between the two modeling approaches used to verify the 3D model of the 100-story building

4.2 MODELING VERIFICATION

The developed models of the ten reference buildings are verified by comparing the dynamic characteristics obtained from the ETABS models used in the design with those from the fiber-based models developed for inelastic analyses. Table 27 summarizes the elastic periods obtained from the design and the fiber-based models, while Figure 40 depicts the comparison between the results of the two modeling approach.

The comparison shows that the elastic periods obtained from the design models are slightly longer than those obtained from the fiber-based models. This is attributable to the steel reinforcement considered in the fiber-based models unlike the design models in which the stiffness is based on the concrete cross-sections. Moreover, the actual material strength values considered in the fiber-based models increase stiffness and reduce periods. The results verify the fiber-based models developed for the ten reference buildings and lend weight to the results presented in subsequent sections.

Table 27. Elastic periods of vibration obtained from the design and the fiber-based models

Reference building	Elastic period (Sec.) – Fiber-based models			Elastic period (Sec.) – Design models		
	T1	T2	T3	T1	T2	T3
2-story	0.56	0.20	0.05	0.59	0.20	0
8-story	1.38	0.45	0.23	1.49	0.49	0.26
18-story	1.37	0.32	0.13	1.57	0.44	0.21
26-story	2.27	0.55	0.23	2.43	0.68	0.33
40-story	3.83	1.02	0.45	3.90	1.06	0.49
50-story	5.22	1.41	0.64	5.30	1.43	0.67
56-story	4.73	1.29	0.59	5.20	1.48	0.71
66-story	5.41	1.51	0.70	5.80	1.67	0.81
80-story	5.77	1.42	0.60	6.08	1.59	0.74
100-story	7.77	1.94	0.81	8.11	2.14	1.04

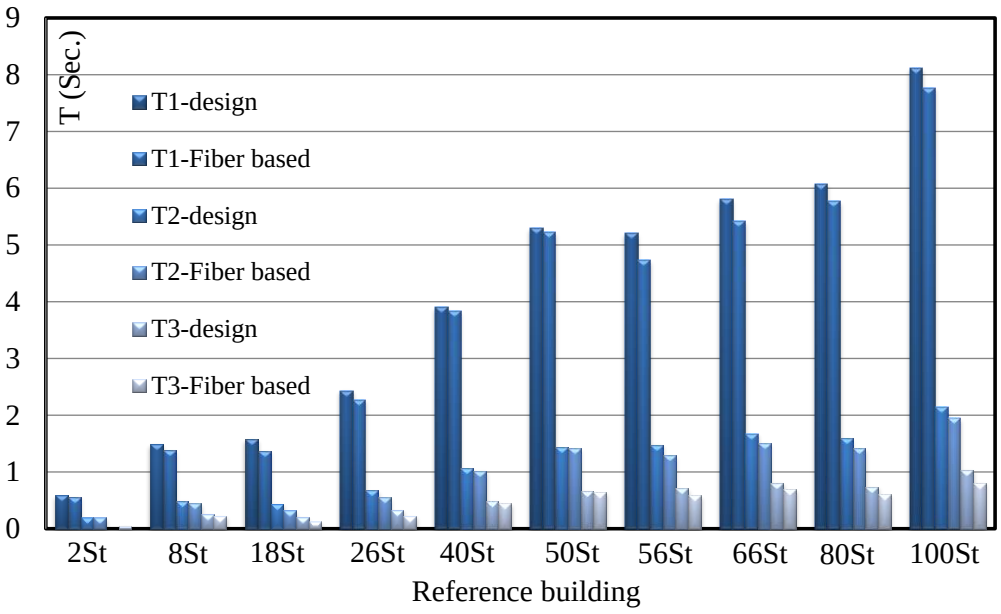

Figure 40. Comparison between the elastic periods obtained from the design and fiber-based models

4.3 SELECTION OF INPUT GROUND MOTIONS

Two sets of natural earthquake ground motions are selected for deriving the vulnerability relationships of the investigated reference structures. The selected natural input ground motions represent two seismic scenarios: (i) severe distant earthquake scenario, as shown in Table 28; and (ii) moderate close earthquake scenario, as shown in Table 29. These two seismic scenarios were proposed in previous studies covering the seismic hazard assessment of the study region (e.g. Aldama-Bustos et al., 2009; Mwafy et al., 2006).

Forty natural ground motions are selected from the pacific earthquake engineering research center (PEER) and the European strong-motion databases to represent the above-mentioned seismic scenarios (Ambraseys et al., 2004; PEER, 2013). Twenty of the selected natural records (R1–R20) represent severe far-field earthquakes, while the other twenty real records (R21–R40) represent moderate near-source events, as shown in Table 28 and Table 29, respectively.

The natural records are selected based on the following criteria: (i) Epicentral Distance: ranges from 91 to 161 km for severe distant earthquakes and from 2.86 to 29.9 km for moderate close events. (ii) Magnitude: ranges from 6.93 to 7.62 for severe distant earthquakes and from 5.14 to 6.04 for moderate close ground motions. (iii) Site Class: stiff soil ‘C’ and very dense soil ‘D’. (iv) Spectral Amplification: to match the design spectrum of the studied area (ASCE-7, 2010; DMA, 2013). Figure 41 shows the elastic response spectra of the selected twenty real input ground motions to represent the severe distant earthquake scenario, while Figure 42 shows the elastic response spectra of the selected twenty earthquake records to represent the moderate close seismic scenario.

The selected earthquake records are initially scaled to a design peak ground acceleration (PGA) of 0.16g before applying to the reference structures. This PGA was recommended in previous seismic hazard studies for the reference area (Mwafy et al., 2006). The number of input ground motions employed in the present study and their selection criteria ensure that the investigated buildings are assessed under diverse sets of input ground motions and potential seismic scenarios that represent the studied area.

Table 28. Characteristics of the selected twenty natural input ground motions to represent severe distant events

Ref	Earthquake	Station	Symbol	Comp.	Date	Mag. (M_w)	Site class	Ep. Dist. (km)	Duration (sec.)	PGA (m/s^2)	a/v g/ms^{-1}	a/v classification
R1	Bucharest	Building res. Institute	bu	EW	04-03-1977	7.53	stiff	161	18	1.73	0.60	
R2	Chi-Chi	CWB 99999 ILA013	ch	EW	20-09-1999	7.62	v. dense	135	117	1.36	0.52	
R3	Loma Prieta	Emeryville	ev	260	18-10-1989	6.93	v. dense	96.5	39	2.45	0.57	
R4	Loma Prieta	Golden Gate Bridge	ggb	270	18-10-1989	6.93	v. dense	100	38	2.29	0.61	
R5	Hector Mine	Indio - Coachella Canal	hmi	0	16-10-1999	7.13	stiff	99	60	0.90	0.70	
R6	Izmit	Ambarli-Termik	iza	EW	17-08-1999	7.64	stiff	113	150	1.80	0.60	
R7	Izmit	Istanbul-Zeytinburnu	izz	NS	17-08-1999	7.64	stiff	96	129.24	1.08	0.77	
R8	Kocaeli	Bursa Tofas	kob	E	17-08-1999	7.51	stiff	95	139	1.06	0.49	
R9	Kocaeli	Hava Alani	koh	90	17-08-1999	7.51	v. dense	102	106.615	0.92	0.46	
R10	Loma Prieta	Alameda Naval Air Stn Hanger	lpa	270	18-10-1989	6.93	stiff	91	29	2.39	0.73	low
R11	Loma Prieta	Berkeley LBL	lpb	90	18-10-1989	6.93	v. dense	98	39	1.15	0.65	
R12	Loma Prieta	Oakland-Outer Harbor Wharf	lpo	0	18-10-1989	6.93	stiff	94	40	2.75	0.67	
R13	Manjil	Abhar	maa	N57E	20-06-1990	7.42	stiff	91	29.49	1.30	0.62	
R14	Manjil	Tonekabun	mat	N132	20-06-1990	7.42	v. dense	131	40	1.22	0.76	
R15	Chi-Chi	TAP005	tap05	E	20-09-1999	7.62	stiff	156	134	1.34	0.49	
R16	Chi-Chi	TAP010	tap10	E	20-09-1999	7.62	stiff	151	144	1.19	0.50	
R17	Chi-Chi	TAP021	tap21	E	20-09-1999	7.62	stiff	151	125	1.15	0.47	
R18	Chi-Chi	TAP032	tap32	N	20-09-1999	7.62	v. dense	144	90	1.13	0.64	
R19	Chi-Chi	TAP090	tap90	E	20-09-1999	7.62	stiff	156	125	1.28	0.41	
R20	Chi-Chi	TAP095	tap95	N	20-09-1999	7.62	stiff	158	123	0.96	0.52	

a/v: PGA/PGV, a/v classification (<0.8 Low & >1.2 high), shear wave velocity (Vs_{30}) of very dense soil = 360-760 m/s, and for stiff soil = 180-360 m/s

Table 29. Characteristics of the selected twenty natural input ground motions to represent moderate close events

Ref	Earthquake	Station	Symbol	Comp.	Date	Mag. (Mw)	Site class	Ep. Dist. (km)	Duration (sec.)	PGA (m/s^2)	a/v g/ms^{-1}	a/v classification
R21	Coyote Lake	San Juan Bautista, 24 polk St	cl	213	06-08-1979	5.74	v. dense	19.7	26	0.991	1.424	
R22	Livermore-02	Livermore-Morgan Terr Park	liv	355	27-01-1980	5.42	v. dense	14.1	15	2.235	2.581	
R23	Hollister-04	City Hall	hol	271	28-11-1974	5.14	v. dense	9.8	20	1.651	1.480	
R24	Whittier Narrows-01	Brea Dam (L Abut)	wn589	130	01-10-1987	5.99	v. dense	24.0	20	1.299	1.460	
R25	Whittier Narrows-01	LA-Centry City CC North	wn601	90	01-10-1987	5.99	stiff	29.9	30	0.851	1.788	
R26	Whittier Narrows-01	LB-Orange Ave	wn619	228	01-10-1987	5.99	stiff	24.5	21	2.111	1.468	
R27	Northridge-06	Panorama City-Roscoe	nor	90	20-03-1994	5.28	stiff	11.8	7.2	1.141	1.916	
R28	Montenegro	Petrovac-Hotel Oliva	mon	Y	15-04-1979	5.80	v. dense	24.0	28	0.873	1.426	
R29	Umbria Ma.	Castelnuovo-Assisi	um	NE	26-09-1997	6.04	v. dense	22.0	45	1.600	1.254	
R30	Lazio Abr. Y	Cassino-Sant Elia	la	EW	05-07-1984	5.93	v. dense	16.0	30	1.123	1.590	high
R31	Mammoth Lakes-02	Mammoth Lakes H. S.	ml2	344	25-05-1980	5.69	v. dense	3.49	12	4.064	1.957	
R32	Mammoth Lakes-06	Fish & Game (FIS)	ml6	0	27-05-1980	5.94	stiff	12.02	11	3.979	2.753	
R33	Coalinga-04	Anticline Ridge Free-Field	co394	270	09-07-1983	5.18	v. dense	6.34	15	3.220	2.048	
R34	Coalinga-04	Anticline Ridge Pad	co395	270	09-07-1983	5.18	v. dense	6.34	14	3.246	2.350	
R35	Coalinga-05	Burnett Construction	co405	360	22-07-1983	5.77	stiff	12.38	21	2.915	1.988	
R36	Whittier Narrows-01	Alhambra - Fremont School	wn626	180	01-10-1987	5.99	v. dense	6.77	26	3.806	1.514	
R37	Whittier Narrows-01	Garvey Res. - Control Bldg	wn629	60	01-10-1987	5.99	v. dense	2.86	38	3.775	2.432	
R38	Whittier Narrows-01	LA - 116th St School	wn639	360	01-10-1987	5.99	stiff	21.26	25	3.343	1.888	
R39	Whittier Narrows-01	LA - Obregon Park	wn645	360	01-10-1987	5.99	stiff	9.05	30	4.161	1.748	
R40	Friuli	Breginj-Fabrika IGLI	fri	Y	15-09-1976	6.00	v. dense	21.0	9.9	4.956	2.333	

a/v: PGA/PGV, a/v classification (<0.8 Low & >1.2 high), shear wave velocity (Vs_{30}) of very dense soil = 360-760 m/s, and for stiff soil = 180-360 m/s

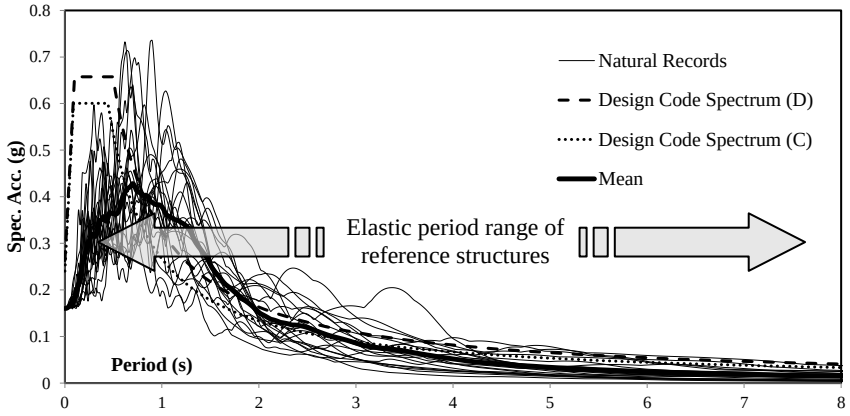

Figure 41. Response spectra of the twenty natural input ground motions that represent the severe distant earthquake scenario along with the mean spectrum and the design code spectra for site classes "C" and "D"

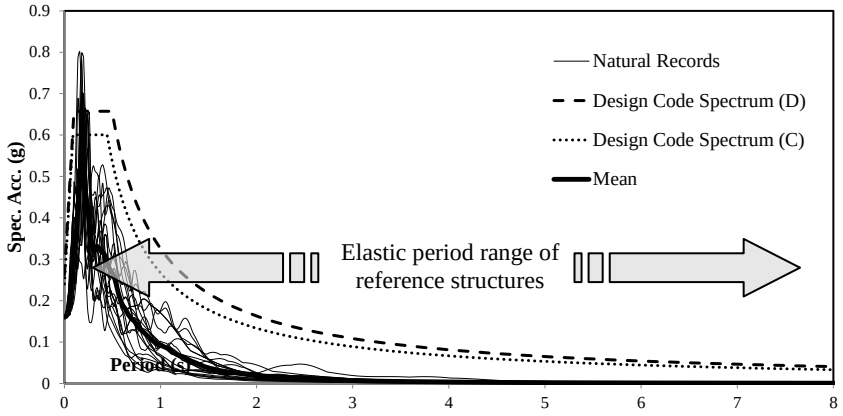

Figure 42. Response spectra of the twenty natural input ground motions that represent the moderate close earthquake scenario along with the mean spectrum and the design code spectra for site classes "C" and "D"

4.4 CONCLUDING REMARKS

Detailed fiber-based analytical models were developed for the ten reference buildings using the inelastic analysis platform ZEUS-NL. All models were effectively idealized to enable monitoring the stresses and strains during the inelastic dynamic simulations. The adopted modeling approaches of different structural systems were discussed in detail in this chapter. For the 2 and 8-story buildings, which represent the FSC structural system, a 3D idealization was adopted. For the 18, 26, 40, 50, 56 and 66-story buildings, which represent the SW system, a 2D

idealization was adopted due to the symmetry of the buildings layouts and the negligible torsional effect. The latter modeling approach enabled reducing the number of elements and the analysis time significantly. Finally, a 3D idealization was adopted for the 80 and 100-story buildings, which represent the TIT system, to accurately idealize the internal and the external tubes and their intricate seismic response.

Earthquake ground motions for the vulnerability assessment of the diverse set of reference buildings were selected based on previous seismic hazard studies. The uncertainty in seismic demands due to the variability in input ground motions was effectively accounted for using forty earthquake records representing two seismic scenarios. These two seismic scenarios were proposed in a number of previous studies covering the seismic hazard assessment of the study area.

The earthquake records were selected from strong motion databases based on their epicentral distance, magnitude, site class and spectral amplification to match the design spectrum of the studied area. Twenty of the selected natural records represented the severe distant earthquake scenario, while the remaining twenty natural records represented the moderate close earthquake scenario. The selected earthquake records were initially scaled to the design intensity before applying to the reference structures. The adopted detailed approaches for modeling the reference structures and for selecting input ground motions ensure that the investigated wide range of buildings are assessed using reliable numerical models under possible seismic scenarios representing the study area.

CHAPTER 5: PERFORMANCE CRITERIA

5.1 INTRODUCTION

The selection of limit states plays a very important role in the derivation of vulnerability functions. Due to the diversity of the reference structural systems and the importance of limit states in vulnerability assessment, a large number of IPAs and IDAs are conducted and their results have been utilized to select suitable performance criteria for the present study. Additionally, a comprehensive literature review of previous studies is undertaken to properly select the limit states. The performance criteria adopted in the present study are also verified with the values adopted by the seismic provisions in order to arrive at reliable fragility curves for the ten reference structures, as described in detail in subsequent sections.

5.2 INELASTIC PUSHOVER ANALYSIS

5.2.1 Pushover Analysis Procedure

The inelastic pushover analysis procedure is used to estimate the lateral capacity of a structure in the inelastic domain. This analysis procedure significantly reduces time and effort as compared with time history and incremental dynamic analyses, which require the use of a wide range of input ground motions. The static pushover analysis method has been developed and verified through several previous studies (e.g. Antoniou and Pinho, 2004; Bracci et al., 1997; Chopra and Goel, 2002; Fajfar and Gaspersic, 1996; Gupta and Kunnath, 2000; Krawinkler and Seneviratna, 1998; Mwafy and Elnashai, 2001; Saiidi and Sozen, 1981).

The IPA of a structure is a static non-linear analysis with incrementally increasing lateral loads under permanent vertical loads. The lateral load pattern, which is distributed along the building height, is proportionally increased until a certain limit state or a target displacement of the structure is reached. This analysis procedure allows for monitoring the sequence of yielding and failure as well as tracing the lateral capacity progress of the structure.

Based on the recommendations of the modern design codes (e.g. ASCE-41, 2007), two lateral load patterns are used in the current study. The first load pattern is an inverted triangular lateral load distribution (PT), matching the fundamental mode shape. The second load pattern is a uniform lateral load distribution (PU), resembling lateral forces that are proportional with mass. Based on the recommendations of previous studies (e.g. Mwafy et al., 2006; Mwafy and Elnashai, 2001), the PT load pattern is used with the low-rise structures, namely the 2 and 8-story buildings, since they are governed by the first mode of vibration. The PU load pattern is used with the other structures (18 to 100-story buildings) due to the significant contribution of higher modes to the seismic performance of high-rise buildings. The inelastic pushover analysis procedure is used in the present study to monitor the local and global yielding as well as to estimate the lateral capacity, interstory drift ratios (IDRs), and overstrength factors of the reference buildings.

5.2.2 Estimation of Lateral Capacity

Pushover analysis is conducted to determine the lateral capacity of the reference structures and to monitor the local and global yielding. The predefined lateral loads discussed above are applied along the height of reference building and

then incrementally increased up to the expected collapse limit state or until a significant local damage is detected. Figure 43 to Figure 45 illustrate the progress of the lateral capacity curves for the FSC, SW and TIT structural systems, respectively. The first indication of yielding in vertical and horizontal members, global yielding, ultimate strength, and the corresponding IDRs are shown in Figure 43 to Figure 45.

The global yielding is estimated from an elastic-perfectly plastic idealization of the capacity curves, where the initial stiffness is considered as the secant stiffness at 75% of the ultimate strength (Park, 1988). The starting point of the post-elastic branch is considered as the global yielding threshold (e.g. Elnashai and Mwafy, 2002; Park, 1988). Figure 46 shows the distribution of the IDRs for the reference buildings in the transverse direction. The IDR distributions provide insights in the potential deficiencies in strength or stiffness. The response of the reference buildings at the yield and collapse limit states is the main focus of the present study. For the FSC system, the first indication of local yielding is shifted from columns to horizontal members with increasing the building height, as shown in Figure 43. The first yielding in the 2-story building is detected in the external columns, which are weaker in the transverse direction. The strong marginal beams used in the FSC system postponed the yielding of horizontal members, as shown in Figure 43.

For the SW system, the first indication of the local yielding is also shifted from shear walls to horizontal members with increasing the building height, as shown in Figure 44. This is mainly due to the reduced lateral stiffness with increasing building height. For instance, the initial lateral stiffness of the 18-story building is 170 MN/m, while it is 80 MN/m for the 66-story. The higher stiffness of the shorter shear walls attracts higher lateral loads, and hence yielding is observed

earlier. For the TIT system, which consists of very rigid internal cores and external columns with beams forming the external tube, the first indication of the local yielding is noticed in the external tube, while the yielding of internal cores is observed at a later stage of lateral load, as shown in Figure 45.

The ultimate capacity of the reference structures is estimated and mapped with IDRs, as shown in Figure 43 to Figure 45. It is observed that the IDRs at ultimate strength increases with increasing the building height of different structural systems, as shown in Figure 43 to Figure 46. It is also noteworthy that shifting the first indication of yielding from the vertical members to the horizontal members and to be at a higher base shear, as shown in Figure 43 to Figure 45, is indeed more favorable and follows the strong-column weak-beam concept recommended by modern design codes.

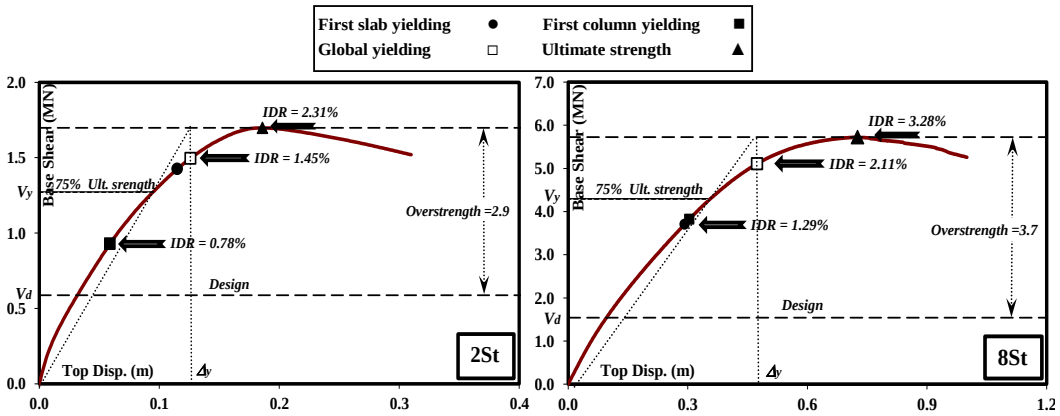

Figure 43. Mapping of the lateral capacity curves with local response for the FSC structures in the transverse direction

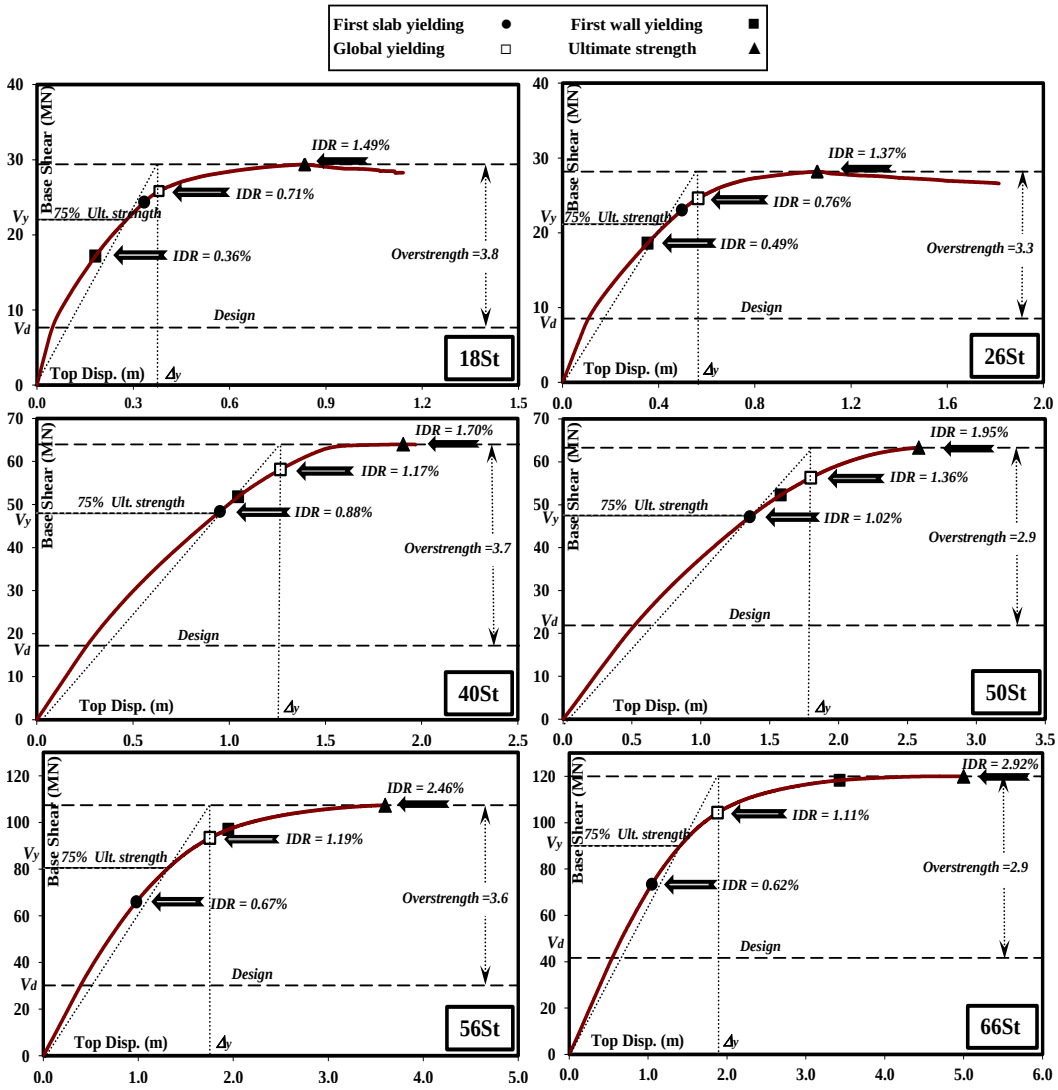

Figure 44. Mapping of the lateral capacity curves with local response for the SW structures in the transverse direction

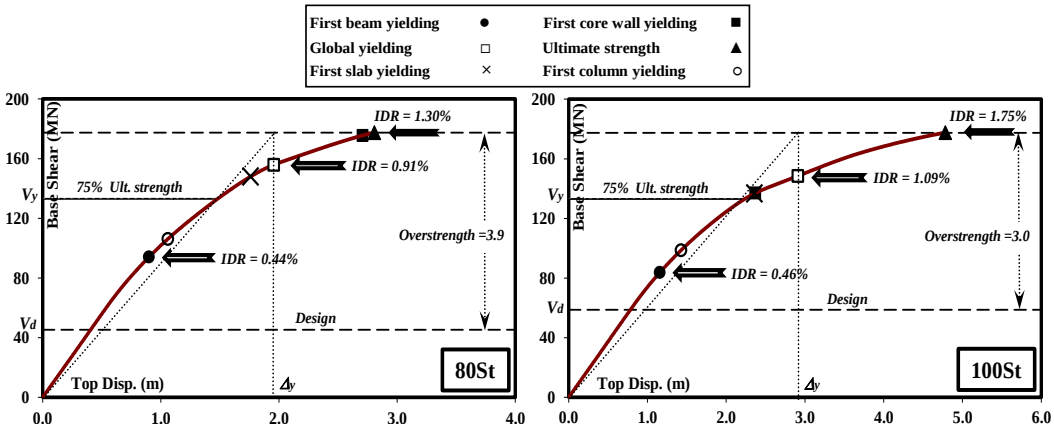

Figure 45. Mapping of the lateral capacity curves with local response for the TIT structures in the transverse direction

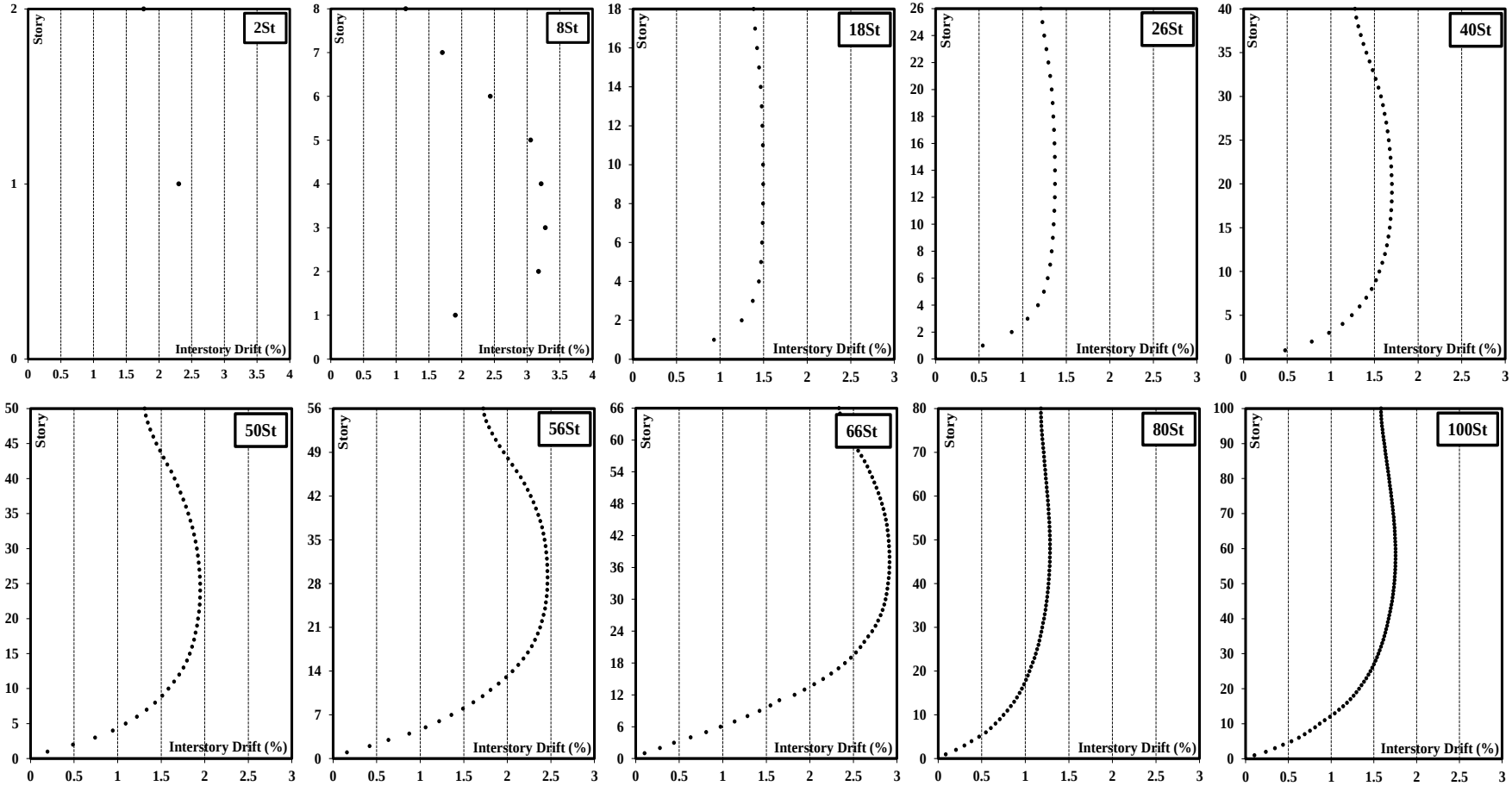

Figure 46. Distributions of interstory drift ratios at ultimate strength for the ten reference buildings in the transverse direction

5.3 TIME HISTORY ANALYSIS

This analysis procedure is conducted in the present study since the inelastic static pushover analysis has a number of limitations, particularly for structures influenced by higher modes. The later analysis cannot thus predict the actual seismic performance of structures with a high degree of precision. Two sets of natural ground motions are carefully selected to represent the study area, as discussed in Chapter 4. Forty real earthquakes are employed to evaluate the expected inelastic seismic performance of the ten reference structures.

The THA results are presented in terms of base shear and top displacement histories as well as the distributions of IDRs along the building height. Figure 47 shows the base shear time histories of the 2-story building at twice the design earthquake intensity (0.32g) under the 20 natural ground motions that represent the severe distant earthquake scenario. The top displacement histories of the 2-story building are shown in Figure 48 for the 20 long period ground motions at twice the design earthquake intensity (0.32g). Although the presented results are for earthquake records that represent the same seismic scenario, the response histories clearly show the high variability of seismic demands under the effect of different input ground motions. This confirms the importance of selecting a wide range of input ground motions in vulnerability assessment. The base shear and top displacement time histories for the other reference structures are presented in Appendix A. Figure 49 to Figure 51 depicts the IDR distributions of the FSC, TIT and SW buildings, respectively, at the twice the design earthquake intensity (0.32g).

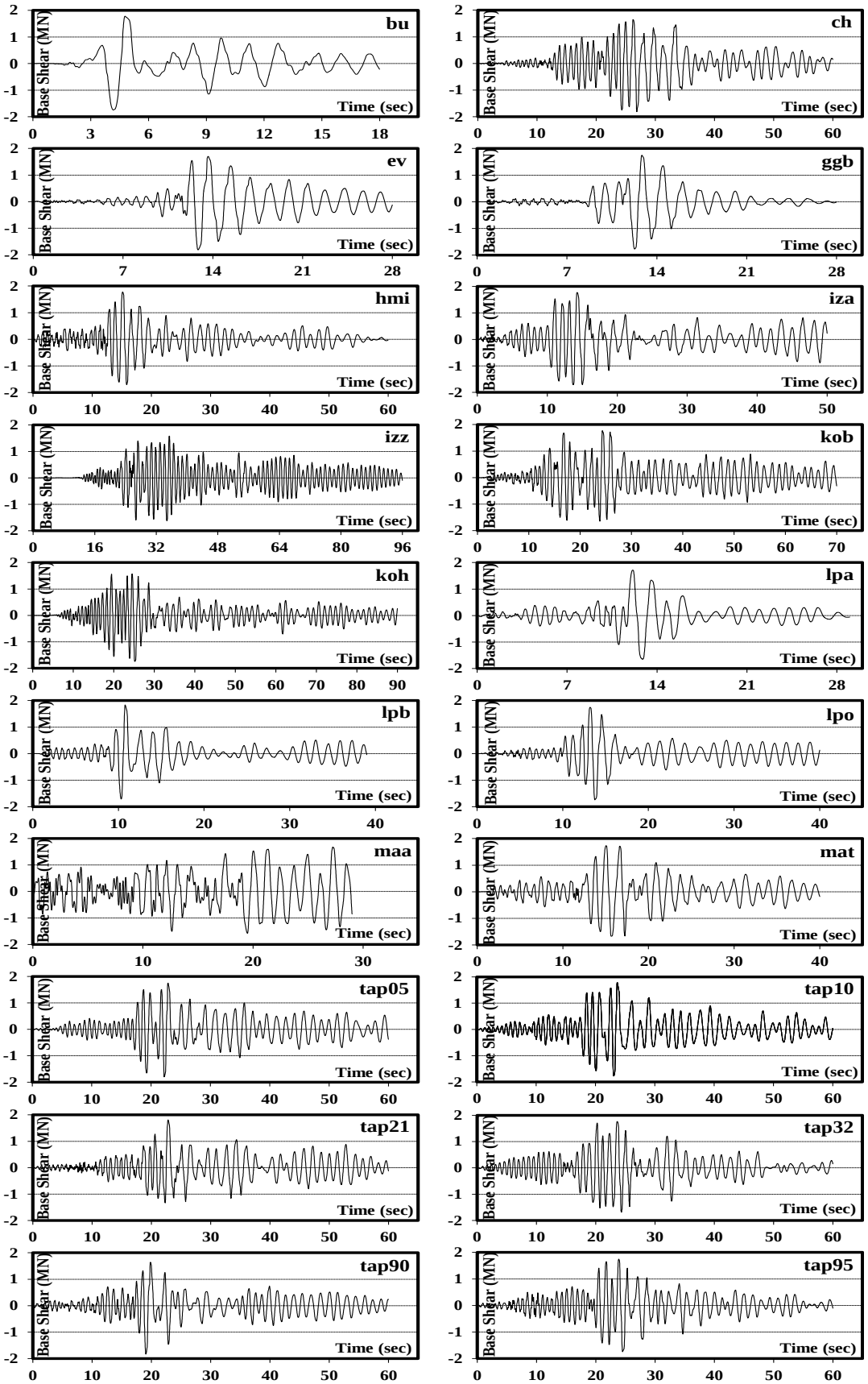

Figure 47. Sample base shear time histories of the 2-story building at twice the design intensity (0.32g) under severe distant earthquakes

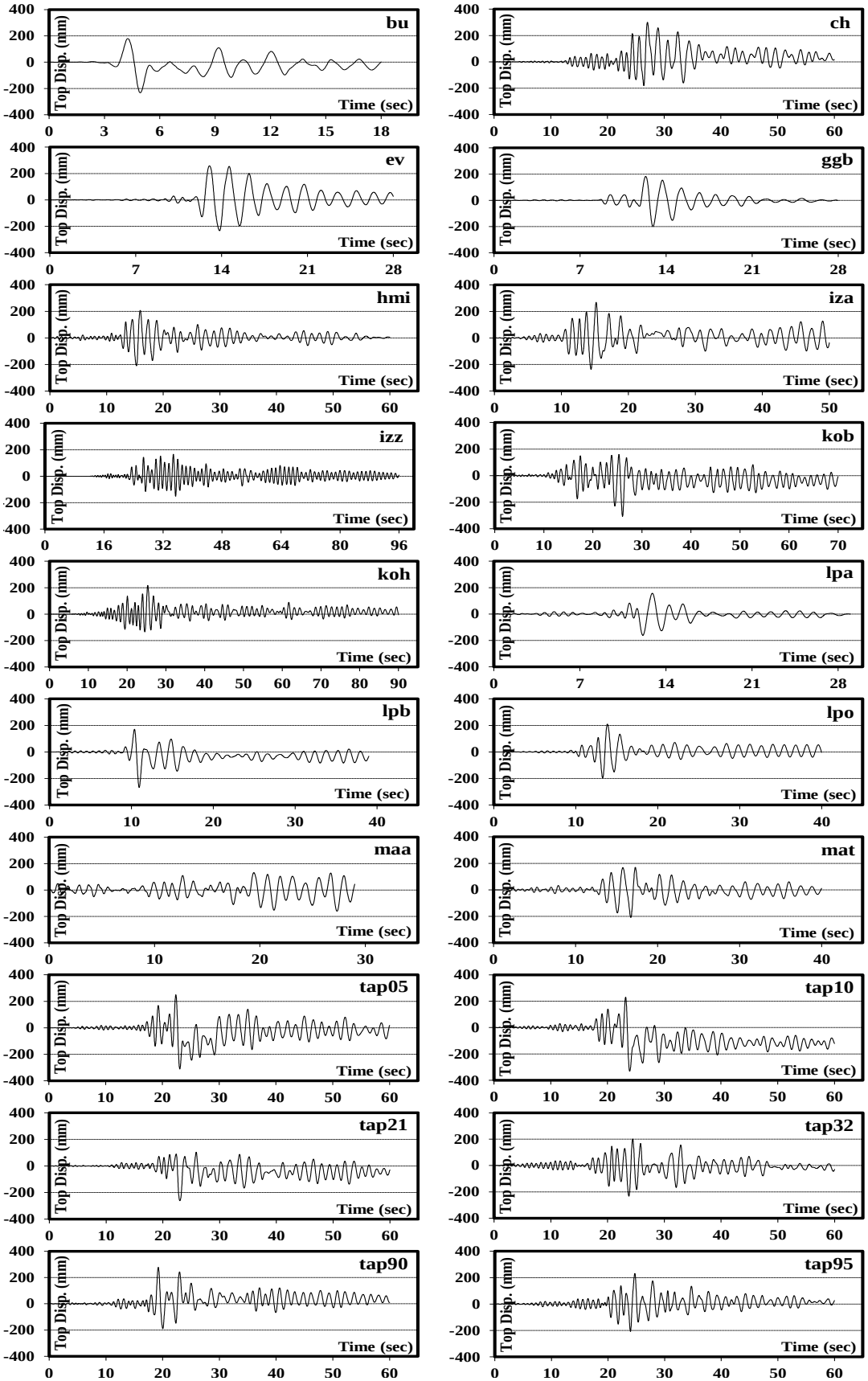

Figure 48. Sample top displacement time histories of the 2-story building at twice the design intensity (0.32g) under severe distant earthquakes

The THA results are utilized to confirm the immediate occupancy limit state for different structural systems, as explained hereafter. A large number of THAs applied incrementally to the reference structures up to collapse (i.e. incremental dynamic analyses, IDAs) are also conducted to estimate the limit states of different structural systems, as discussed in subsequent sections.

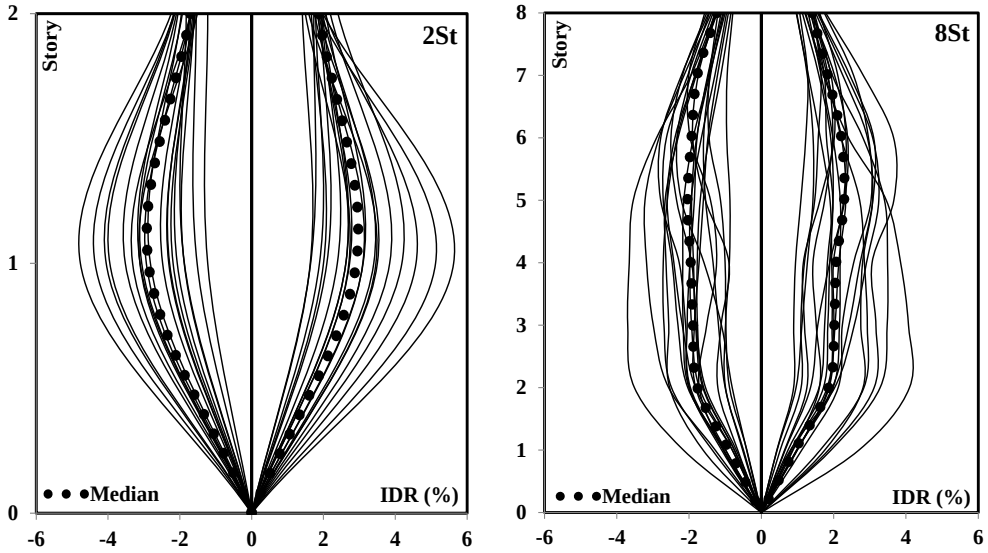

Figure 49. Sample of IDR distributions for the FSC structures at twice the design intensity under severe distant earthquakes

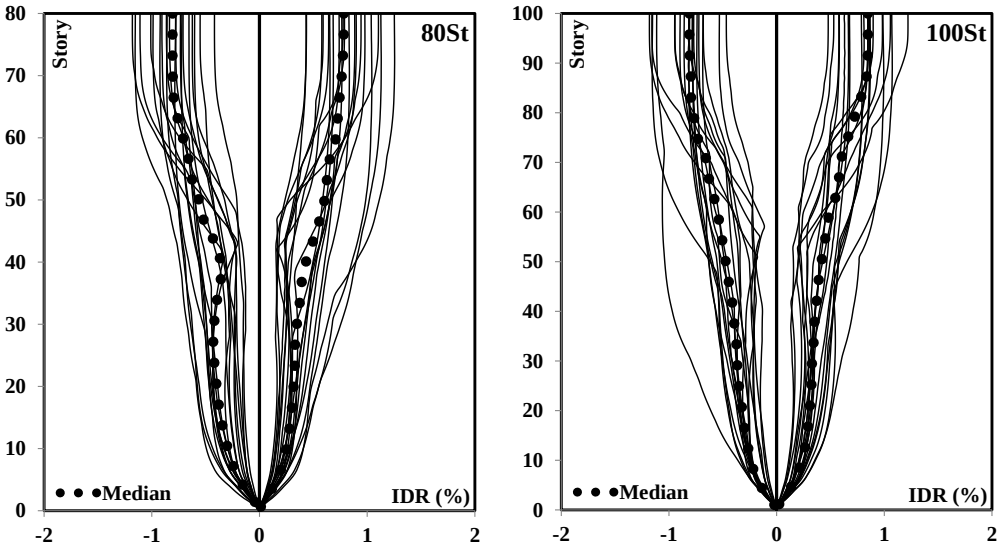

Figure 50. Sample of IDR distributions for the TIT structures at twice the design intensity under severe distant earthquakes

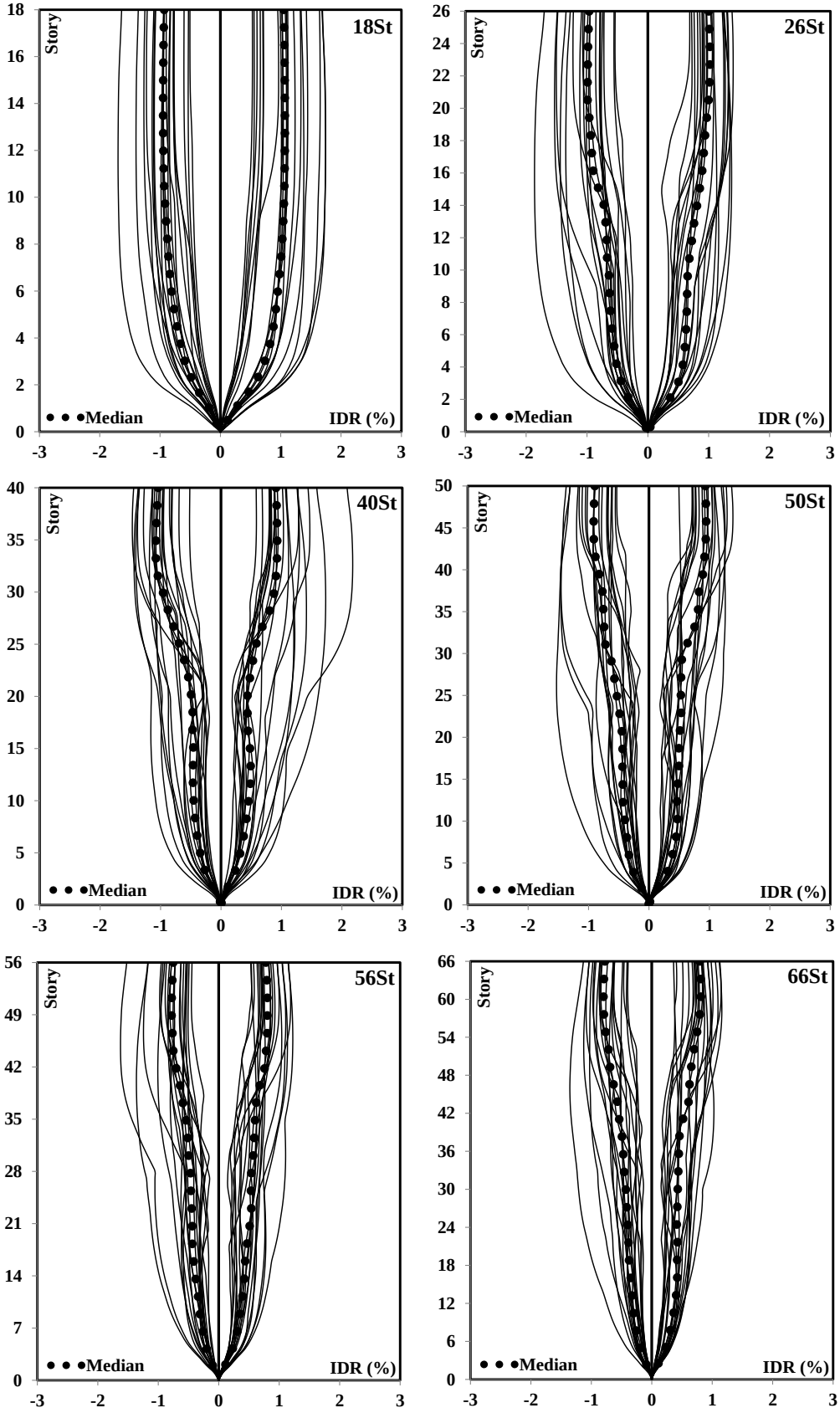

Figure 51. Sample of IDR distributions for the SW structures at twice the design intensity under severe distant earthquakes

5.4 INCREMENTAL DYNAMIC ANALYSIS

This analysis procedure is used to assess the inelastic seismic response of a structure under seismic loads with increasing severity. It was developed within the framework of the probabilistic seismic risk analysis in order to estimate the physical damage of a given structure (Vamvatsikos and Cornell, 2002). This analysis involves conducting multiple non-linear inelastic time history analyses for a structural model under a suite of selected ground motions; each is scaled to several levels of seismic intensity (Mwafy et al., 2014; Mwafy and Elnashai, 2001).

5.4.1 Scaling Approach

The input ground motions employed in the present work are scaled based on their PGAs so that the seismic forces are directly related to the input accelerations. This scaling approach is in line with the design codes, and thus it has been used in several previous studies (e.g. Ji et al., 2007a; Kwon and Elnashai, 2006; Mwafy, 2012a). The scaling levels are selected to force the structure throughout the entire range of behavior, from the elastic to the inelastic range and finally to collapse.

To derive a wide range of vulnerability functions using IDA for seismic risk analysis, the analytical models of the ten reference structures are combined with the two seismic scenarios selected to suite the study area, as discussed before. Each input ground motion is incrementally scaled to different intensity levels so that the structural behavior at all performance levels discussed hereafter can be monitored and assessed. Different scaling factors are utilized in IDA for each earthquake scenario to effectively utilize the computational power and enhance the resolution of the fragility curves. A scaling factor of 0.08g, which corresponds to half the design

earthquake intensity considered in the present study, is selected for the severe distant earthquake scenario. Fourteen analyses are performed for each input ground motion-building combination, starting from a PGA of 0.08g to 1.12g, or up to the satisfaction of the collapse limit state.

The above-mentioned scaling procedure is very tight for the moderate near-source earthquakes since high PGAs are required to reach the collapse performance criterion, especially for long period buildings. Therefore, a PGA of 0.32g is adopted for scaling the moderate near-source records for the 2 to 26-story buildings. Fourteen analyses are carried out for each input ground motion-building combination, beginning from a PGA of 0.32g to 4.48g, or up to collapse. For the 40 to 100-story buildings, a PGA of 0.64g, which corresponds to four times the design ground motion, is selected for scaling the moderate close earthquake scenario. Fourteen analyses are carried out for each ground motion-building combination, starting from a PGA of 0.96g to 9.28g or up to the satisfaction of the collapse performance level.

5.4.2 Incremental Dynamic Analysis Results

The global response parameters of the ten reference structures, namely base shear, top displacement and IDR, are obtained from more than 5000 inelastic THAs. The most important IDA results are presented in terms of an IDA curve for each record-building combination. Additional results are obtained from IDA such as maximum base shear, top displacement and IDR at each intensity level. In order to accurately estimate and confirm the selected immediate occupancy (IO) and collapse prevention (CP) limit states, IDA curves (in terms of max IDR and spectral

acceleration, S_a) are developed in the present study for different structural systems, as illustrated in Figure 52 to Figure 54.

The IDA curves shown in Figure 52 to Figure 54 are developed based on the twenty natural ground motions representing the severe distant earthquakes since this scenario is more significant than the moderate close earthquake scenario (e.g. Mwafy, 2012a; Mwafy et al., 2006). The IO limit state is estimated at the first indication of yielding which is considered at the first notable deviation in the initial slope of the IDA curve. The CP limit state is estimated at the last point on the IDA curve with a tangent slope equal to 20% of the elastic slope or at a very high IDR of 10% (Vamvatsikos and Cornell, 2002).

It is noted that the points representing the first indication of yielding are typically close to each other, unlike the points representing collapse, which spread in a wide range, as shown in Figure 52 to Figure 54. The presented results in Figure 52 to Figure 54 reflect the higher uncertainty in estimating the CP limit state compared with the IO counterpart.

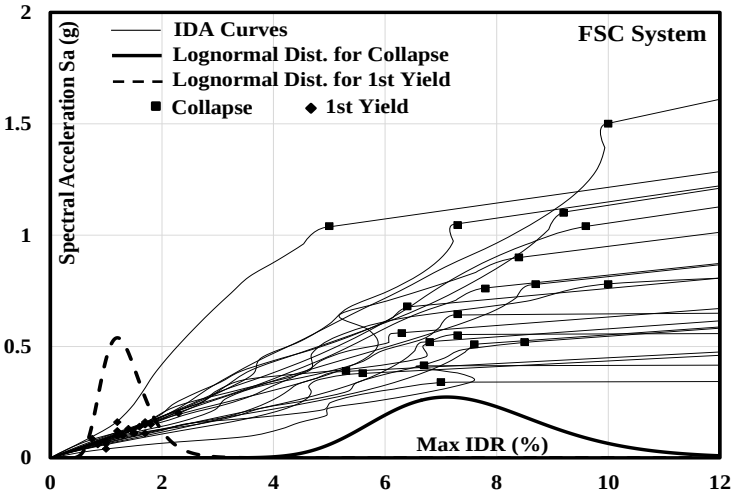

Figure 52. IDA curves used to estimate the IO and CP limit states for the FSC structural system using 20 severe distant earthquake records

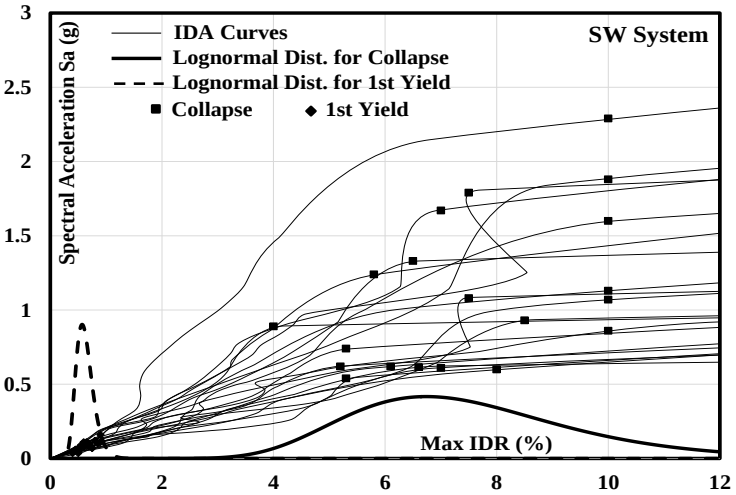

Figure 53. IDA curves used to estimate the IO and CP limit states for the SW structural system using 20 severe distant earthquake records

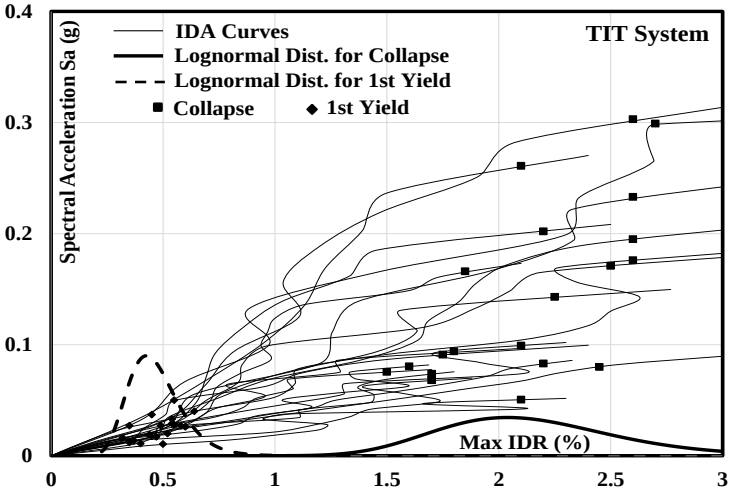

Figure 54. IDA curves used to estimate the IO and CP limit states for the TIT structural system using 20 severe distant earthquake records

5.5 SELECTION OF LIMIT STATES

Following ASCE 41 (2007), three limit states are adopted in the present study for the derivation of vulnerability relationships, namely immediate occupancy (IO), life safety (LS), and collapse prevention (CP). These are related to minor yielding, extensive damage with a significant margin against collapse, and extensive concrete crushing and buckling of reinforcing steel, respectively. The interstory drift is considered in the present study as the primary performance criterion to represent the damage of the reference buildings since it can be easily related to local and global response (ASCE-41, 2007). Table 30 summarizes the IDR corresponding to different limit states for the three structural systems along with the values recommended by code provisions and previous experimental and analytical studies. Based on the IDA results, IDRs of 1.0%, 0.5% and 0.4% are adopted for the IO limit state of the FSC, SW and TIT systems, respectively. These conservative limit states are consistent with/slightly lower than ASCE 41 (2007) as well as IPA and THA results, as shown in Table 30. For the TIT system, the IDA results are slightly lower than ASCE 41 (2007) due to the very rigid internal core walls of this system.

As a result of the significantly high limit states obtained from the IDAs at the CP limit state, a conservative IDR of 4.0% is adopted for the FSC system based on the study of Dymiotis et al. (1999), as shown in Table 30. The latter CP limit state is also consistent with ASCE 41 (2007). Similarly, based on the recent experimental study of Lehman et al. (2013), IDR of 2.27% is adopted for the CP limit state of the SW system. This CP threshold is slightly higher than the ASCE 41 (2007). Due to the scarcity of previous studies covering the response of the TIT system, IDR of 1.8% is adopted for the CP limit state based on IDA results. The latter CP limit state

for the TIT system is slightly lower than ASCE 41 (2007). The TIT system is a combination of external columns and beams forming an external tube as well as very rigid internal core walls. Observing the yield and collapse performance indicators earlier in the tube buildings compared with other systems supports adopting conservative limit states for this system. Finally, the LS performance criterion, which falls between the IO and CP limit states, represents a significant damage sustained by the structure with an acceptable margin of safety against failure. This margin is considered 50% of the CP limit state in ASCE 41 (2007), and hence is adopted in the present study.

Table 30. Summary of IDR corresponding to different limit states for the three reference structural systems along with the values recommended by code provisions and previous experimental and analytical studies

Selection Approach		Structural System								
		FSC System			SW System			TIT System		
		Limit State - Interstory Drift (%)								
		IO	LS*	CP	IO	LS*	CP	IO	LS*	CP
(ASCE-41, 2007)		1.00	2.00	4.00	0.50	1.00	2.00	0.50	1.00	2.00
Previous studies	(Dymiotis et al., 1999) - before Failure	…	…	**4.00**	…	…	…	…	…	…
	(Dymiotis et al., 1999) - at Failure	…	…	6.60	…	…	…	…	…	…
	(Haselton et al., 2010) - 16 percentile	…	…	5.90	…	…	…	…	…	…
	(Haselton et al., 2010) - 50 percentile	…	…	7.20	…	…	…	…	…	…
	(Haselton et al., 2010) - 84 percentile	…	…	8.90	…	…	…	…	…	…
	(Ghobarah, 2004)	0.40	1.80	3.00	0.40	1.50	2.50	…	…	…
	(Beyer et al., 2008)	…	…	…	0.30	…	2.39	…	…	…
	(Panagiotou et al., 2010)	…	…	…	0.35	0.89	2.36	…	…	…
	(Lehman et al., 2013)	…	…	…	0.50	1.00	**2.27**	…	…	…
Current study	IPA	1.30	…	…	0.50	…	…	0.50	…	…
	THA - 16 percentile	1.40	…	…	0.60	…	…	0.40	…	…
	THA - 50 percentile	1.60	…	…	0.70	…	…	0.50	…	…
	THA - 84 percentile	1.80	…	…	0.80	…	…	0.70	…	…
	IDA - 16 percentile	**1.00**	…	6.00	**0.50**	…	5.50	**0.40**	…	**1.80**
	IDA - 50 percentile	1.30	…	7.40	0.60	…	7.30	0.50	…	2.10
	IDA - 84 percentile	1.80	…	9.10	0.80	…	9.50	0.60	…	2.50
Selected Limit State		**1.00**	**2.00**	**4.00**	**0.50**	**1.135**	**2.27**	**0.40**	**0.90**	**1.80**

IO: Immediate Occupancy; LS: Life Safety; CP: Collapse Prevention.

IPA: Inelastic Pushover Analysis at first indication of yield; THA: Time History Analysis at first indication of yield; IDA: Incremental Dynamic Analysis at first indication of yield and at collapse (Vamvatsikos and Cornell, 2002).

*: LS limit state is considered 50% of the CP counterpart.

The selection of limit states for different structural systems based on the comprehensive IPAs, THAs and IDAs results as well as previous experimental and

analytical studies and code-recommended values lend weight to the performance criteria of the current study. It is worth noting that the shear failure is not considered as a failure criterion for the limit state selection. High base shear is observed from the short period records, which may have impact on the limit states. More research is needed to investigate the impact of shear response on limit states, particularly under the effect of moderate near-source earthquakes.

5.6 CONCLUDING REMARKS

A large number of IPAs, THAs and IDAs were performed as well as a literature review of previous studies was conducted to select realistic performance criteria and to verify the selected values with the code provisions. The seismic response of the ten reference structures at different limit states was monitored. The IPA results were used to trace the local and global yielding and to estimate the lateral capacity and IDR distributions of the reference buildings. The IPA results were utilized to verify the IO limit state for different structural systems.

The THA was performed using forty natural ground motions. The results were presented in terms of base shear and top displacement histories as well as the distributions of IDRs along the building height. These results were employed to confirm the IO limit state for different structural systems. The IDA was conducted to accurately assess the inelastic behavior of the reference structures under seismic loads with increasing severity. The selected ground motions were scaled to different intensity levels to monitor the structural behavior at different limit states. The response parameters of the reference structures were obtained from more than 5,000 inelastic analyses.

The IDA curves (in terms of max IDR and spectral acceleration S_a) were developed. The IO limit state was estimated at the first notable deviation in the initial slope of the IDA curve, while the CP limit state was estimated at a tangent slope equal to 20% of the elastic slope. It was noted that the points representing the first indication of yielding were close to each other, unlike the collapse points, which spread in a wide range. This reflected the higher uncertainty in estimating the CP limit state compared with the IO counterpart.

Three limit states were adopted for the derivation of vulnerability relationships, namely IO, LS, and CP. The interstory drift was considered as the primary performance criterion to estimate the damage states of the reference buildings. Based on the IDA results, IDRs of 1.0%, 0.5% and 0.4% were adopted for the IO limit state of the FSC, SW and TIT structural systems, respectively. For the CP limit state, IDRs of 4.0%, 2.27% and 1.80% were adopted for the FSC, SW and TIT structural systems, respectively. The selection of the IO and CP limit states was based on IDA results and the recommendations of previous experimental and analytical studies. The LS limit state, which falls between the IO and CP performance criteria, was considered equal to 50% of the CP limit state. The selected limit states of the reference structures were based on comprehensive IPAs, THAs and IDAs results as well as previous experimental and analytical studies and code-recommended values, which lent weight to the performance criteria of the current study.

CHAPTER 6: VULNERABILITY ASSESSMENT OF MODERN MULTI-STORY BUILDINGS

6.1 INTRODUCTION

Vulnerability functions relate the input ground motion intensity to the probability of exceeding limit states. The selected forty natural ground motions in the current study are scaled based on their PGA, which is the considered a measure of ground motion intensity, as described in detail in Chapter 5. The following equation is used to derive the fragility functions (Wen et al., 2004):

$$P(LS|GMI) = 1 - \Phi\left[\lambda_{CL} - \lambda_{D|GMI} \Big/ \left(\sqrt{\beta^2_{D|GMI} + \beta^2_{CL} + \beta^2_{M}}\right)\right] \quad (4)$$

where, P(LS|GMI) is the probability of exceeding a limit state given the ground motion intensity (GMI); Φ is the standard normal cumulative distribution function; λ_{CL} = ln (median of drift capacity for a particular limit state); $\lambda_{D|GMI}$ = ln (calculated median demand drift given the ground motion intensity from the fitted power law equation); $\beta_{D|GMI}$ is demand uncertainty = $\sqrt{\ln(1 + s^2)}$, where s^2 is the standard error of the demand drift data; β_{CL} is drift capacity uncertainty; and β_M is modeling uncertainty. The β_{CL} and β_M are assumed in the present study to be 0.30 and 0.20, respectively, based on previous studies (e.g. Jeong et al., 2012; Wen et al., 2004). The detailed modeling approach adopted for idealizing the ten reference structures of the present study and the verifications conducted for the developed numerical models support the adopted value for β_M.

6.2 DERIVATION OF VULNERABILITY FUNCTIONS USING IDA

The vulnerability relationships of the ten reference structures are derived through over 5,000 IDAs using forty natural earthquake records in order to arrive at a reliable estimation of physical damage from different earthquake scenarios. Figure 55 depicts the IDA results for the ten reference buildings obtained from the twenty natural records representing the severe distant earthquake scenario. The IDA results of the reference structures obtained from the moderate close earthquake scenario are presented in Figure 56. The power law used for deriving the vulnerability relationships using Equation 4 and the IO, LS and CP limit states adopted in the present study are also shown in Figure 55 and Figure 56.

Figure 55 and Figure 56 show that different limit states are exceeded at significantly higher PGAs under the near-source earthquake records compared with the severe distant input ground motions. This is attributed to the high spectral amplifications of severe distant earthquakes up to 2.0 sec, which match the fundamental and/or the higher mode periods of the reference buildings, as shown in Table 27, Figure 40 and Figure 41. Despite the lower mass participation of the higher modes of vibration, when the tall buildings are excited by the severe far-field earthquake records these modes are amplified. The PGA-IDR statistical distributions are used to calculate the probability of exceedance for each of the selected limit states at different intensity levels.

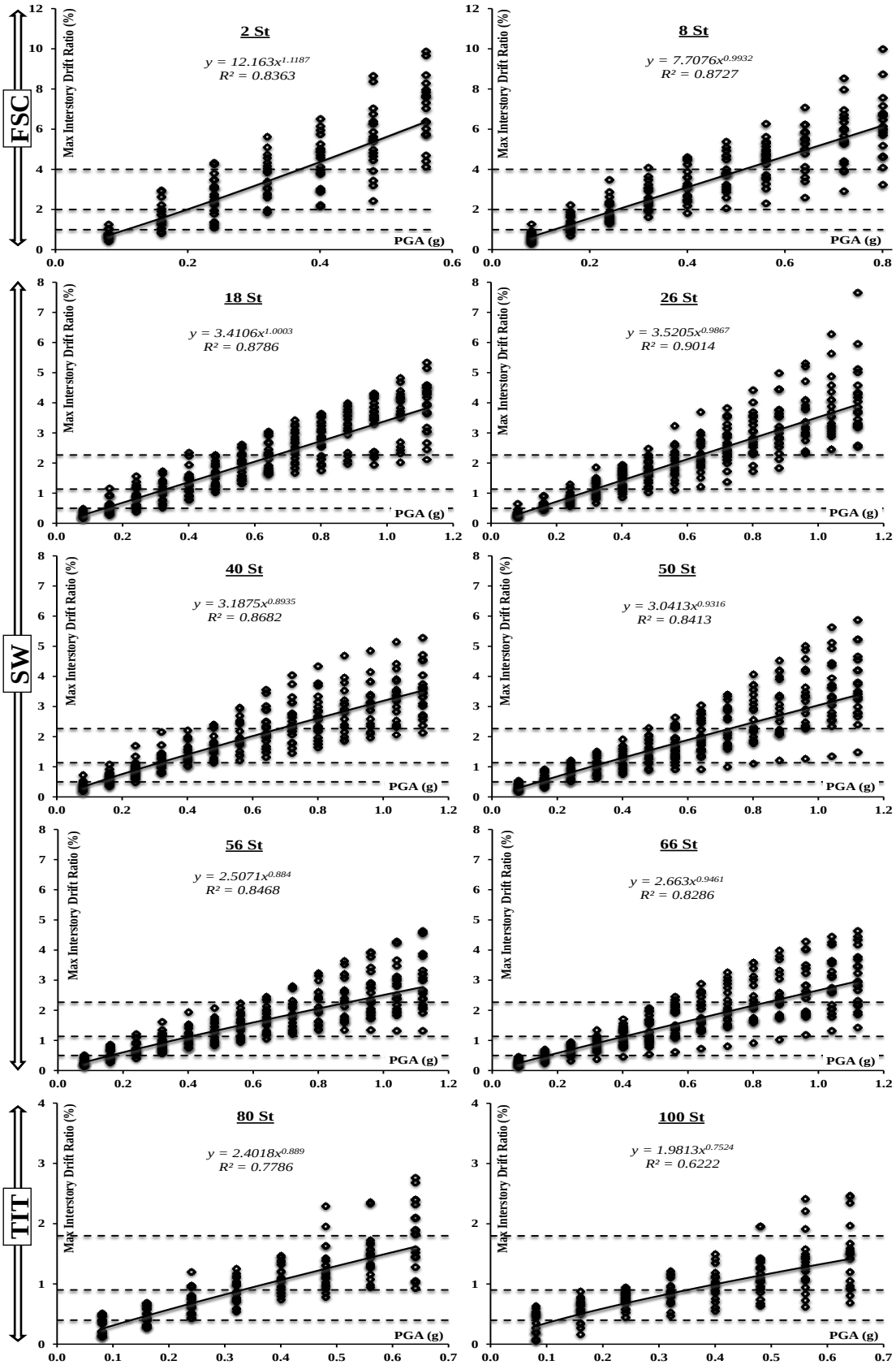

Figure 55. IDA results of ten reference structures using 20 natural records representing severe distant earthquakes along with the power law equations and limit states (IO, LS and CP from bottom to top, respectively)

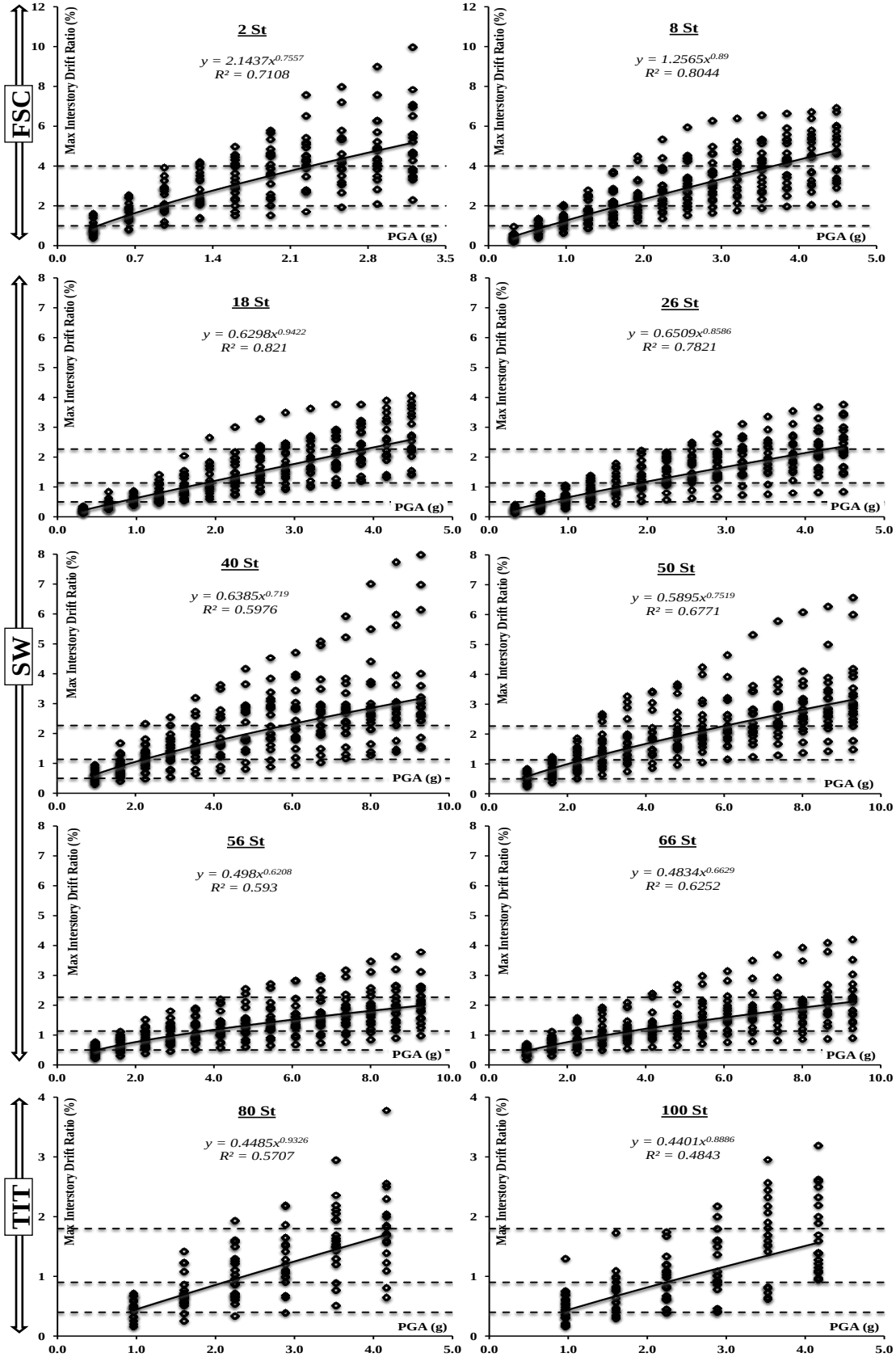

Figure 56. IDA results of ten reference structures using 20 natural records representing moderate close earthquakes along with the power law equations and limit states (IO, LS and CP from bottom to top, respectively)

The fragility relationships of the ten reference structures are derived by plotting the estimated probability data versus PGAs. Figure 57 shows the vulnerability relationships of the reference buildings under the severe distant earthquake scenario, while Figure 58 depicts the vulnerability functions from the moderate close earthquake scenario. It is observed that the slopes of the derived fragility functions decrease as the performance criterion shifts from the IO to CP. The sharp slope of the IO limit state curve is due to the high lateral stiffness in the elastic range, which significantly decreases the dispersion of the IDRs obtained from various input ground motions. In contrast, the slopes of the CP fragilities decrease due to the higher variability of the demand in the inelastic range.

Figure 59 compares the fragility curves obtained from the severe distant and moderate close scenarios for the 8, 18, 66 and 100-story buildings, which represent three different structural systems and building heights. The comparisons show that the damage probabilities of the reference structures under the moderate close earthquake scenario are insignificant compared to the severe distant records, particularly at the design and twice the design intensity levels.

The results obtained from the present study clearly reflect the low vulnerability of multi-story buildings in the study area to the short period earthquake scenario, as confirmed from Figure 57 to Figure 59. The high impacts of long period input ground motions on the vulnerability of different structural systems with different building heights suggest the need to pay more attention to this earthquake scenario in seismic vulnerability assessment studies.

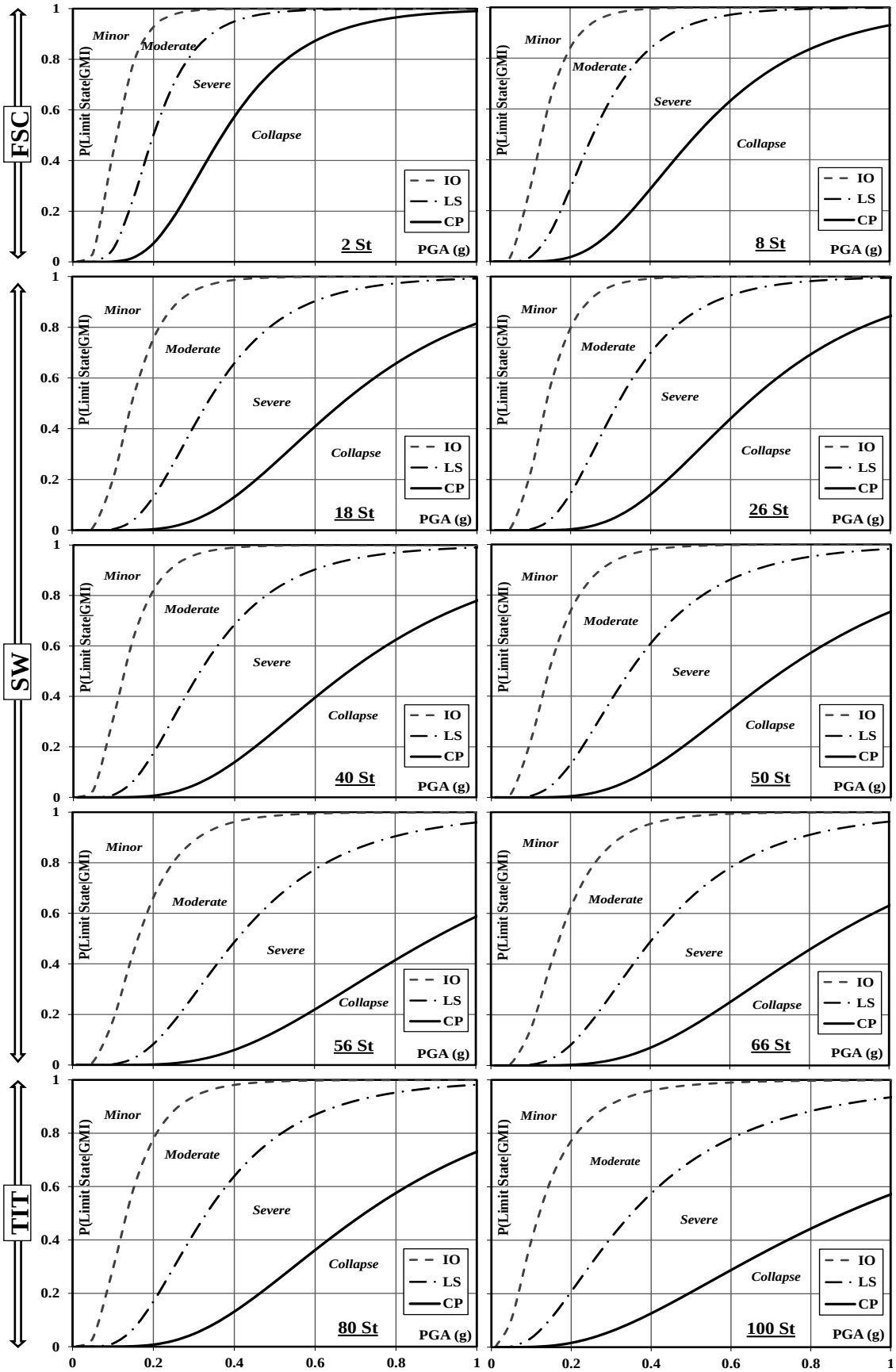

Figure 57. Vulnerability relationships of ten reference buildings obtained from IDAs using twenty severe distant earthquake records

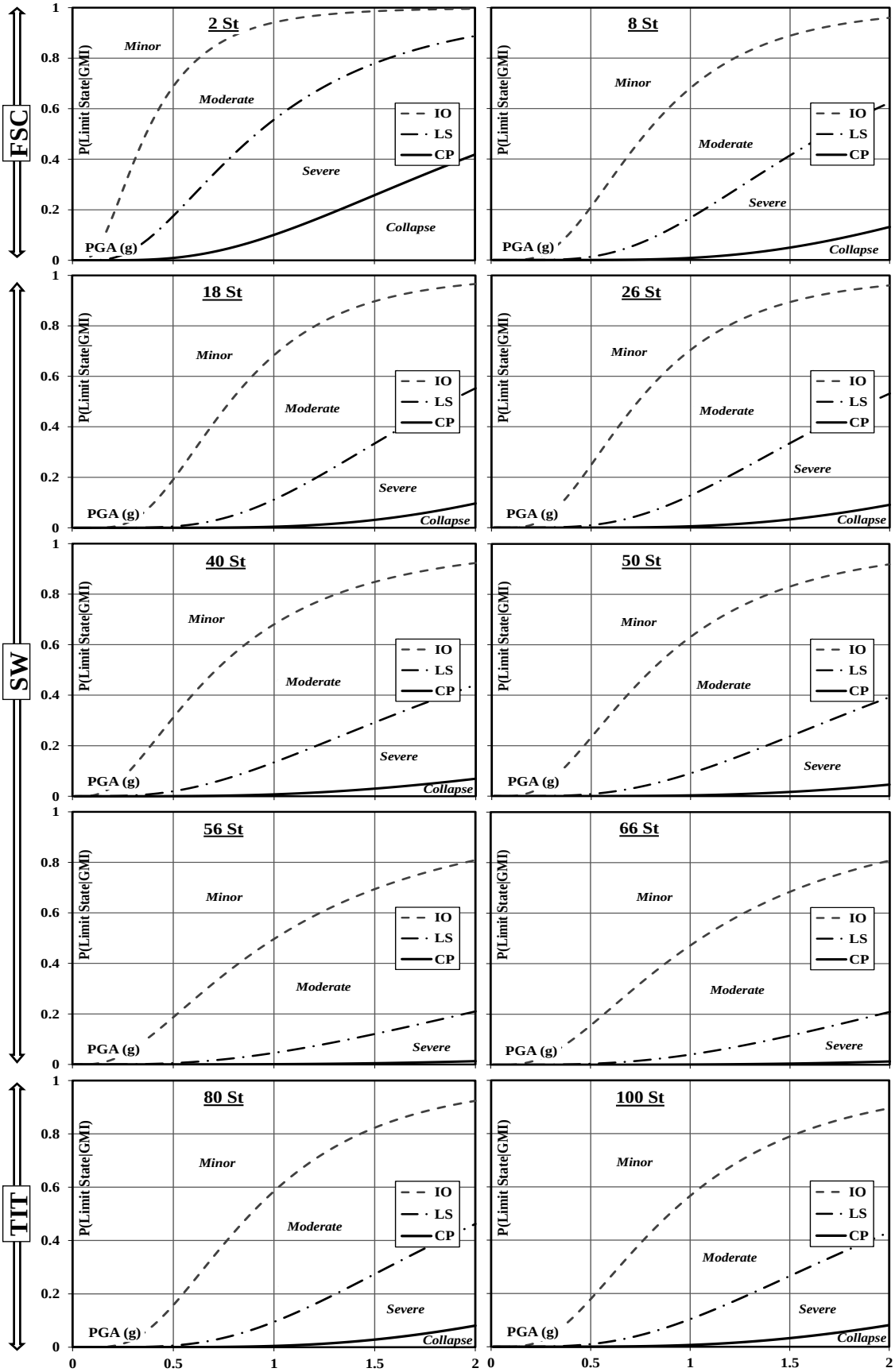

Figure 58. Vulnerability relationships of ten reference buildings obtained from IDAs using twenty moderate close earthquake records

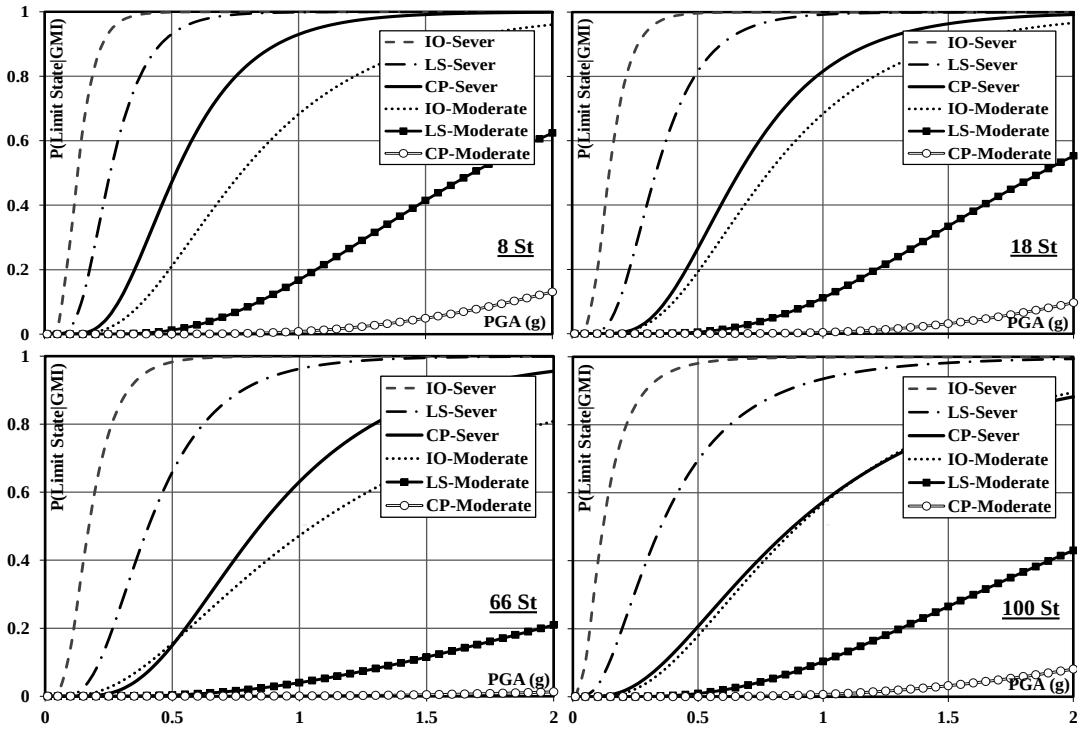

Figure 59. Comparisons between the fragility relationships obtained from the severe distant and moderate close earthquake scenarios for the 8, 18, 66 and 100-story buildings, which represent different structural systems

For the three investigated structural systems, Figure 60 compares the fragility relationships of buildings with different heights under the severe distant earthquake scenario. The comparisons illustrated in Figure 60 show a direct relationship between the damage level and building height. The developed fragility curves for the shorter buildings are steeper than those of taller structures. This indicates that earthquake records have more impact on shorter structures than taller buildings, especially for FSC and SW systems. This observation is also shown in the fragilities of TIT structural system at high PGAs. The above-mentioned observation is emphasized under the effect of both moderate near-source and severe far-field earthquakes. This is justified by the reduced participation of the prominent period of vibration to the seismic response with increasing the building height.

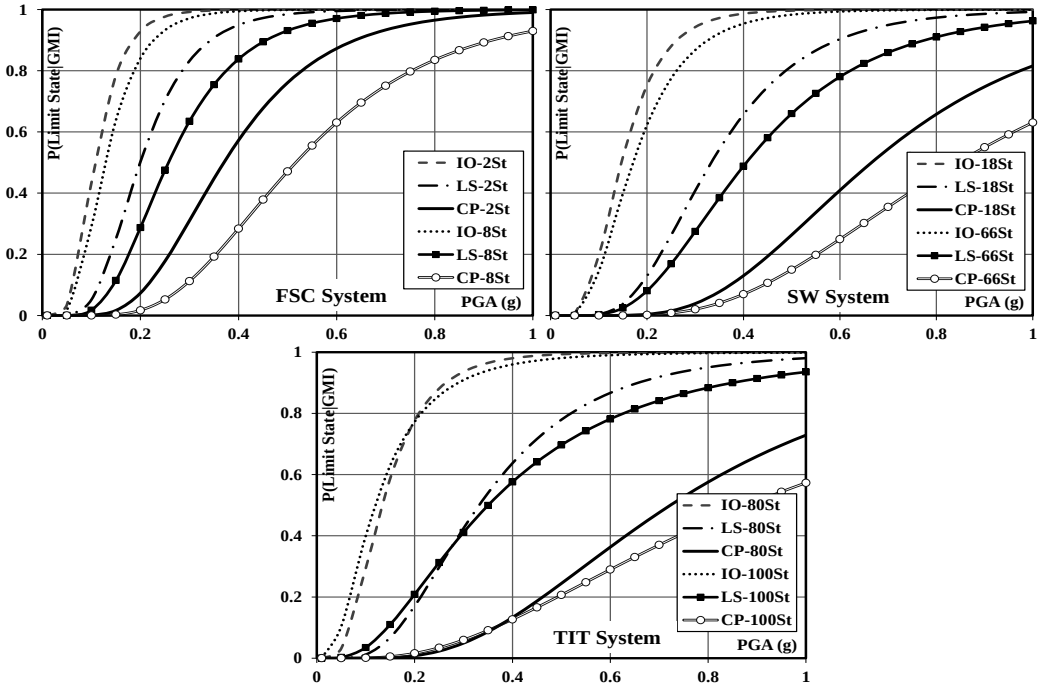

Figure 60. Comparisons between the fragility relationships of building with various heights for three different structural system under severe distant earthquakes

6.3 3D FRAGILITY CURVES OF DIFFERENT STRUCTURAL SYSTEMS

Three dimensional vulnerability relationships are developed for the different structural systems and performance limit states employed in the present study using the severe distant and moderate close earthquake scenarios. Figure 61 and Figure 62 illustrate the 3D fragility curves of the FSC, SW and TIT systems in terms of building height. While the X and Y-axes represent the ground motion intensity and the probability of exceedance, respectively, the third axis represents the number of stories. The IO, LS and CP performance criteria are separately presented for different systems to enable adding the third axis, which represents the number of stories. This versatile 3D format of vulnerability curves enables the interpolation of results from the derived vulnerability relationships to arrive at the fragilities of a wide range of structures with different heights and systems.

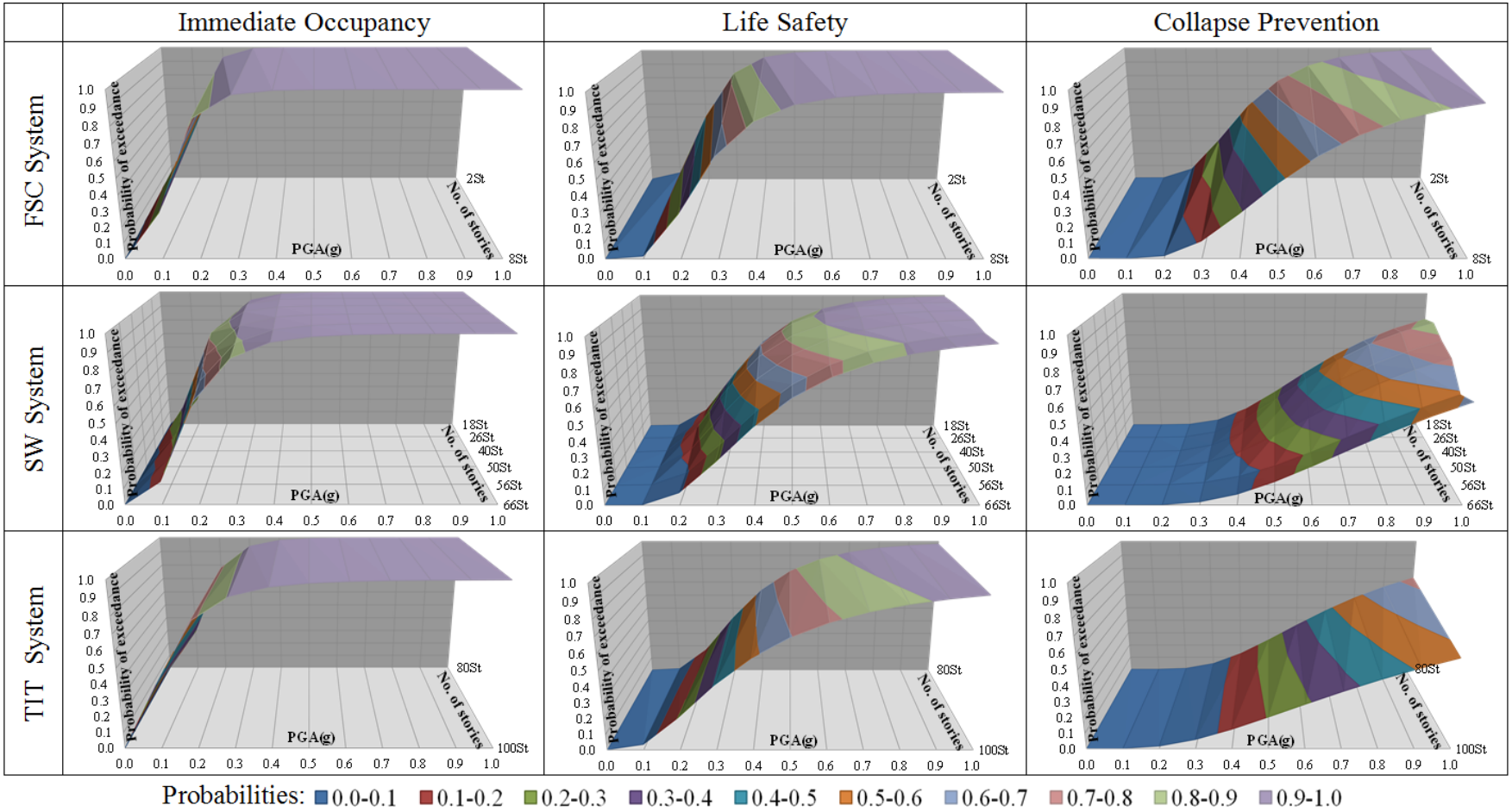

Figure 61. 3D fragility curves of different structural systems in terms of building height using the severe distant earthquake scenario

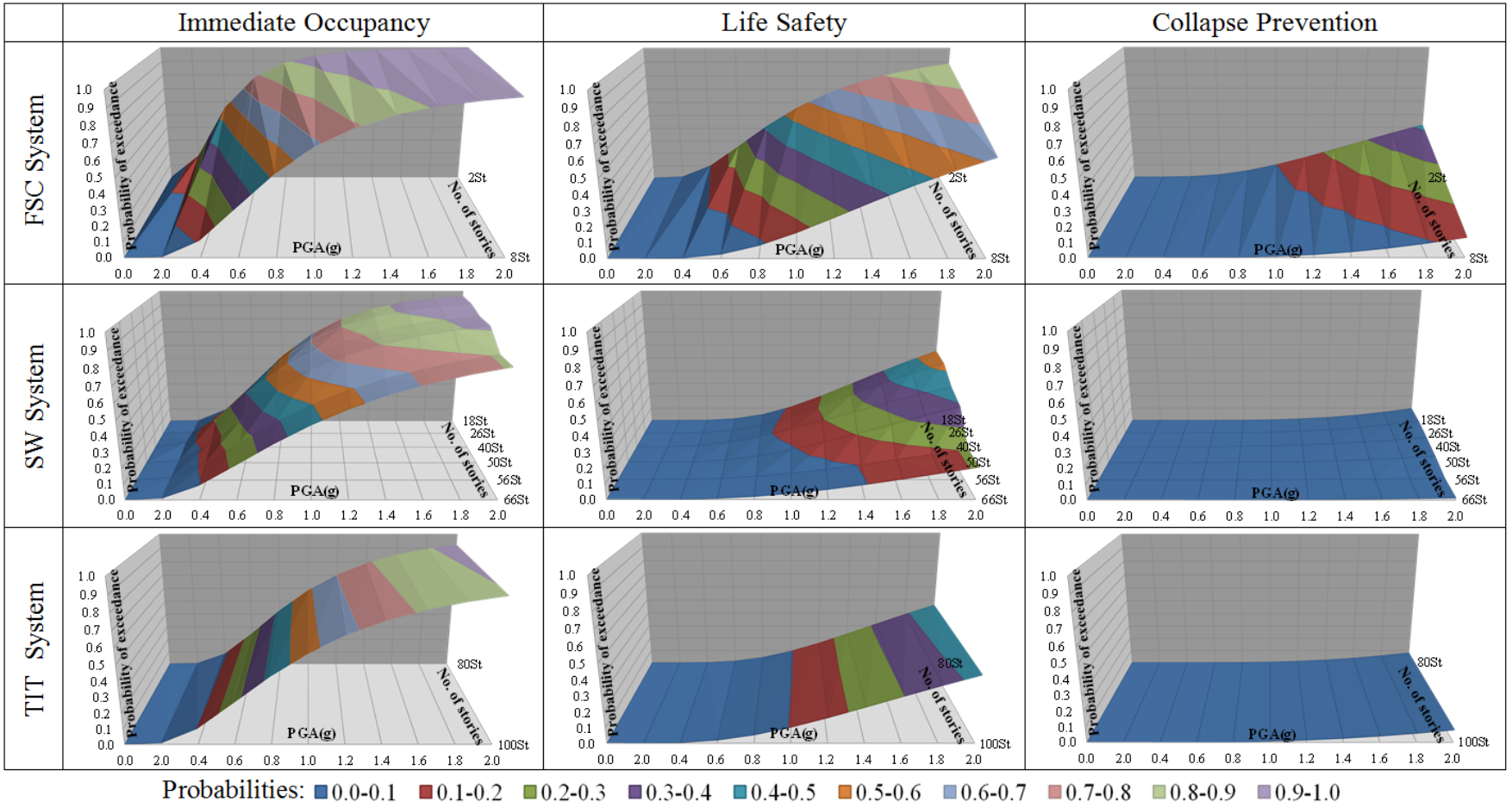

Figure 62. 3D fragility curves of different structural systems in terms of building height using the moderate close earthquake scenario

To provide a more informative presentation of this comprehensive vulnerability assessment study, Figure 63 depicts the limit state exceedance probabilities of the ten reference buildings under the severe distant ground motion scenario at the design and twice the design earthquake intensities.

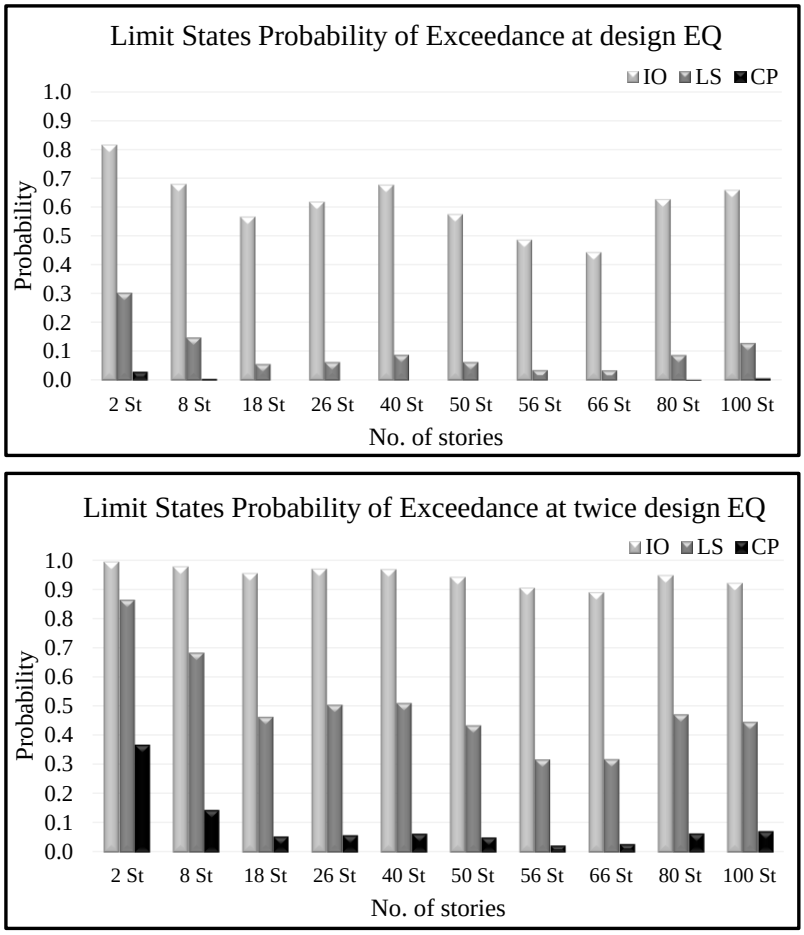

Figure 63. Limit state exceedance probabilities of the reference structures under the severe distant earthquakes at the design and twice the design earthquake levels

The results of the probabilistic vulnerability assessment using different seismic scenarios anticipated at the study area confirm the satisfactory performance of the SW and TIT structural systems under the design earthquake and their acceptable response under twice the design intensity, as shown shown in Figure 57, Figure 58 and Figure 63. This is particularly true for the LS and CP limit states.

These observations are in line with the modern code approach for the seismic design of RC buildings.

On the other hand, the results at the design and at twice the design earthquake intensity confirm the vulnerability of the FSC system, which is a common system in the study area for low and mid-rise buildings, to the severe distant earthquakes, particularly at twice the design PGA. This observation confirms the pressing need for mitigation actions to reduce the potential earthquake losses of the FSC structural system. The observed vulnerability of this system is attributed to the ineffective framing action provided by flat slabs and columns. The developed vulnerability functions in this comprehensive study are essential elements to arrive at a reliable loss assessment system for the study region.

6.4 SEISMIC DESIGN RESPONSE FACTORS

The seismic design response factors, Ω, R and C, are estimated in the present study through the extensive IPA and THA discussed in Chapter 5. These analyses are also used to calculate the first yield overstrength factor (Ω_{fy}) for the reference buildings, which is needed to estimate the R factors. Figure 64 shows comparisons between the Ω_{fy} obtained from IPA and THA, while Figure 65 compares between the design strength of the reference structures and the strength at first yield obtained from IPA and THA. It is clear that the Ω_{fy} values obtained from IPA are lower than those from THA, particularly for mid- and high-rise buildings. This is due to the effect of higher modes of vibrations, which amplify the strength obtained from THA. Moreover, the design overstrength factors of the reference buildings are calculated and presented in Figure 43 to Figure 45. These results are summarized in Table 31.

Clearly, the calculated Ω factors are higher than the code values for all reference structures except for the 2-story building. This implies that the Ω factor of the low-rise flat slab-columns system should be decreased by 10% as a result of its inefficient lateral force resisting system.

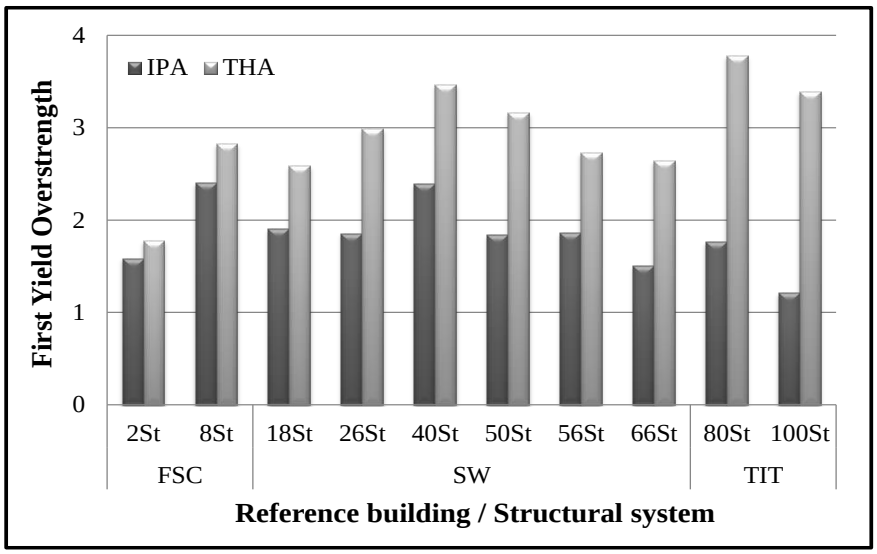

Figure 64. Comparison between first yield overstrength (Ω_{fy}) of the reference structures obtained from IPA and THA

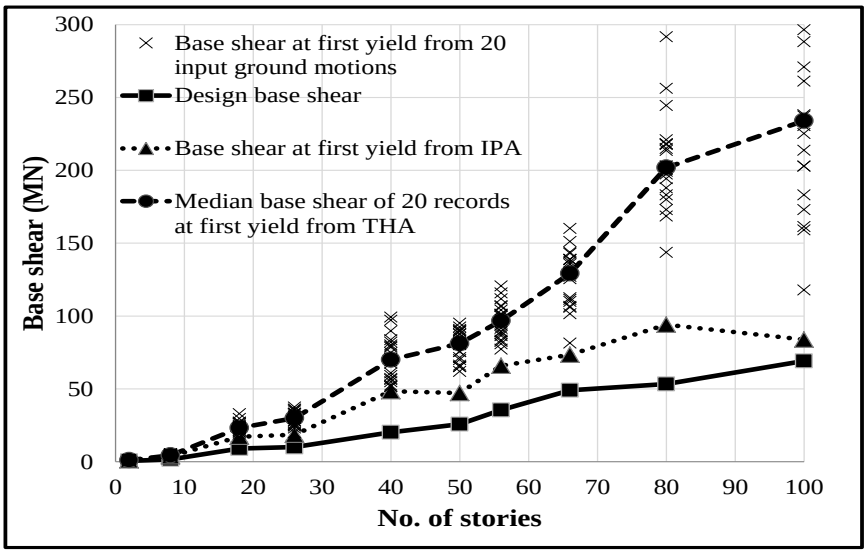

Figure 65. Comparison between the design strength of the reference structures and the strength at first yield obtained from IPAs and THAs

Table 31. Comparison between the design overstrength factors of the ten reference buildings and the code values

System	Building	Design strength (kN)	Ultimate strength (kN)	Ω – Calculated	Ω – Code
FSC	2-story	588	1697	2.9	3.0
	8-story	1541	5725	3.7	
SW	18-story	9015	29379	3.8	2.5
	26-story	10042	28174	3.3	
	40-story	20247	63994	3.7	
	50-story	25725	63288	2.9	
	56-story	35470	107359	3.6	
	66-story	49025	119950	2.9	
TIT	80-story	53396	177385	3.9	2.5
	100-story	69157	177429	3.0	

The PGAs and IDRs at the first indication of yield and collapse are summarized in Table 32 and Table 33, respectively. These results are obtained from THAs using the most critical earthquake scenario (i.e. the twenty natural input ground motions that represent severe distant earthquakes). For the sake of brevity, only the minimum, maximum and median values obtained from the selected set of earthquake records are shown in Table 32 and Table 33. The results show a notable difference between the response of the reference buildings under the effect of different input ground motions although they were selected to represent certain earthquake scenarios. The median values of the PGAs at the first indication of yield and collapse are presented in Figure 66.

Table 32. Summary of THA results at the first indication of yielding

System	Building	Peak ground acceleration (g)			Interstory drift ratio (%)		
		Minimum	Maximum	Median	Minimum	Maximum	Median
FSC	2-story	0.06	0.16	0.10	0.77	1.10	0.84
	8-story	0.08	0.32	0.24	1.29	1.91	1.63
SW	18-story	0.08	0.32	0.16	0.45	0.70	0.59
	26-story	0.08	0.24	0.24	0.58	0.90	0.69
	40-story	0.16	0.40	0.26	0.85	1.14	0.98
	50-story	0.16	0.48	0.32	0.83	1.11	0.95
	56-story	0.16	0.32	0.24	0.43	0.87	0.67
	66-story	0.16	0.48	0.24	0.54	0.77	0.67
TIT	80-story	0.08	0.32	0.16	0.35	0.62	0.50
	100-story	0.08	0.40	0.16	0.48	0.72	0.59

Table 33. Summary of THA results at the first indication of collapse

System	Building	Peak ground acceleration (g)			Interstory drift ratio (%)		
		Minimum	Maximum	Median	Minimum	Maximum	Median
FSC	2-story	0.22	0.54	0.36	3.86	4.18	3.99
	8-story	0.32	0.96	0.51	3.88	4.13	4.00
SW	18-story	0.40	1.20	0.64	2.25	2.40	2.30
	26-story	0.46	0.96	0.66	2.28	2.40	2.32
	40-story	0.48	1.20	0.72	2.27	2.49	2.35
	50-story	0.48	1.68	0.78	2.27	2.51	2.34
	56-story	0.64	1.28	0.88	2.19	2.47	2.33
	66-story	0.56	1.60	0.88	2.22	2.46	2.35
TIT	80-story	0.44	1.04	0.64	1.69	1.96	1.83
	100-story	0.44	1.28	0.74	1.70	1.98	1.83

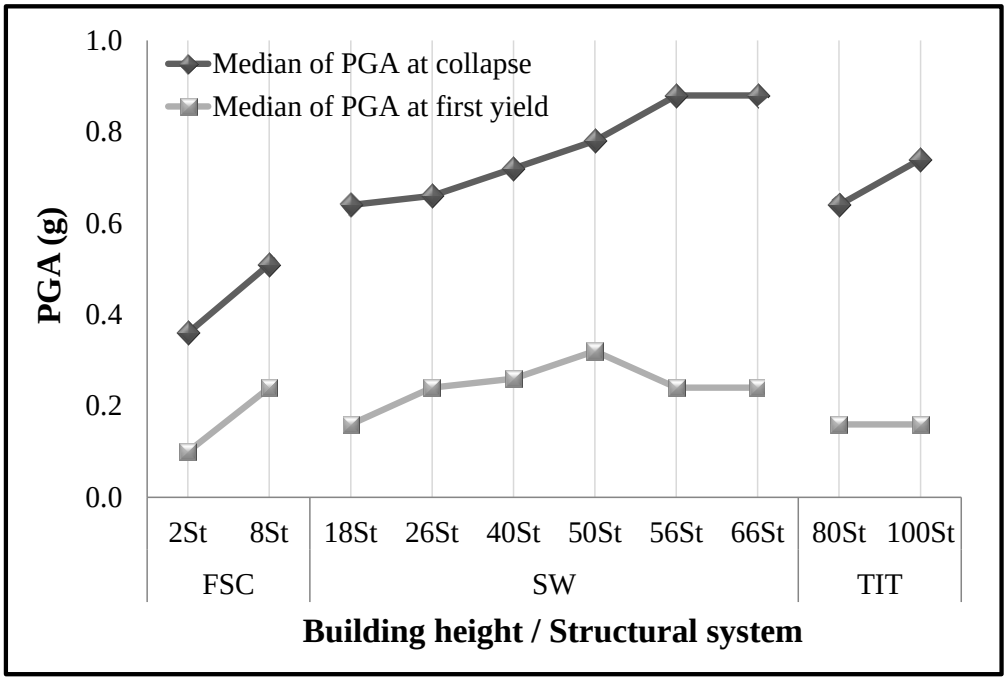

Figure 66. Comparison between the median of PGAs at first indication of yield and collapse obtained from THA

The THA results at the first indication of yield and collapse obtained from the twenty natural input ground motions that represent the severe distant seismic scenario are illustrated in Figure 67 for the ten reference structures along with the collapse-to-yield PGA and IDR ratios. As explained in Equation 3, the collapse-to-yield PGA ratios are utilized along with the first yield overstrength (Ω_{fy}) factors to estimate the R factors, while the collapse-to-yield IDR ratios are used to estimate the C factors for the reference buildings.

The collapse-to-yield PGA and IDR ratios do not show a clear trend with increasing the building height or within the group of buildings with similar structural systems. This is attributable to the fact that a wide range of structural variables (i.e. layouts, systems and heights) are investigated in the present study. The PGAs at the first indication of yielding are marginally influenced by increasing the building height or changing structural system, as shown in Table 32 and Figure 66. However, Table 33 and Figure 66 emphasize the direct relationship between the building height and the PGA at the first indication of collapse. For taller buildings, collapse is noticed at higher PGAs for each of the three considered structural systems. This implies that, within each structural system, the impacts of earthquakes decrease as the building height increases since higher PGA are required to cause collapse.

The collapse-to-yield PGA ratios shown in Figure 67 are employed to calculate the R factors of the reference structures using Equation 3, where the Ω_{fy} factors are calculated from both IPA and THA, as depicted in Figure 68 and Figure 69, respectively. The design R factors (R Code), which are 5.0, 4.0 and 5.0 for the FSC, SW and TIT systems, respectively, are also shown in Figure 68 and Figure 69 (ASCE-7, 2010). Both of the median R values obtained from individual input ground motions and those obtained from the median collapse-to-yield PGAs illustrated in Figure 67 are presented in Figure 68 and Figure 69.

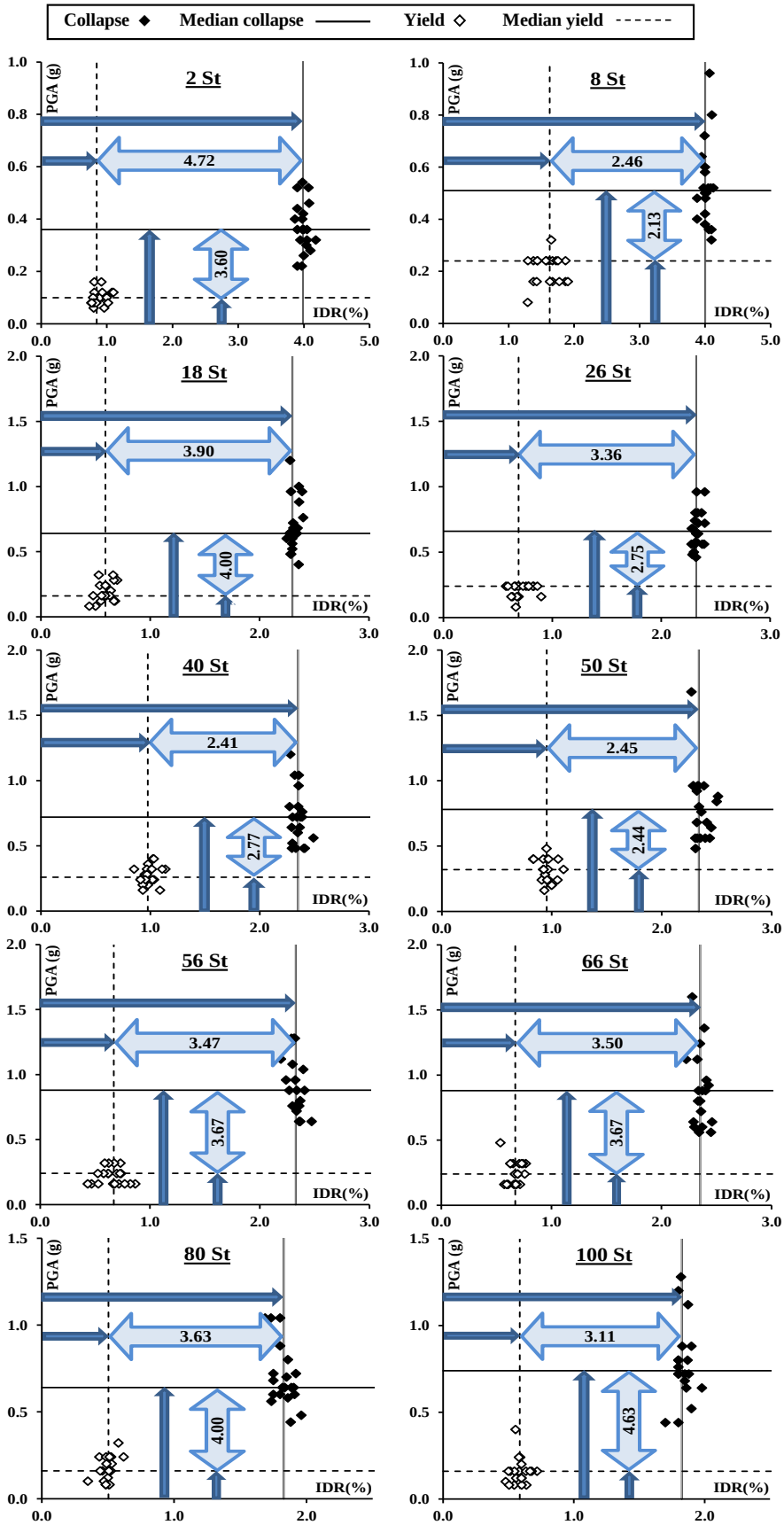

Figure 67. THA results at yield and collapse along with collapse-to-yield PGA and IDR ratios for the reference buildings using severe distant records

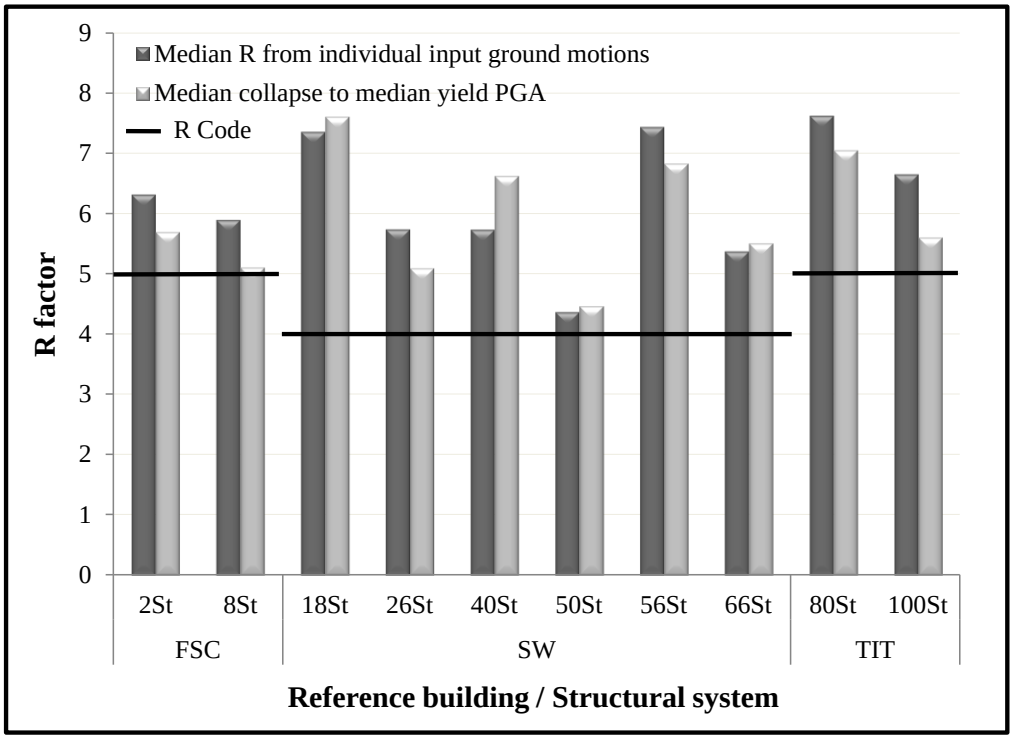

Figure 68. Comparison between the code values and the response modification factors of the reference buildings calculated using collapse-to-yield PGAs from THA and Ω_{fy} from IPA

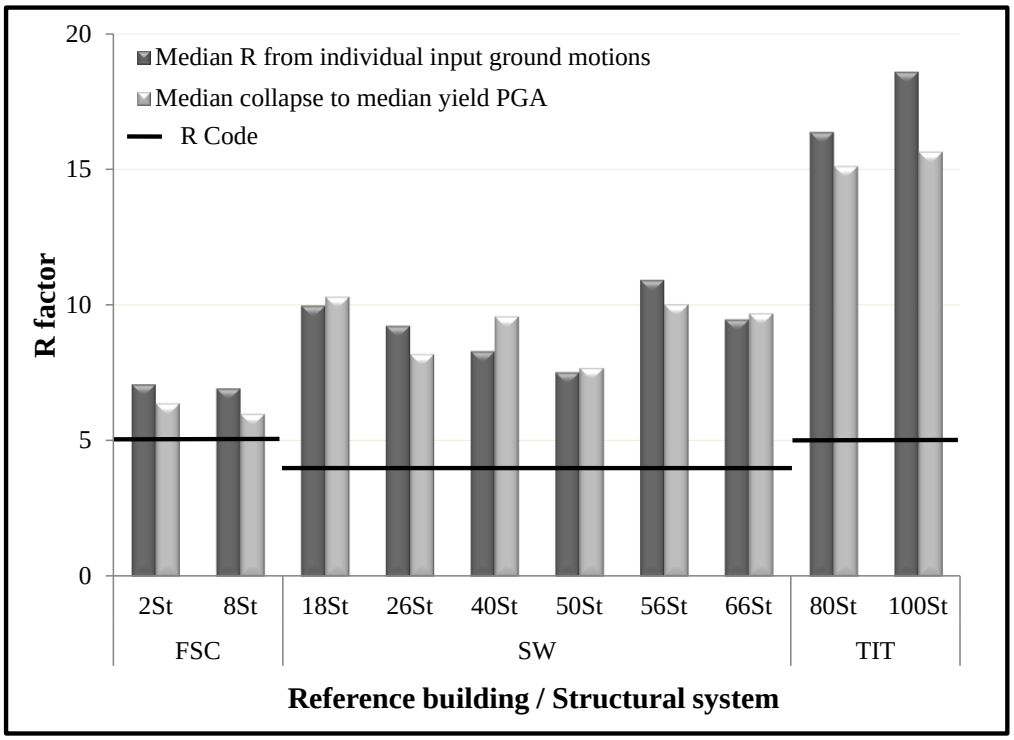

Figure 69. Comparison between the code values and the response modification factors of the reference buildings calculated using collapse-to-yield PGAs and Ω_{fy} from THA

It is shown from Figure 68 and Figure 69 that the median R factors of the reference buildings are generally higher than the values recommended by the design code, particularly for the SW and TIT systems (ASCE-7, 2010). Moreover, the median R factors for the mid- and high-rise buildings are significantly higher than the values recommended by the design code when considering the reliable THA approach to evaluate the Ω_{fy} factors, as shown in Figure 69. With very few exceptions, it is noticed that the R factor decreases with increasing the building height for the same building layout.

The results of this comprehensive study show that the margin of safety of R factor of the SW and TIT systems is much higher than the FSC system. The results presented in Figure 68 and Figure 69 imply that the R factors of the SW and TIT systems can be increased by at least 10%. The R factors can be increased further if THA results are considered. However, it is recommended to carefully investigate the impacts of the proposed increase of the R factors on the seismic response of the SW and TIT systems before implementing additional reductions in seismic forces.

Figure 70 summarizes the C factors of the reference structures, which are estimated using the twenty far-field records. The C factor is considered in the present study to be equal to the collapse-to-yield IDRs. The design C factors (C Code), which are 4.5, 4.0 and 4.5 for the FSC, SW and TIT systems, respectively, are also shown in Figure 70 (ASCE-7, 2010). Both of the median C values obtained from individual earthquake records and those obtained from the median collapse-to-yield IDRs illustrated in Figure 67 are presented in Figure 70. It is shown that the median C factors of the SW and TIT systems are adequately conservative when compared with the values recommended by the design code (ASCE-7, 2010), while the code

value is slightly non-conservative for the low-rise FSC system. The results suggest that the C factor of the low-rise flat slab-columns buildings, which lacks an efficient lateral force resisting system, should be increased by 10%.

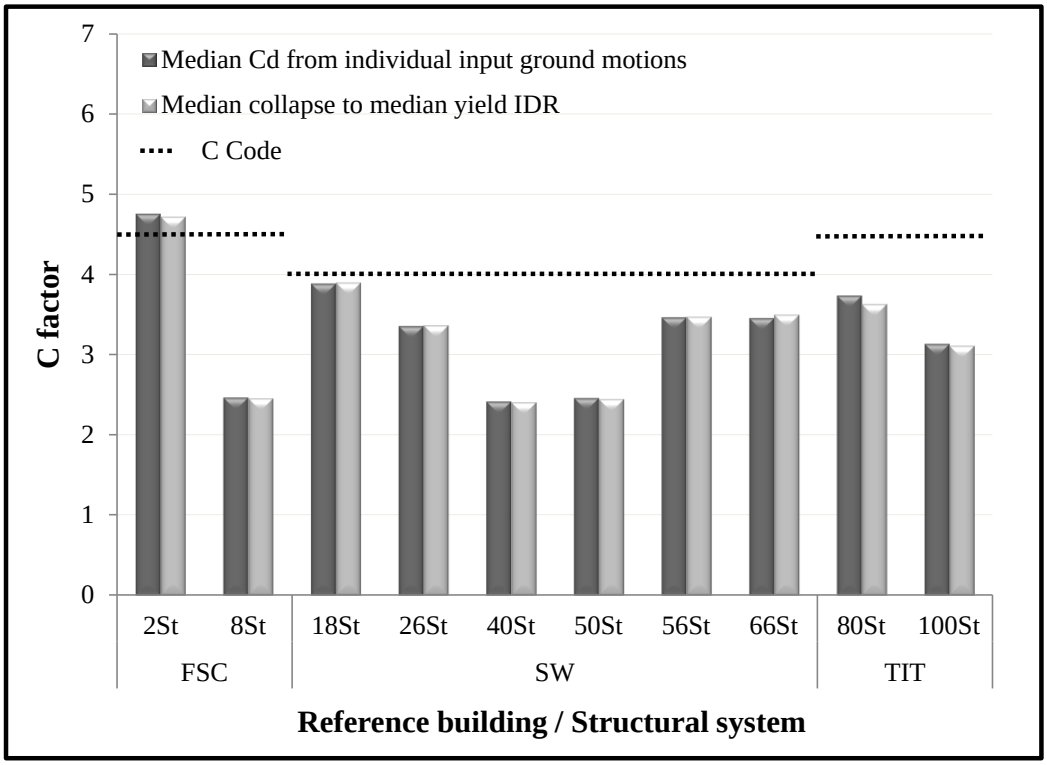

Figure 70. Deflection amplification factors of the reference buildings obtained from THA along with the code values

Within the same structural system, the observed variations in the R and C factors of the reference buildings are mainly due to the differences in the building heights and layouts, which result in different seismic demands. The results confirm the significance of studying a wide range of buildings with different geometric characteristics in order to arrive at an accurate and reliable assessment of the seismic design response factors.

6.5 PERIOD RELATIONSHIPS

The period of vibration is an important dynamic characteristic of structures. It is essential in seismic design to accurately estimate the design forces of the building. RC structures experience strength deterioration and stiffness degradation during earthquake shaking due to the concrete cracking and steel yielding of different structural elements. This damage results in elongation in the fundamental period, which is important for the evaluation of the structural performance. The structure becomes soft and responds with higher natural periods after the first significant yield (e.g. Elnashai and Mwafy, 2002; Udwadia and Trifunac, 1973). To evaluate the period elongation of the reference buildings at different limit states, the inelastic periods are calculated in the current study based on THA results using the fast Fourier transformation (FFT) algorithm (e.g. Kwon and Kim, 2010; Trifunac et al., 2001).

The elastic and elongated periods are estimated through EVAs and THAs using the fiber-based and the design models of the reference structures. Figure 71 shows a comparison between the elastic fundamental periods obtained from the design models and fiber-based models of the ten reference structures, which represent different structural systems, buildings layouts and heights. The comparison shows that the elastic periods obtained from the design models are slightly longer than those obtained from the fiber-based models. As discussed in Chapter 4, this is attributable to the steel reinforcement considered in the fiber-based models unlike the design models in which the stiffness is only based on the concrete cross-sections. Moreover, the actual material strength values considered in the fiber-based models increase

stiffness and reduce periods. The presented results validate the fiber-based numerical models of the reference structures, which are used to estimate the elongated periods.

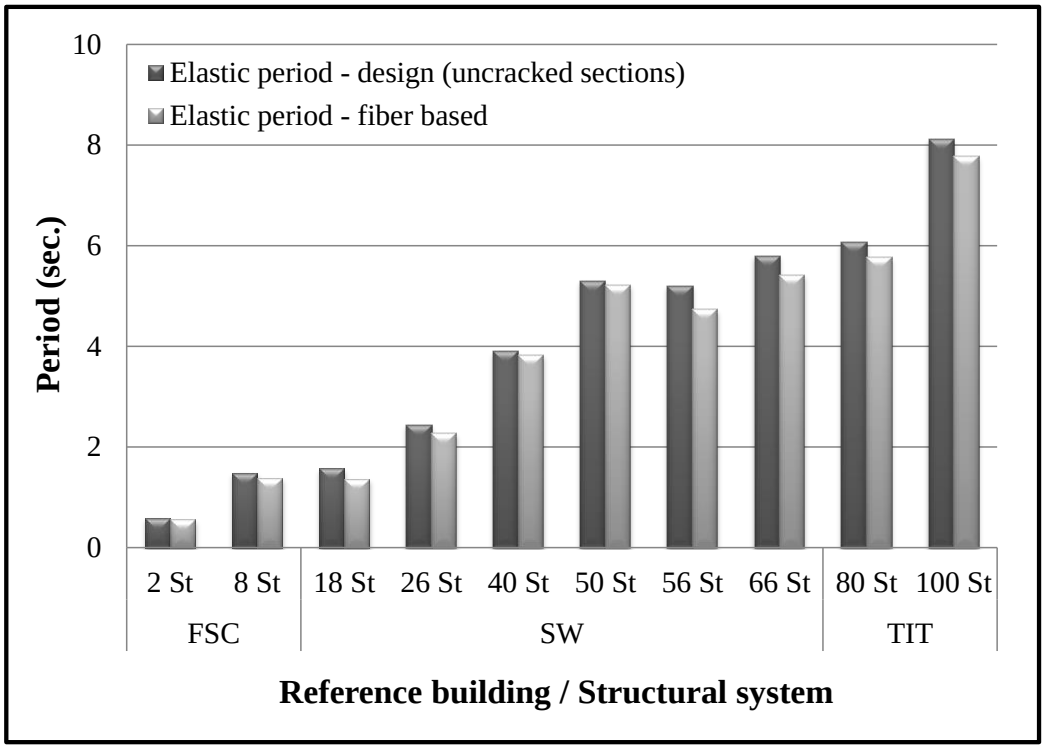

Figure 71. Comparison between elastic fundamental periods obtained from the design and the fiber-based models of the ten reference structures

The elongated fundamental periods of the reference buildings are calculated at the adopted LS and CP performance criteria in the present study for different structural systems, as discussed in Chapter 5. Figure 72 depicts a comparison between the elastic fundamental periods obtained from EVA and the inelastic periods estimated from THA at the LS and CP limit states. The period elongations at the above-mentioned performance limit states are illustrated in Figure 73.

The results show that the periods of vibration are elongated at the LS limit state by 220%, 160% and 110% (i.e. elongation of 2.2, 1.6 and 1.1) for the FSC, SW and TIT structural systems, respectively. At the CP performance level, the average

period elongation is 2.8, 2.0 and 1.3 for the above-mentioned three systems, respectively. These levels of elongation clearly reflect the damage states of the structure under seismic loads.

The observed high period elongation of the FSC system is attributed to the spread of inelasticity and damage in all structural members throughout the building height. The low period elongation of the TIT system is due to the limited inelasticity and concentration of damage in the very rigid internal core walls that represent the inner tube. The period elongation of the SW system falls between the two above-mentioned structural systems.

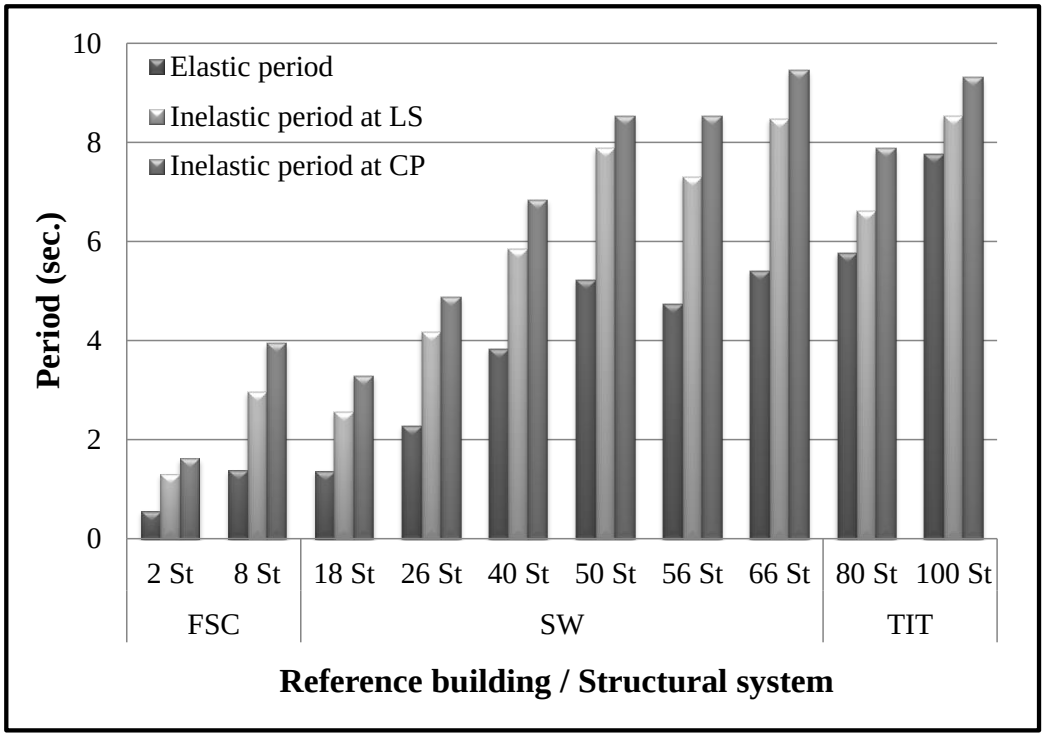

Figure 72. Comparison between the elastic fundamental periods obtained from EVA and the inelastic periods estimated from THA at the LS and CP limit states

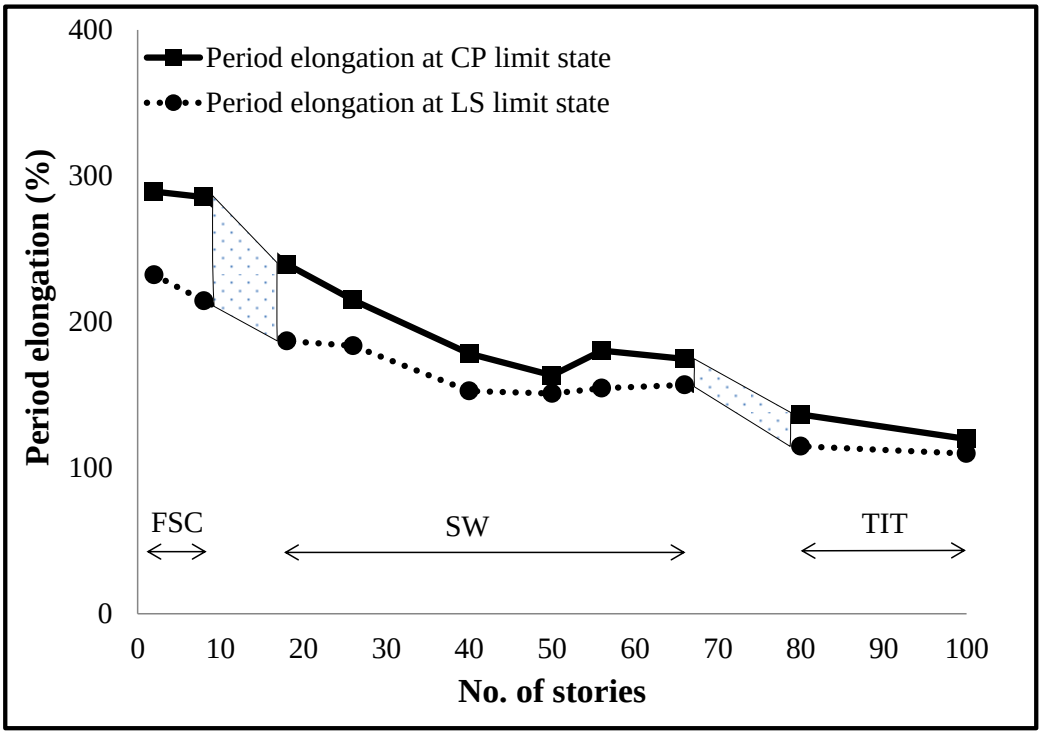

Figure 73. Comparison between the inelastic period elongation at the LS and CP limit states obtained from THA for the reference buildings

Effective stiffness values are typically used in elastic seismic analysis and design procedures. ACI-318 (2011) recommends an effective stiffness of 0.7EI for uncracked walls, 0.7EI for columns and 0.35EI for beams, where EI is the stiffness of the uncracked section. ASCE-41 (2007) recommends 0.8EI, 0.7EI and 0.5EI for uncracked walls, columns and beams, respectively. Paulay and Priestley (1992) suggested 0.8EI for uncracked walls and columns and 0.4EI for rectangular beams. In order to evaluate the effective stiffness of structural members used in design procedures, comparisons are conducted between the values recommended by the code provisions and previous studies with the results of the current work, as illustrated in Figure 74 and Figure 75.

The results presented in Figure 74 and Figure 75 show that the actual elongated periods of the FSC system at the LS limit state are higher than those

obtained using the effective stiffness values recommended by the code provisions and previous studies. On the contrary, the elongated periods of the TIT system are notably lower than those obtained using the effective stiffness values recommended by the code provisions and previous studies. The elongated periods of the SW system are higher than those obtained using the recommended effective stiffness for the 18- to 50-story buildings, while the 56- and 66-story buildings show comparable periods from inelastic analysis and the recommended effective stiffness.

Based on the present study results, it is proposed to reduce the effective stiffness of the FSC columns to 0.5EI. The suggested reduction in the column stiffness slightly increases the period of the 2- and 8-story buildings without exceeding the actual inelastic periods at the LS limit state. For the SW system, it is clear that the period elongation is related to the building height and layout. To avoid suggesting non-conservative stiffness values, it is recommended to use the values adopted by ASCE-41 and Paulay and Priestley for walls (i.e. 0.80EI).

For the TIT system, the results clearly reflect that the effective stiffness values recommended by design provisions and previous studies are highly non-conservative since they result in much longer periods than the actual inelastic periods at the LS limit state. This is expected to endanger the structure since the non-conservative periods may result in underestimating design forces. It is therefore recommended to use the full stiffness of structural members to arrive at conservative inelastic periods for the design of the TIT system.

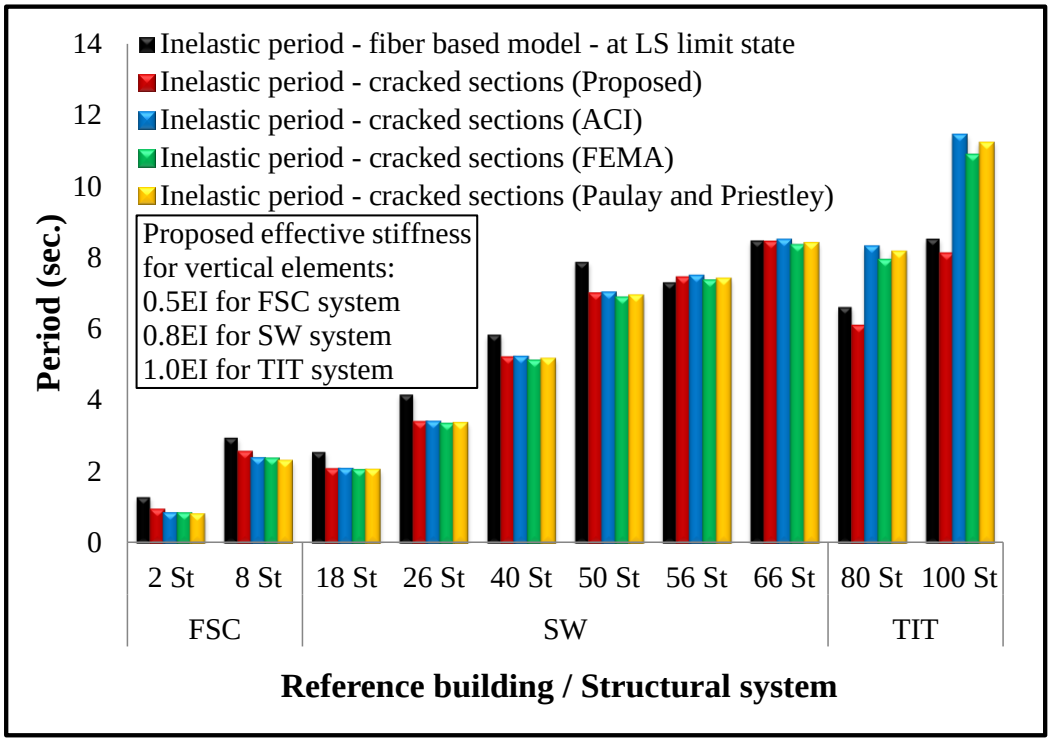

Figure 74. Comparison between the inelastic fundamental periods obtained from the design models using different effective stiffness values along with those calculated from THA at the LS limit state

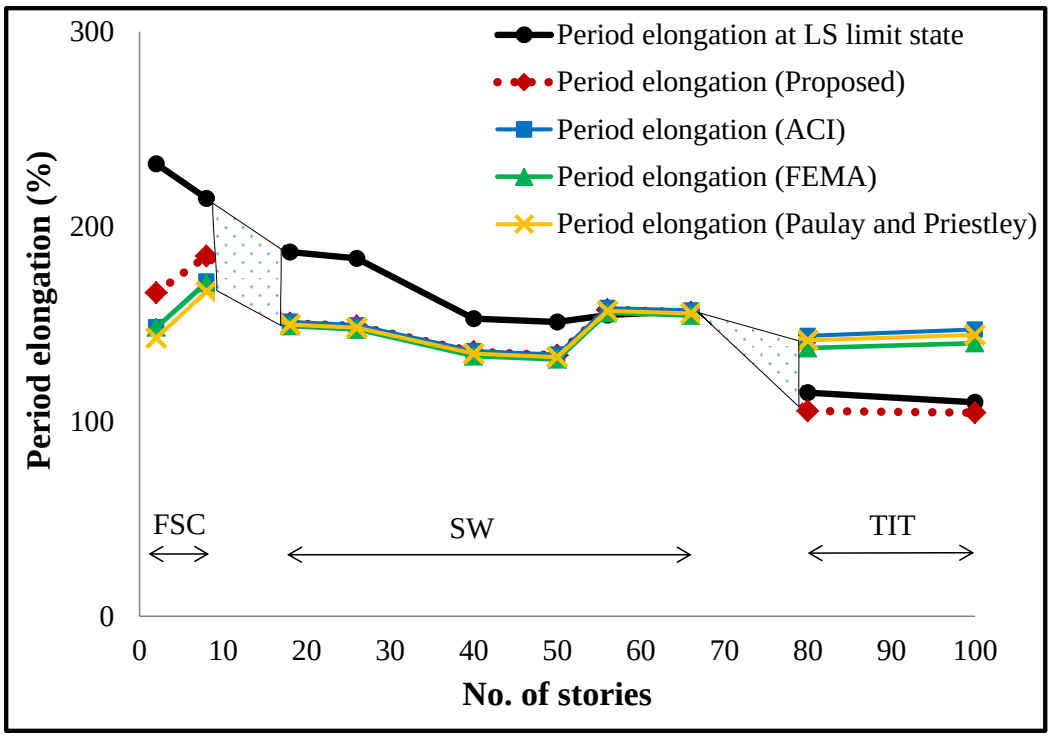

Figure 75. Comparison between the period elongations obtained using different effective stiffness values along with those calculated at the LS limit state

6.6 CONCLUDING REMARKS

The vulnerability functions of ten reference structures were derived in this study using 40 real input ground motion and over 5,000 inelastic analyses in order to arrive at a reliable estimation of physical damage under different possible earthquake scenarios. 3D vulnerability relationships in terms of building height were also developed for three different structural systems. The limit states exceedance probabilities were calculated from the fragility functions and used to assess the seismic performance of the reference structures. The seismic design response factors of the three structural systems covered in this study were estimated using IPA and THA results. The elastic and elongated periods of the reference structures were also calculated using free vibration analysis and THA. Comparisons between the periods of vibration estimated using the effective stiffness values recommended by the code provisions and previous studies with the inelastic periods of the reference structures were conducted to assess the values used in elastic design procedures.

The results indicated that the performance limit states were exceeded at significantly higher PGAs under the moderate near-source earthquake records compared with severe distant input ground motions. The limit states exceedance probabilities of the reference structures under the former earthquake scenario were insignificant compared to the severe distant records, particularly at the design and twice the design PGA levels. The impacts of the severe earthquake scenario on the vulnerability of structural systems with different building heights were confirmed from the results of the present study. The developed fragility curves confirmed that earthquakes have more impact on shorter buildings than taller structures, particularly for the FSC and SW structural systems. The versatile 3D format proposed in this

study for the vulnerability curves enables the interpolation of results from the derived functions to arrive at the fragilities of a wide range of structures with different heights and systems.

The results of the probabilistic vulnerability assessment confirmed the satisfactory performance of the SW and TIT systems under the design earthquake and their acceptable response under twice the design intensity. On the other hand, the results at the above-mentioned earthquake intensities confirmed the vulnerability of the low and mid-rise FSC system to the severe distant earthquakes, particularly at twice the design PGA. This observation confirmed the pressing need for mitigation actions to reduce the potential earthquake losses of the FSC system.

The calculated overstrength factors of the reference structures were higher than the code values except for the low-rise FSC system. This suggested reducing the overstrength factor of the low-rise FSC system by 10% due to its inefficient lateral force resisting system. The calculated response modification factors were higher than the code values, particularly for the SW and TIT systems. The median R factors for the mid- and high-rise buildings were significantly higher than the values recommended by the design code when considering the reliable THA approach to evaluate the R factors. The results confirmed that the R factors of the SW and TIT systems could be safely increased by at least 10%. The median of the deflection amplification factors for the SW and TIT systems were adequately conservative when compared with the values recommended by ASCE-7, while the code value was non-conservative for the low-rise FSC system. The results indicated that the deflection amplification factor of the low-rise FSC system should be increased by 10%.

The period elongation at the LS limit state was 2.2, 1.6 and 1.1 for the FSC, SW and TIT systems, respectively. At the CP performance level, the average period elongation was 2.8, 2.0 and 1.3 for the above-mentioned systems, respectively. The high elongation of the FSC system was attributed to the spread of inelasticity and damage in all structural members at different limit states. The observed minor elongation of the TIT system, particularly at LS, was due to the limited inelasticity and concentration of damage in the very rigid internal core walls. It was proposed to employ a column effective stiffness of 0.5EI for the FSC system. For the SW system, it was recommended to use an effective stiffness of 0.8EI for walls, which is adopted by ASCE-41. For the TIT system, the results confirmed that the effective stiffness recommended by design provisions and previous studies were highly non-conservative, and hence it was recommended to use non-cracked sections to arrive at conservative periods of vibration for design. The calculated seismic design response factors in this study confirmed the significance of considering a wide range of buildings with different geometric characteristics in order to arrive at accurate and reliable estimates of important seismic design parameters.

CHAPTER 7: SUMMARY AND CONCLUSIONS

7.1 SUMMARY

This study involved the selection, design and development of verified fiber-based simulation models for ten reference structures representing the modern multi-story building inventory in the UAE. Over 5,000 IPAs and IDAs were performed using forty earthquake ground motions, which enabled deriving 3D vulnerability functions for the contemporary buildings in the region. The tasks undertaken in the present study are summarized below.

7.1.1 Design and Analytical Modeling of Reference Structures

Ten reference structures of 2, 8, 18, 26, 40, 50, 56, 66, 80 and 100 stories were selected to represent the modern building inventory in a highly populated and earthquake-prone area in the UAE. The selected buildings had six varying layouts as well as three different lateral force-resisting systems, namely flat slab-columns (FSC), shear walls (SW) and tube in tube (TIT) systems. The ten reference buildings were fully designed and detailed as per the building codes and construction practice adopted in the UAE. Detailed fiber-based analytical models were developed and verified for the ten reference buildings. The developed fiber-based models were verified by comparing their dynamic characteristics with those obtained from the design models as well as the results of previous studies.

7.1.2 Selection of Input Ground Motions and Performance Criteria

The uncertainty in seismic demands due to the variability in input ground motions was effectively accounted for by using forty natural earthquake records. The real input ground motions were selected based on their epicentral distance, magnitude, site class, and spectral amplification to match the design spectrum of the study area. Twenty of the selected ground motions represented a severe distant earthquake scenario, while the other twenty earthquake records represented a moderate near-field seismic scenario. Due to the diversity of the investigated structural systems and the significance of limit states in vulnerability assessment, the performance criteria were selected based on the comprehensive results of the present study, previous experimental and analytical studies, and code-recommended values.

7.1.3 Vulnerability Assessment

The vulnerability functions of the ten reference structures were derived using a large number of IDAs in order to arrive at a reliable estimate of physical damage under different possible earthquake scenarios. 3D vulnerability relationships in terms of building height were also developed for different structural systems and performance criteria. The seismic design response factors of the structural systems covered in this study were estimated using IPA and IDA results. The elastic and elongated periods were calculated using free vibration analysis and THA. The periods of vibration estimated using the effective stiffness values recommended by code provisions and previous studies along with those calculated from the THA results of the present study were compared to provide insights into the most suitable effective stiffness values for seismic design.

7.2 CONCLUSIONS

The most important observations and conclusions of this study are as follows:

7.2.1 Modeling Verification and Performance Criteria

- The comprehensive analysis results confirmed that the final design of high-rise buildings should be verified using inelastic THA. This is consistent with the recent guidelines for performance-based seismic design of tall buildings.
- Three limit states were selected for the derivation of vulnerability relationships based on the results of the present study, previous experimental and analytical studies, and the code-recommended values. For the IO limit state of the FSC, SW and TIT structural systems, IDRs of 1.0%, 0.5% and 0.4%, respectively, were adopted. For the CP limit state, IDRs of 4.0%, 2.27% and 1.80% were adopted for the three structural systems, respectively. The LS limit state was considered 50% of the CP limit state.

7.2.2 Vulnerability Relationships and Damage Probabilities

- This comprehensive study enabled deriving 3D vulnerability functions for the contemporary buildings that include different structural systems and building heights for the direct implementation in a loss estimation system for the region. The versatile 3D presentation allows for the interpolation of results from the derived vulnerability relationships to obtain the fragilities of a wide range of structures with different heights and systems.
- The high impacts of the far-field earthquake scenario on the vulnerability of different structural systems with various building heights were confirmed from the results of the present study.

- Unlike the satisfactory performance of the SW and TIT systems, the results of the probabilistic seismic assessment study confirmed the vulnerability of the FSC system to the severe distant earthquakes, particularly at twice the design earthquake intensity. This confirms the pressing need for mitigation actions to reduce the potential earthquake losses of the FSC system.

7.2.3 Evaluation of Seismic Design Response Factors

- The calculated overstrength factors were higher than the code values for all reference structures except for the 2-story building due to its inefficient lateral forces-resisting system. It was suggested to decrease the overstrength factor of the low-rise FSC system by 10%.
- The results clearly indicated that the R factors of the SW and TIT systems could be conservatively increased by at least 10%. An additional increase in the R factors of these systems is possible after a systematic assessment of the impacts of the suggested reduction in seismic loads.
- When compared with the ASCE-7 recommended values, the median of the deflection amplification factors for the SW and TIT systems were adequately conservative, while the code value was non-conservative for the low-rise FSC system. The results indicated the need for increasing the deflection amplification factor of the low-rise FSC system by 10%.

7.2.4 Evaluation of Period Elongation and Effective Stiffness

- The period elongation at the LS limit state was 2.2, 1.6 and 1.1 for the FSC, SW and TIT systems, respectively. At the CP performance level, the average period elongation was 2.8, 2.0 and 1.3 for the above-mentioned structural systems, respectively. The observed high elongation of the FSC system was due to the

spread of inelasticity and damage in structural members at different limit states. The minor elongation of the TIT system, particularly at LS, was attributable to the limited inelasticity and concentration of damage in the very rigid core walls.

- It was suggested in this study to employ an effective stiffness of 0.5EI for the columns of the FSC structural system. For the SW system, the ASCE-41 recommended effective stiffness for walls (0.8EI) is adequately conservative. For the TIT system, the effective stiffness recommended by design provisions and previous studies were highly non-conservative, and hence it was suggested to employ non-cracked sections to arrive at conservative inelastic periods of vibration for design.

7.3 RECOMMENDATIONS FOR FUTURE WORK

Based on the findings and conclusions of the present study, the recommendations for future research are as follows:

- Future studies are highly desirable to integrate the wide range of fragility relationships developed in the present study and in other studies covering different classes of structures in a comprehensive seismic loss assessment and mitigation system for the region.
- The present study focused on regular buildings with different structural systems and heights. Future work is needed to assess the vulnerability of distinctive and irregular structures, which are common in the region. More research is also needed to investigate the vulnerability of infrastructure such as bridges, tunnels and pipeline networks.

- More research is needed to analytically and experimentally investigate the impact of shear response on limit states and fragilities, particularly under the effect of moderate near-source earthquakes.
- Future work is needed to investigate the impact of the proposed modifications in seismic design response factors on the seismic performance of buildings with different structural systems, and to calibrate this with the design codes implemented in the region.
- More research is needed to assess the vulnerability and possible mitigation actions of the conventional/prestressed flat slab-column system and comparable systems such as the hollow core slab system, which are widespread in the region, with different building configurations.
- Future work is required to investigate the need to revise the currently adopted period relationships in building codes according to different structural systems and building heights.

REFERENCES

Abdalla, J. A., & Al-Homoud, A. S. (2004). Seismic hazard assessment of United Arab Emirates and its surroundings. *Journal of Earthquake Engineering, 8*(6), 817-837.

ACI-318. (2011). *Building Code Requirements for Structural Concrete and Commentary*. Detroit, Michigan: American Concrete Institute.

Al-Haddad, M., Siddiqi, G., Al-Zaid, R., Arafah, A., Necioglu, A., & Turkelli, N. (1994). A basis for evaluation of seismic hazard and design criteria for Saudi Arabia. *Earthquake Spectra, 10*(2), 231-258.

Al-Homoud, A. (2003). The Fujairah United Arab Emirates (UAE) earthquake of March 11, 2002 a reminder for the immediate need to develop and implement a national hazard mitigation strategy. *The Proceedings of the EGS-AGU-EUG Joint Assembly*, Nice, France.

Al Khatibi, E., Abou Elenean, K., Megahed, A., & El-Hussain, I. (2014). Improved characterization of local seismicity using the Dubai Seismic Network, United Arab Emirates. *Journal of Asian Earth Sciences, 90*(1), 34-44.

Al Marzooqi, Y., Abou Elenean, K., Megahed, A., (...), & Al Khatibi, E. (2008). Source parameters of March 10 and September 13, 2007, United Arab Emirates earthquakes. *Tectonophysics, 460*(1), 237-247.

Aldama-Bustos, G., Bommer, J., Fenton, C., & Stafford, P. (2009). Probabilistic seismic hazard analysis for rock sites in the cities of Abu Dhabi, Dubai and Ra's Al Khaymah, United Arab Emirates. *Georisk, 3*(1), 1-29.

Ali, M. M., & Moon, K. S. (2007). Structural developments in tall buildings: current trends and future prospects. *Architectural Science Review, 50*(3), 205-223.

Alwaeli, W., Mwafy, A., Pilakoutas, K., & Guadagnini, M. (2014). Framework for Developing Fragility Relations of High-Rise RC Wall Buildings Based on Verified Modeling Approach. *The Proceedings of the Second European Conference on Earthquake Engineering and Seismology*, Istanbul, Turkey.

Ambraseys, N. N., Douglas, J., Sigbjornsson, R., (...), & Smit, P. M. (2004). Dissemination of European strong-motion data, Volume 2. *The Proceedings of the 13th Thirteenth World Conference on Earthquake Engineering*, Vancouver, Canada.

Ambraseys, N. N., & Melville, C. P. (2005). *A history of Persian Earthquakes*. Cambridge, UK: Cambridge university press.

Ambraseys, N. N., Melville, C. P., & Adams, R. D. (2005). *The Seismicity of Egypt, Arabia and the Red Sea: a historical review*. Cambridge, UK: Cambridge university press.

Antoniou, S., & Pinho, R. (2004). Development and verification of a displacement-based adaptive pushover procedure. *Journal of Earthquake Engineering, 8*(5), 643-661.

ASCE-7. (2010). *Minimum design loads for buildings and other structures, ASCE Standard ASCE/SEI 7-10*. Reston, VA: American Society of Civil Engineers.

ASCE-41. (2007). *Seismic rehabilitation of existing buildings, ASCE Standard ASCE/SEI 41-07 "formerly FEMA 356"*. Reston, VA: American Society of Civil Engineers.

Ashri, A. (2013). *Seismic Design of Structural Walls in Multi-story Buildings.* Independent Study Report, CEE Department, United Arab Emirates University, Al Ain, UAE.

Beyer, K., Dazio, A., & Priestley, M. (2008). Quasi-static cyclic tests of two U-shaped reinforced concrete walls. *Journal of Earthquake Engineering, 12*(7), 1023-1053.

Borzi, B., & Elnashai, A. (2000). Refined force reduction factors for seismic design. *Engineering Structures, 22*(10), 1244-1260.

Bracci, J. M., Kunnath, S. K., & Reinhorn, A. M. (1997). Seismic performance and retrofit evaluation of reinforced concrete structures. *Journal of Structural Engineering, 123*(1), 3-10.

Calvi, G., Pinho, R., & Crowley, H. (2006a). State-of-the-knowledge on the period elongation of RC buildings during strong ground shaking. *The Proceedings of the PROC (CD) First European Conference on Earthquake Engineering and Seismology*, Geneva, Switzerland.

Calvi, G., Pinho, R., Magenes, G., (...), & Crowley, H. (2006b). Development of seismic vulnerability assessment methodologies over the past 30 years. *ISET Journal of Earthquake Technology, 43*(3), 75-104.

Chopra, A. K., & Goel, R. K. (2002). A modal pushover analysis procedure for estimating seismic demands for buildings. *Earthquake Engineering & Structural Dynamics, 31*(3), 561-582.

Cohen, B. (2004). Urban growth in developing countries: a review of current trends and a caution regarding existing forecasts. *World Development, 32*(1), 23-51.

Cornell, C. A., & Krawinkler, H. (2000). Progress and challenges in seismic performance assessment. *PEER Center News, 3*(2), 1-3.

CSI. (2012a). *ETABS - Integrated building design software*: Computers and Structures, Inc., Berkeley, California.

CSI. (2012b). *SAFE - Design of Slabs, Beams and Foundations - Reinforced and Post-Tensioned Concrete*: Computers and Structures, Inc., Berkeley, California.

CSI. (2012c). *SAP2000 - Structural Analysis Program*: Computers and Structures, Inc., Berkeley, California.

Dipasquale, E., Ju, J.-W., Askar, A., & Çakmak, A. S. (1990). Relation between global damage indices and local stiffness degradation. *Journal of Structural Engineering, 116*(5), 1440-1456.

DMA. (2013). *Abu Dhabi International building code*: Department of Municipal Affairs, Abu Dhabi, UAE.

Dumova-Jovanoska, E. (2004). Fragility curves for RC structures in Skopje region. *The Proceedings of the Proceedings of the 13th World Conference on Earthquake Engineering*, Vancouver, Canada.

Dymiotis, C., Kappos, A. J., & Chryssanthopoulos, M. K. (1999). Seismic reliability of RC frames with uncertain drift and member capacity. *Journal of Structural Engineering, 125*(9), 1038-1047.

EC8. (2004). *Eurocode 8: Design of Structures for earthquake resistance - Part 1: General rules, seismic actions and rules for buildings*: CEN, European Committee for Standardization, Bruxelles.

Elnashai, A., & Broderick, B. (1996). Seismic response of composite frames—II. Calculation of behaviour factors. *Engineering Structures, 18*(9), 707-723.

Elnashai, A., Papanikolaou, V., & Lee, D. (2012). *Zeus-NL - A System for Inelastic Analysis of Structures - User Manual*: Mid-America Earthquake Center, University of Illinois at Urbana-Champaign, Urbana, IL.

Elnashai, A. S., & Mwafy, A. M. (2002). Overstrength and force reduction factors of multistorey reinforced-concrete buildings. *The Structural Design of Tall Buildings, 11*(5), 329-351.

Erberik, M. A., & Elnashai, A. S. (2004). Fragility analysis of flat-slab structures. *Engineering Structures, 26*(7), 937-948.

Fajfar, P., & Gaspersic, P. (1996). The N2 method for the seismic damage analysis of RC buildings. *Earthquake Engineering & Structural Dynamics, 25*(1), 31-46.

FEMA. (2009a). *NEHRP Recommended Seismic Provisions for New Buildings and Other Structures, FEMA P-750*: Federal Emergency Management Agency, Washington, DC.

FEMA. (2009b). *Quantification of building seismic performance factors, FEMA P-695*: Federal Emergency Management Agency, Washington, DC.

Freeman, S. A. (2004). Review of the development of the capacity spectrum method. *ISET Journal of Earthquake Technology, 41*(1), 1-13.

Ghobarah, A. (2004). On drift limits associated with different damage levels. *The Proceedings of the International workshop on performance-based seismic design*, Hamilton, Canada.

Grünthal, G., Bosse, C., Sellami, S., Mayer-Rosa, D., & Giardini, D. (1999). Compilation of the GSHAP regional seismic hazard for Europe, Africa and the Middle East. *Annals of Geophysics, 42*(6), 1215-1223.

GSHAP. (2014). *Global Seismic Hazard Assessment Program*. http://www.seismo.ethz.ch/GSHAP/index.html.

Gupta, B., & Kunnath, S. K. (2000). Adaptive spectra-based pushover procedure for seismic evaluation of structures. *Earthquake Spectra, 16*(2), 367-392.

Gutenberg, B., & Richter, C. F. (1954). *Seismicity of the earth and associated phenomena*. Princeton, NJ: Princeton University Press.

Haselton, C. B., Liel, A. B., Deierlein, G. G., Dean, B. S., & Chou, J. H. (2010). Seismic collapse safety of reinforced concrete buildings. I: Assessment of ductile moment frames. *Journal of Structural Engineering, 137*(4), 481-491.

ICC. (2012). *International building code*: International Code Council, Country Club Hills, IL.

Irfan, M., El-Emam, M., Khan, Z., & Abdalla, J. (2012). Local Site Effects on Seismic Ground Response of Dubai-Sharjah Metropolitan Area. *The Proceedings of the GeoCongress*, Oakland, California.

Jeong, S.-h., & Elnashai, A. S. (2005). Analytical assessment of an irregular RC frame for full-scale 3D Pseudo-dynamic testing part I: analytical model verification. *Journal of Earthquake Engineering, 9*(1), 95-128.

Jeong, S.-H., & Elnashai, A. S. (2007). Probabilistic fragility analysis parameterized by fundamental response quantities. *Engineering Structures, 29*(6), 1238-1251.

Jeong, S.-H., Mwafy, A. M., & Elnashai, A. S. (2012). Probabilistic seismic performance assessment of code-compliant multi-story RC buildings. *Engineering Structures, 34*, 527-537.

Ji, J., Elnashai, A. S., & Kuchma, D. A. (2007a). An analytical framework for seismic fragility analysis of RC high-rise buildings. *Engineering Structures, 29*(12), 3197-3209.

Ji, J., Elnashai, A. S., & Kuchma, D. A. (2007b). *Seismic fragility assessment for reinforced concrete high-rise buildings.* Project Report EE-1, University of Illinois at Urbana-Champaign, Urbana, IL.

Ji, J., Elnashai, A. S., & Kuchma, D. A. (2009). Seismic fragility relationships of reinforced concrete high-rise buildings. *The Structural Design of Tall and Special Buildings, 18*(3), 259-277.

Johnson, P. S. (1998). *Tectonic map of Saudi Arabia and adjacent areas.* Technical Report USGS-TR-98-3, Saudi Arabian Deputy Ministry for Mineral Resources.

Katsanos, E., Sextos, A., & Elnashai, A. (2014). Prediction of inelastic response periods of buildings based on intensity measures and analytical model parameters. *Engineering Structures, 71*(1), 161-177.

Khan, Z., El-Emam, M., Irfan, M., & Abdalla, J. (2013). Probabilistic seismic hazard analysis and spectral accelerations for United Arab Emirates. *Natural Hazards, 67*(2), 569-589.

Krawinkler, H., & Seneviratna, G. (1998). Pros and cons of a pushover analysis of seismic performance evaluation. *Engineering Structures, 20*(4), 452-464.

Kwon, O.-S., & Elnashai, A. (2006). The effect of material and ground motion uncertainty on the seismic vulnerability curves of RC structure. *Engineering Structures, 28*(2), 289-303.

Kwon, O. S., & Kim, E. S. (2010). Evaluation of building period formulas for seismic design. *Earthquake Engineering & Structural Dynamics, 39*(14), 1569-1583.

Laogan, B. T., & Elnashai, A. S. (1999). Structural performance and economics of tall high strength RC buildings in seismic regions. *The Structural Design of Tall Buildings, 8*(3), 171-204.

Lehman, D. E., Turgeon, J. A., Birely, A. C., Hart, C. R., Marley, K. P., Kuchma, D. A., & Lowes, L. N. (2013). Seismic Behavior of a Modern Concrete Coupled Wall. *Journal of Structural Engineering, 139*(8), 1371-1381.

Malkawi, A. I. H., Barakat, S., Shanableh, A., (...), & Altoubat, S. (2007). *Seismic Hazard Assessment and Mitigation of Earthquake Risk in the United Arab Emirates.* Technical Report, A Collaboration Project on Capacity Building in Seismology Between the University of Sharjah and Jordan University of Science and Technology.

Massumi, A., & Moshtagh, E. (2013). A new damage index for RC buildings based on variations of nonlinear fundamental period. *The Structural Design of Tall and Special Buildings, 22*(1), 50-61.

Mosalam, K. M., Ayala, G., White, R. N., & Roth, C. (1997). Seismic fragility of LRC frames with and without masonry infill walls. *Journal of Earthquake Engineering, 1*(4), 693-720.

Mwafy, A. (2013a). Seismic Risk Assessment of Buildings in the Highly Populated Earthquake-Prone Areas of the UAE. *The Proceedings of the Second International Conference on Engineering Geophysics*, Al-Ain, UAE.

Mwafy, A., & Elnashai, A. (2002). Calibration of force reduction factors of RC buildings. *Journal of Earthquake Engineering, 6*(2), 239-273.

Mwafy, A., Hussain, N., & El-Sawy, K. (2014). Seismic performance and cost-effectiveness of high-rise buildings with increasing concrete strength. *The Structural Design of Tall and Special Buildings*, in press.

Mwafy, A. M. (2011). Assessment of seismic design response factors of concrete wall buildings. *Earthquake Engineering and Engineering Vibration, 10*(1), 115-127.

Mwafy, A. M. (2012a). Analytically derived fragility relationships for the modern high-rise buildings in the UAE. *The Structural Design of Tall and Special Buildings, 21*(11), 824-843.

Mwafy, A. M. (2012b). Classification and idealization of the building stock in the UAE for earthquake loss estimation. *The Proceedings of the 15th World Conference on Earthquake Engineering*, Lisbon, Portugal.

Mwafy, A. M. (2013b). *Seismic Vulnerability Assessment of the Building Stock in Highly Populated Areas in the UAE.* Final UAEU-NRF Research Project Report, United Arab Emirates University, Al-Ain, UAE.

Mwafy, A. M., Elnashai, A., Sigbjornsson, R., & Salama, A. (2006). Significance of severe distant and moderate close earthquakes on design and behavior of tall buildings. *The Structural Design of Tall and Special Buildings, 15*(4), 391-416.

Mwafy, A. M., & Elnashai, A. S. (2001). Static pushover versus dynamic collapse analysis of RC buildings. *Engineering Structures, 23*(5), 407-424.

Panagiotou, M., Restrepo, J. I., & Conte, J. P. (2010). Shake-table test of a full-scale 7-story building slice. Phase I: Rectangular wall. *Journal of Structural Engineering, 137*(6), 691-704.

Park, R. (1988). Ductility evaluation from laboratory and analytical testing. *The Proceedings of the Proceedings of the 9th World Conference on Earthquake Engineering*, Tokyo-Kyoto, Japan.

Paulay, T., & Priestley, M. (1992). *Seismic design of reinforced concrete and masonry buildings.* New York: Wiley.

PEER. (2013). *PEER NGA database*: Pacific Earthquake Engineering Research Center, University of California, Berkeley, CA. http://peer.berkeley.edu/nga.

Priestley, M., & Grant, D. (2005). Viscous damping in seismic design and analysis. *Journal of Earthquake Engineering, 9*(sup2), 229-255.

Rossetto, T., & Elnashai, A. (2003). Derivation of vulnerability functions for European-type RC structures based on observational data. *Engineering Structures, 25*(10), 1241-1263.

Rossetto, T., & Elnashai, A. (2005). A new analytical procedure for the derivation of displacement-based vulnerability curves for populations of RC structures. *Engineering Structures, 27*(3), 397-409.

Roufaiel, M. S., & Meyer, C. (1987). Analytical modeling of hysteretic behavior of R/C frames. *Journal of Structural Engineering, 113*(3), 429-444.

Saiidi, M., & Sozen, M. A. (1981). Simple nonlinear seismic analysis of R/C structures. *Journal of the Structural Division, 107*(5), 937-953.

Schultz, M. T., Gouldby, B. P., Simm, J. D., & Wibowo, J. L. (2010). *Beyond the factor of safety: developing fragility curves to characterize system reliability.* DTIC Document. Washington, DC.

SEAOC. (1999). *Recommended lateral force requirements and commentary.* Seventh Edition.: Seismology Committee Structural Engineers Association of California, Sacramento, CA.

Serdar Kirçil, M., & Polat, Z. (2006). Fragility analysis of mid-rise R/C frame buildings. *Engineering Structures, 28*(9), 1335-1345.

Shama, A. A. (2011). Site specific probabilistic seismic hazard analysis at Dubai Creek on the west coast of UAE. *Earthquake Engineering and Engineering Vibration, 10*(1), 143-152.

Sigbjornsson, R., & Elnashai, A. (2006). Hazard assessment of Dubai, United Arab Emirates, for close and distant earthquakes. *Journal of Earthquake Engineering, 10*(05), 749-773.

Singhal, A., & Kiremidjian, A. (1997). *A method for earthquake motion-damage relationships with application to reinforced concrete frames.* National Center for Earthquake Engineering Research Report NCEER-97-0008, State University of New York at Buffalo, Buffalo, NY.

Taranath, B. S. (2004). *Wind and earthquake resistant buildings*. New York: Marcel Dekker.

Taranath, B. S. (2009). *Reinforced concrete design of tall buildings*. Boca Raton, FL: CRC Press.

Tavakoli, B., & Ghafory-Ashtiany, M. (1999). Seismic hazard assessment of Iran. *Annals of Geophysics, 42*(6), 1013-1021.

Trifunac, M., Ivanovic, S., & Todorovska, M. (2001). Apparent periods of a building. I: Fourier analysis. *Journal of Structural Engineering, 127*(5), 517-526.

Tsopelas, P., & Husain, M. (2004). Measures of structural redundancy in reinforced concrete buildings. ii: Redundancy response modification factor RR. *Journal of Structural Engineering, 130*(11), 1659-1666.

Udwadia, F., & Trifunac, M. (1973). Time and amplitude dependent response of structures. *Earthquake Engineering & Structural Dynamics, 2*(4), 359-378.

Vamvatsikos, D., & Cornell, A. (2006). Direct estimation of the seismic demand and capacity of oscillators with multi-linear static pushovers through IDA. *Earthquake Engineering & Structural Dynamics, 35*(9), 1097-1117.

Vamvatsikos, D., & Cornell, C. A. (2002). Incremental dynamic analysis. *Earthquake Engineering & Structural Dynamics*, *31*(3), 491-514.

Vernant, P., Nilforoushan, F., Hatzfeld, D., (...), & Bayer, R. (2004). Present-day crustal deformation and plate kinematics in the Middle East constrained by GPS measurements in Iran and northern Oman. *Geophysical Journal International*, *157*(1), 381-398, International Institute of Earthquake Engineering and Seismology.

Wen, Y., Ellingwood, B., & Bracci, J. (2004). *Vulnerability function framework for consequence-based engineering.* Mid-America Earthquake Center Project DS-4 Report. University of Illinois at Urbana-Champaign, Urbana, IL.

Williams, M. S., & Sexsmith, R. G. (1995). Seismic damage indices for concrete structures: a state-of-the-art review. *Earthquake Spectra*, *11*(2), 319-349.

Wyss, M., & Al-Homoud, A. S. (2004). Scenarios of seismic risk in the United Arab Emirates, an approximate estimate. *Natural Hazards, 32*(3), 375-393.

Zare, M. (2002). *Attenuation relation and coefficients of movement in Iran.* International Institute of Earthquake Engineering and Seismology, Iran.

APPENDIX A: SAMPLES OF VULNERABILITY ASSESSMENT RESULTS

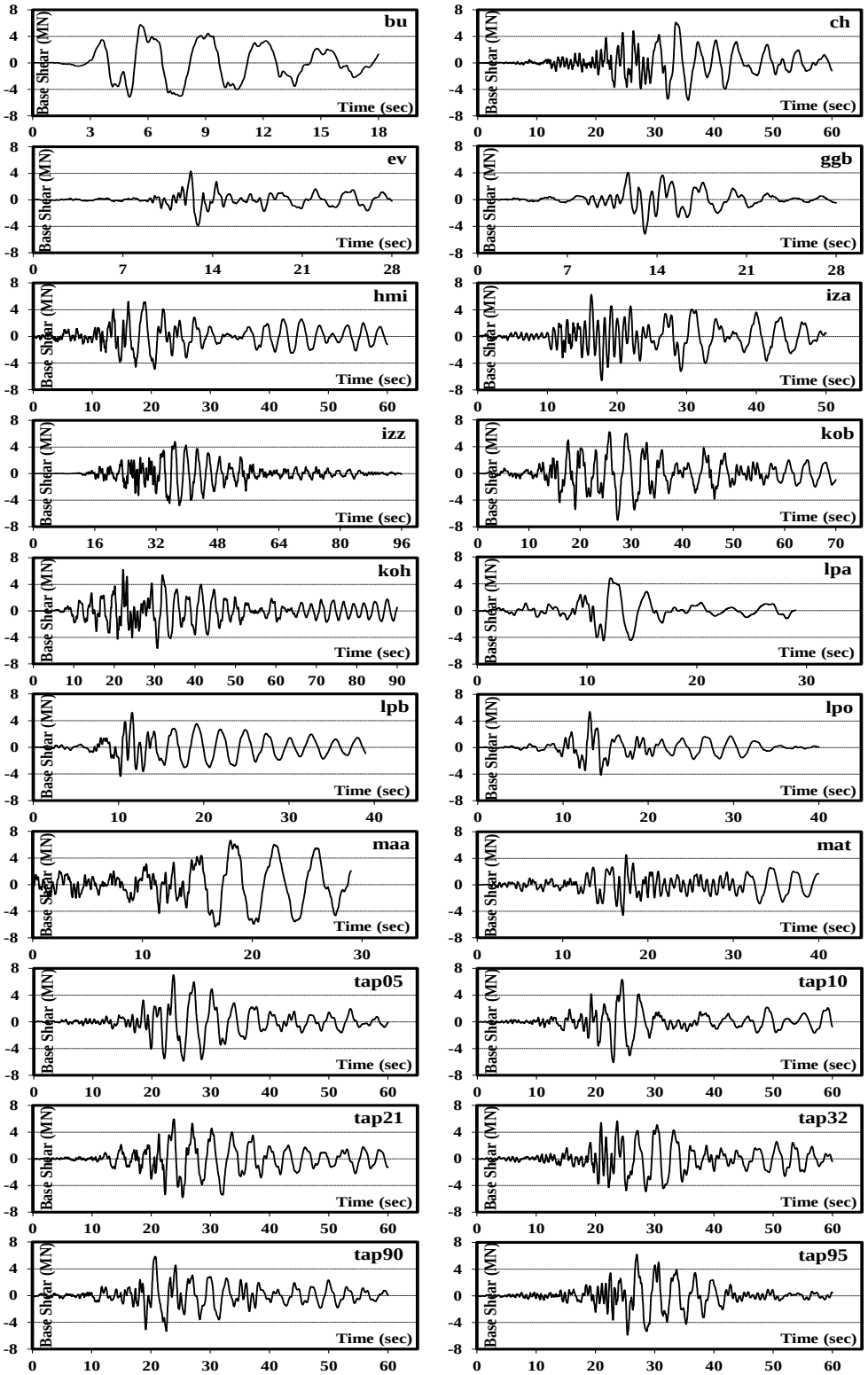

Figure A.1. Sample of base shear time histories of the 8-story building at twice the design intensity (0.32g) under the twenty severe distant earthquakes

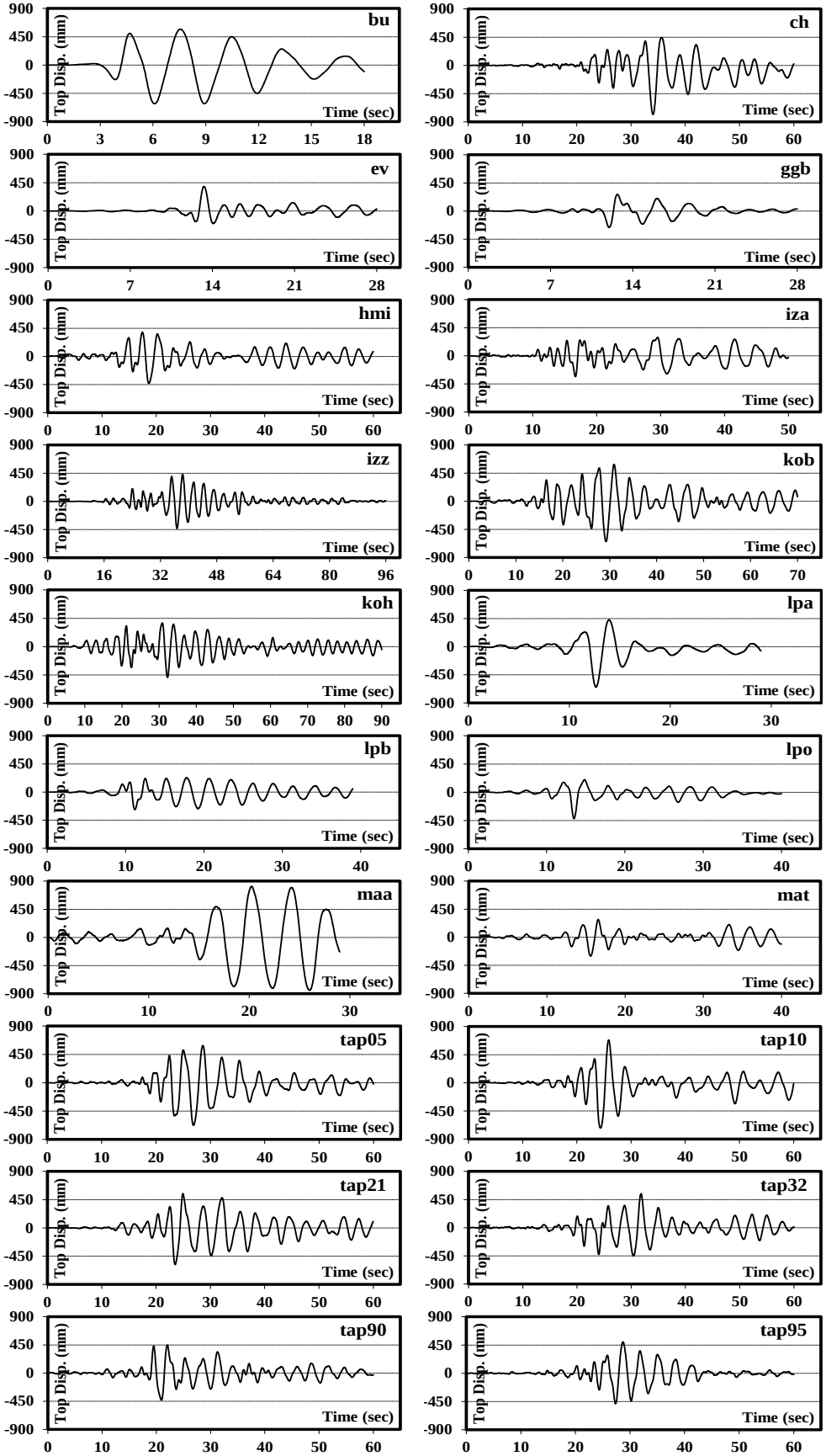

Figure A.2. Sample of top displacement time histories of the 8-story building at twice the design intensity (0.32g) under the twenty severe distant earthquakes

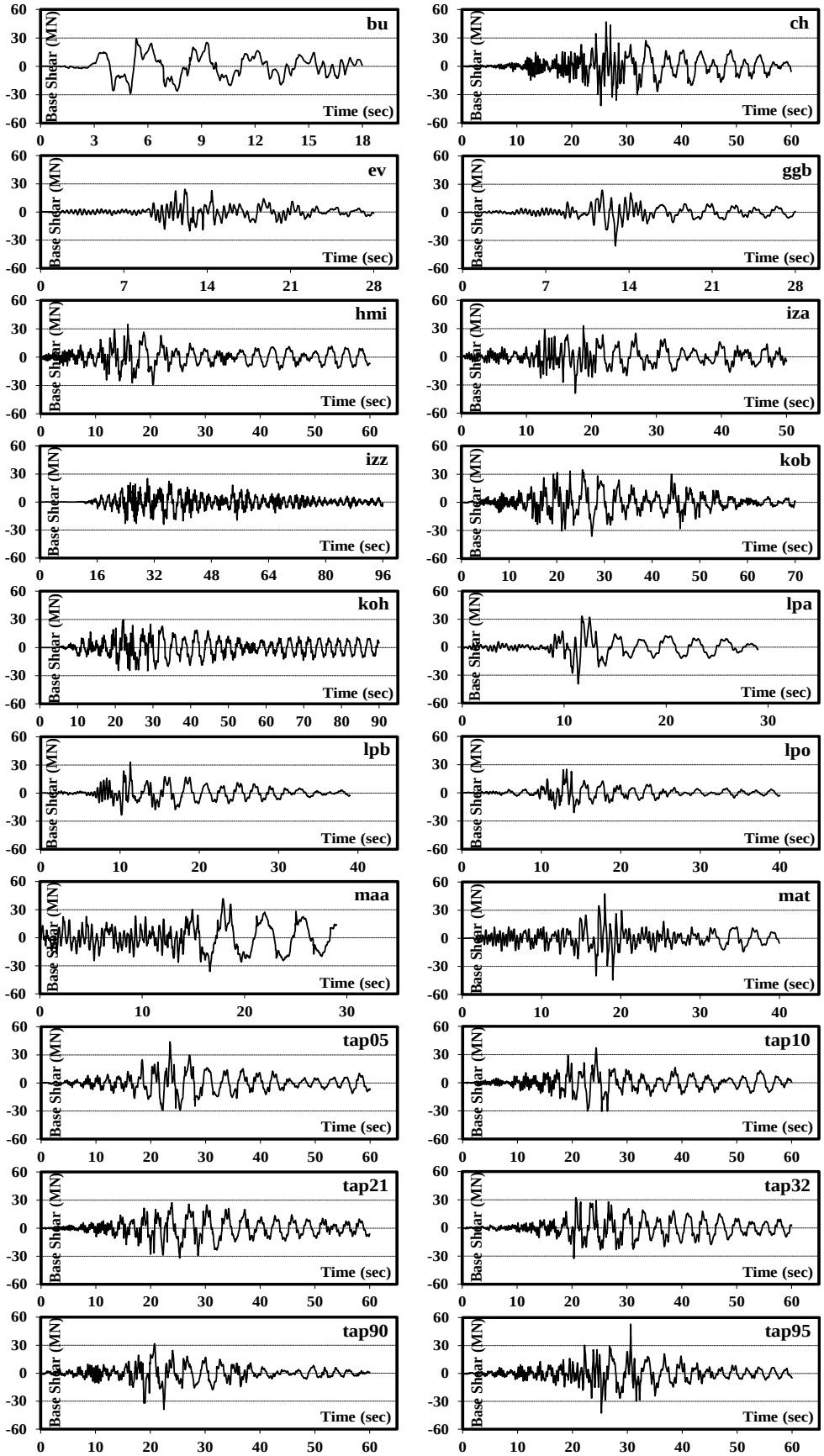

Figure A.3. Sample of base shear time histories of the 18-story building at twice the design intensity (0.32g) under the twenty severe distant earthquakes

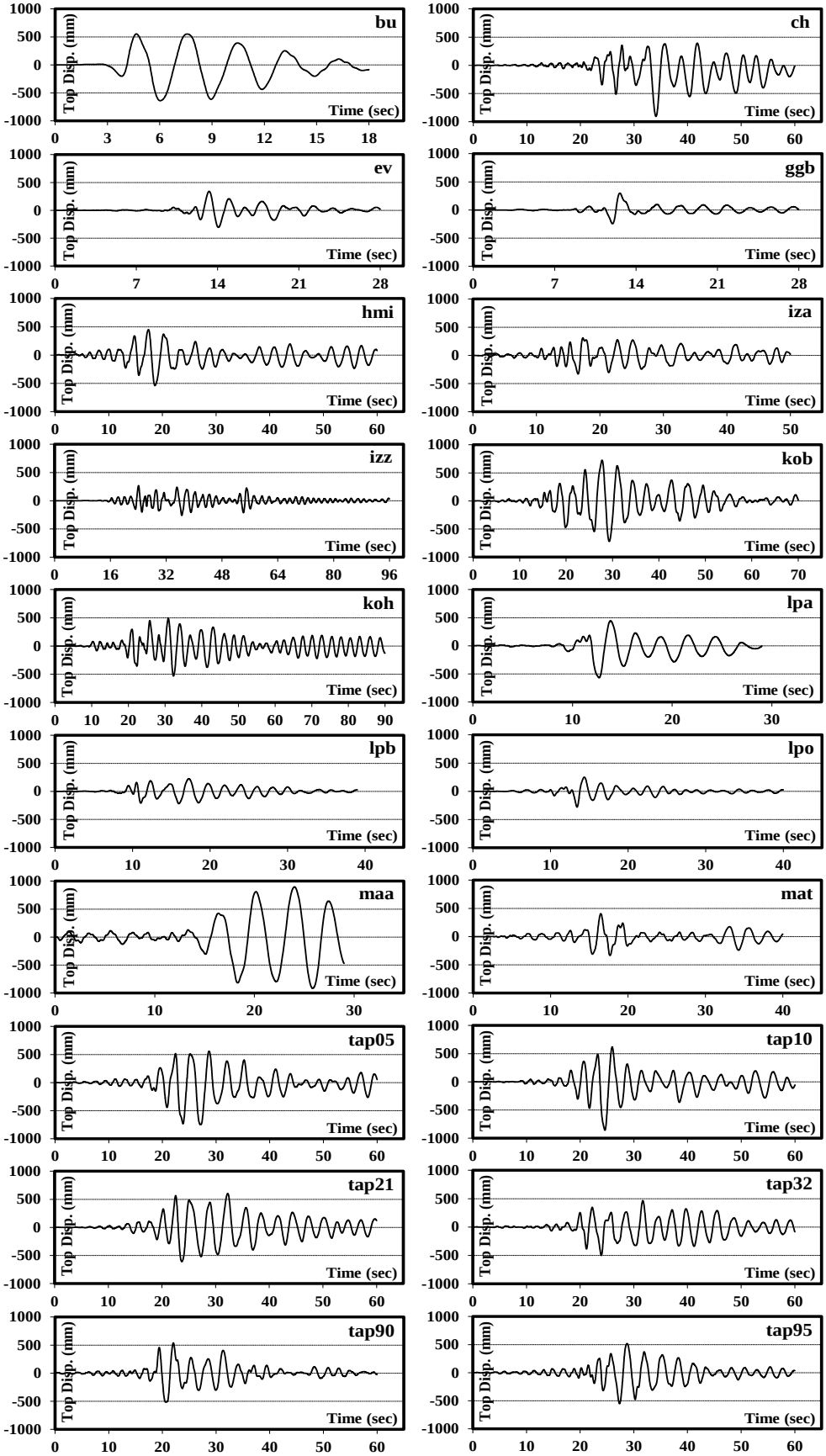

Figure A.4. Sample of top displacement time histories of the 18-story building at twice the design intensity (0.32g) under the twenty severe distant earthquakes

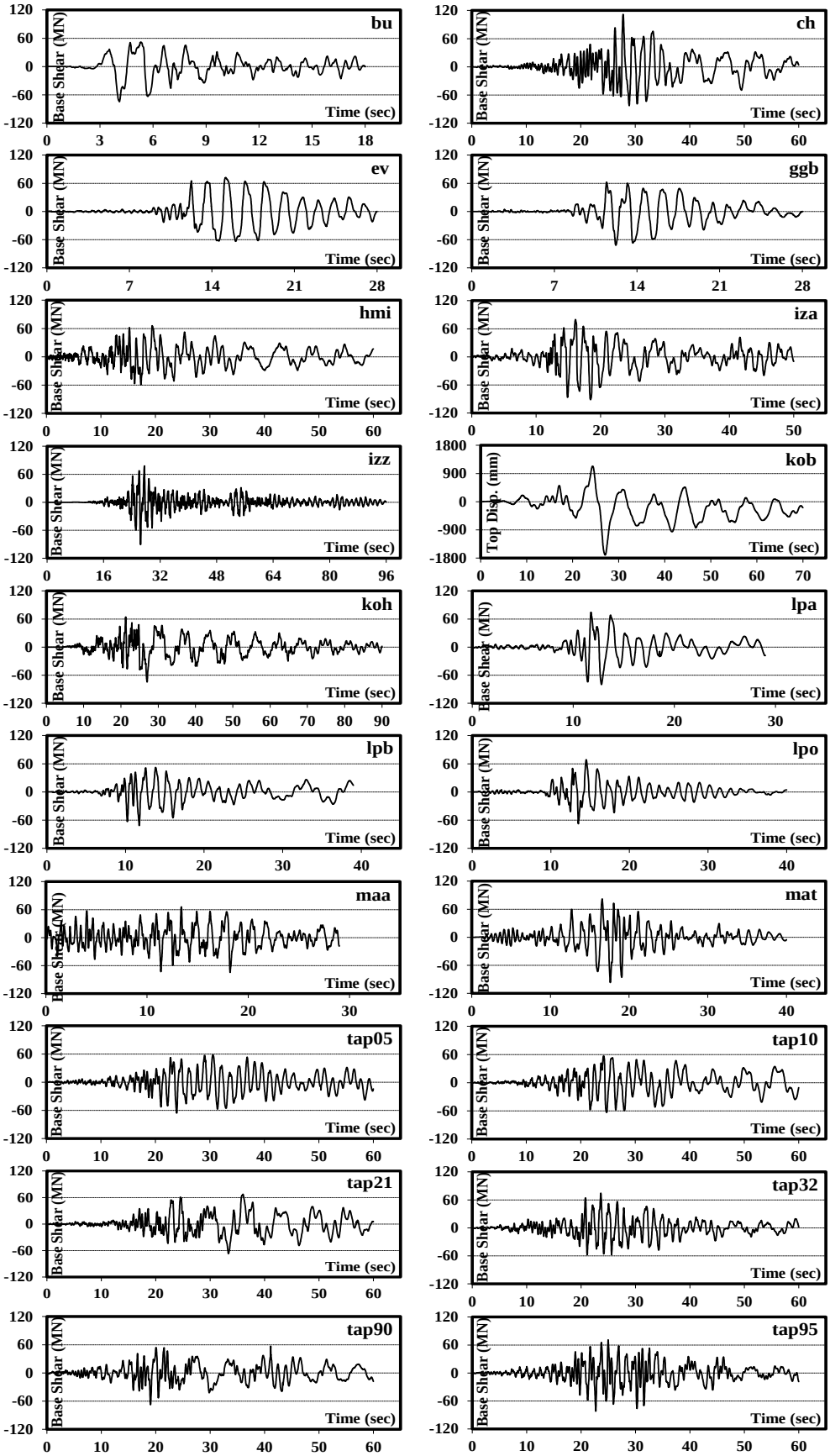

Figure A.5. Sample of base shear time histories of the 40-story building at twice the design intensity (0.32g) under the twenty severe distant earthquakes

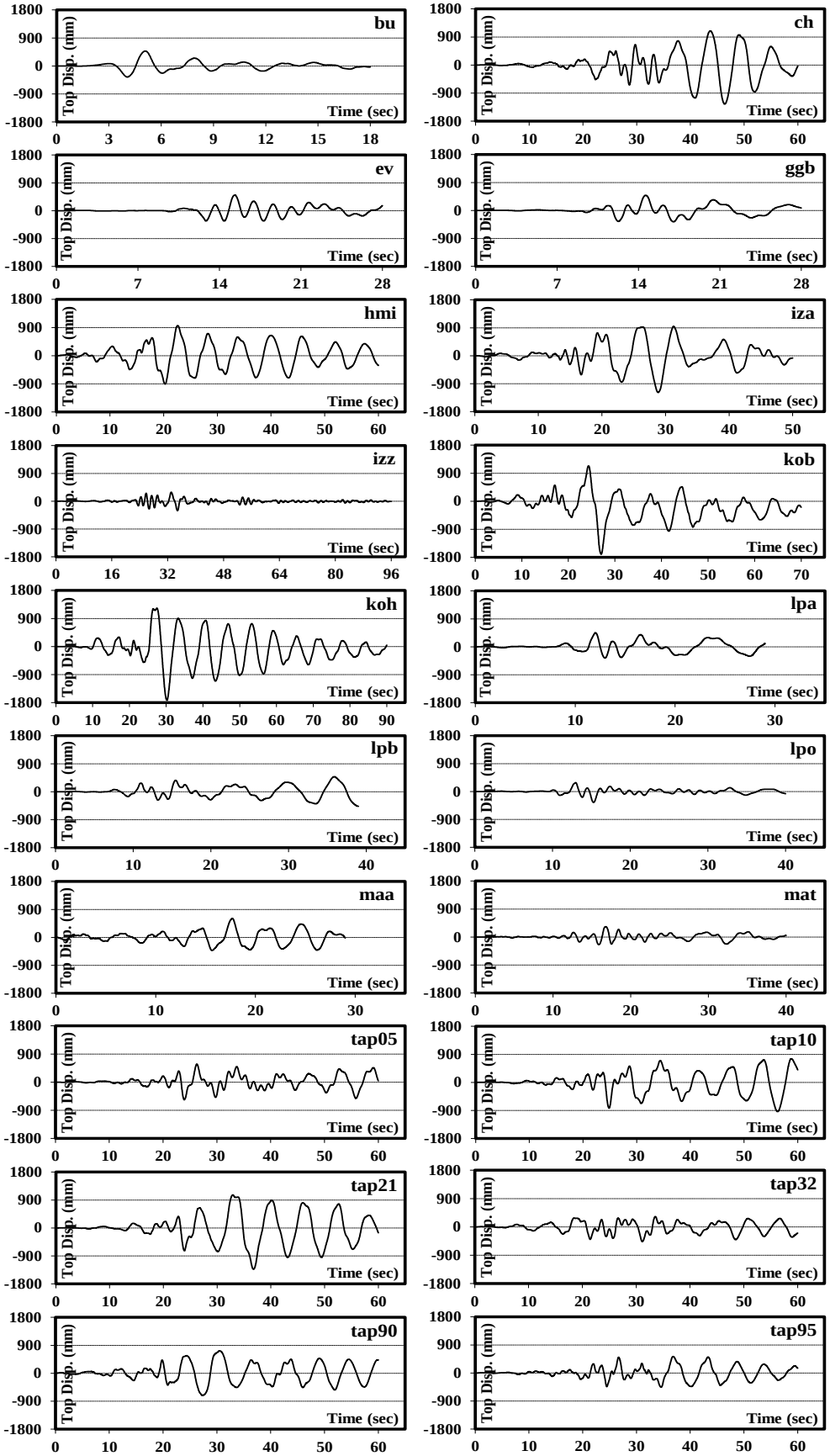

Figure A.6. Sample of top displacement time histories of the 40-story building at twice the design intensity (0.32g) under the twenty severe distant earthquakes

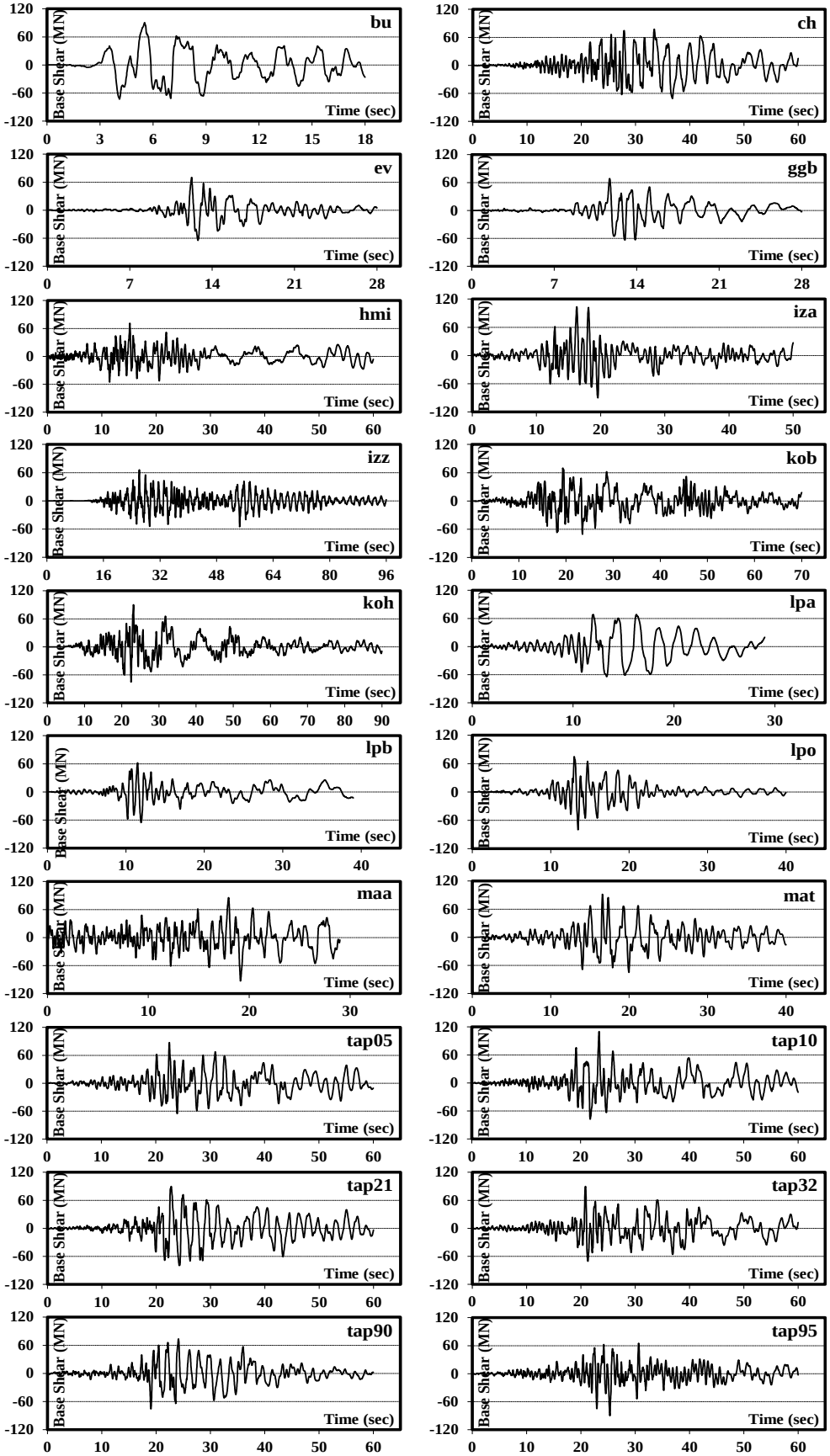

Figure A.7. Sample of base shear time histories of the 50-story building at twice the design intensity (0.32g) under the twenty severe distant earthquakes

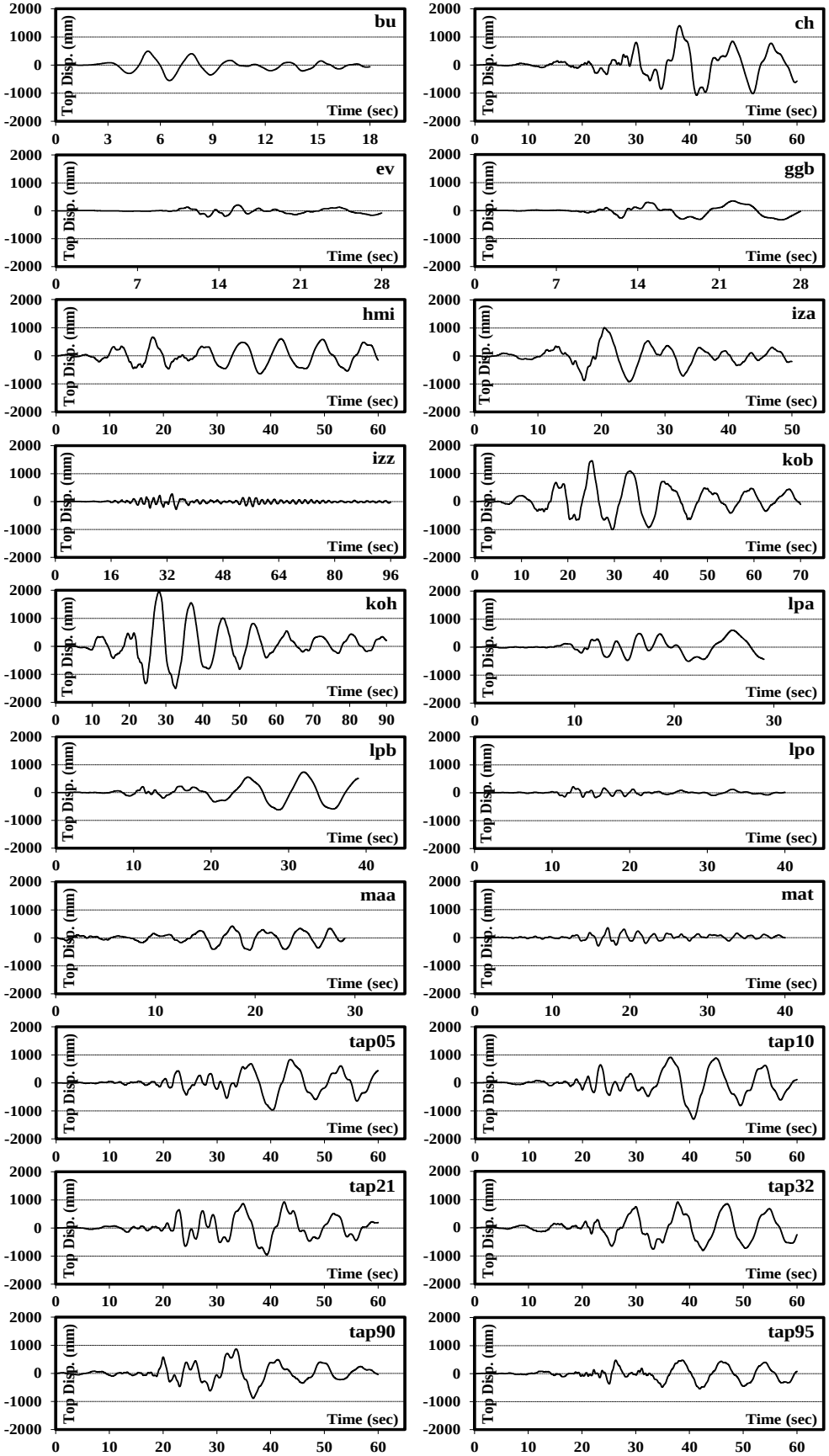

Figure A.8. Sample of top displacement time histories of the 50-story building at twice the design intensity (0.32g) under the twenty severe distant earthquakes

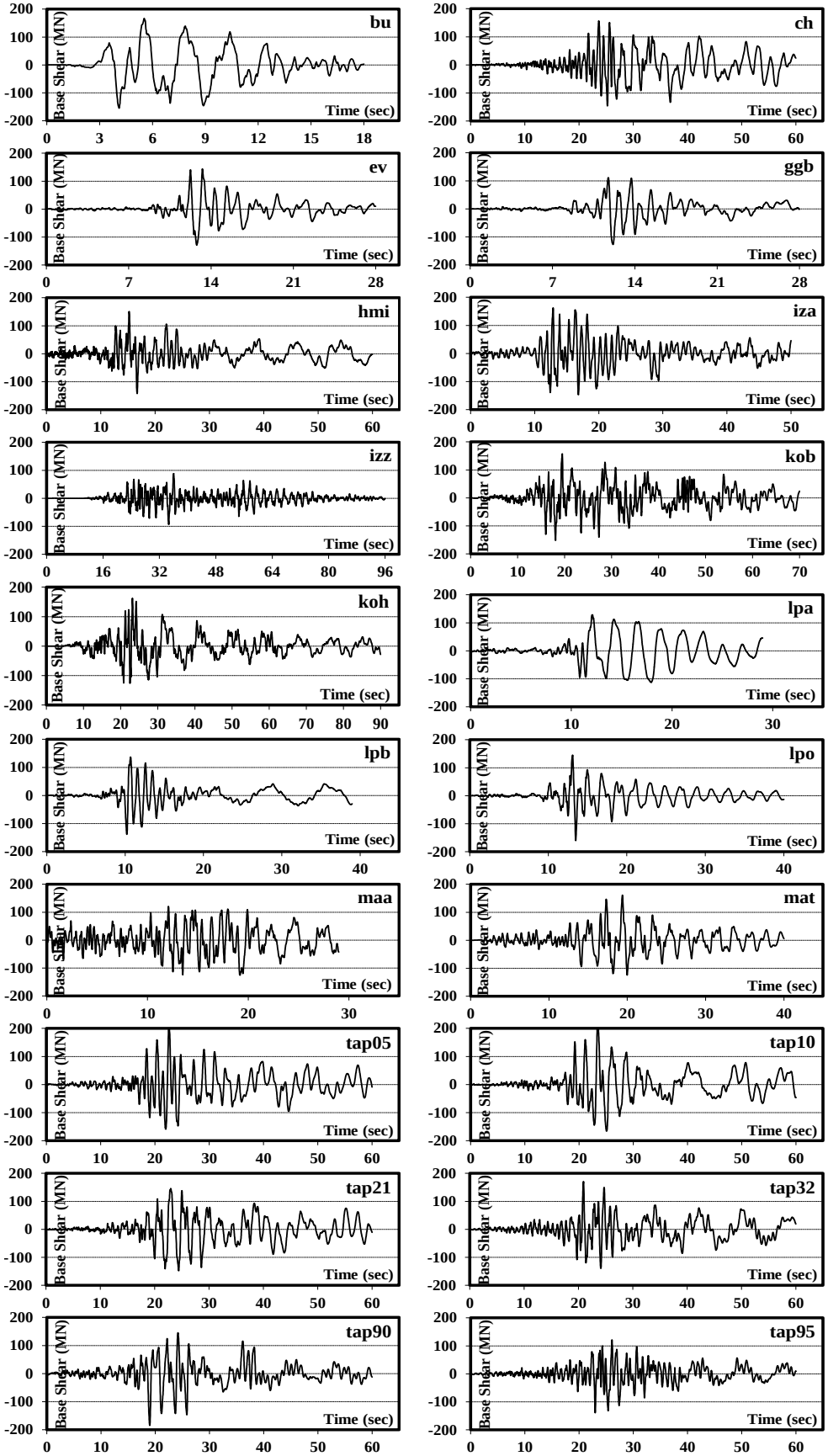

Figure A.9. Sample of base shear time histories of the 66-story building at twice the design intensity (0.32g) under the twenty severe distant earthquakes

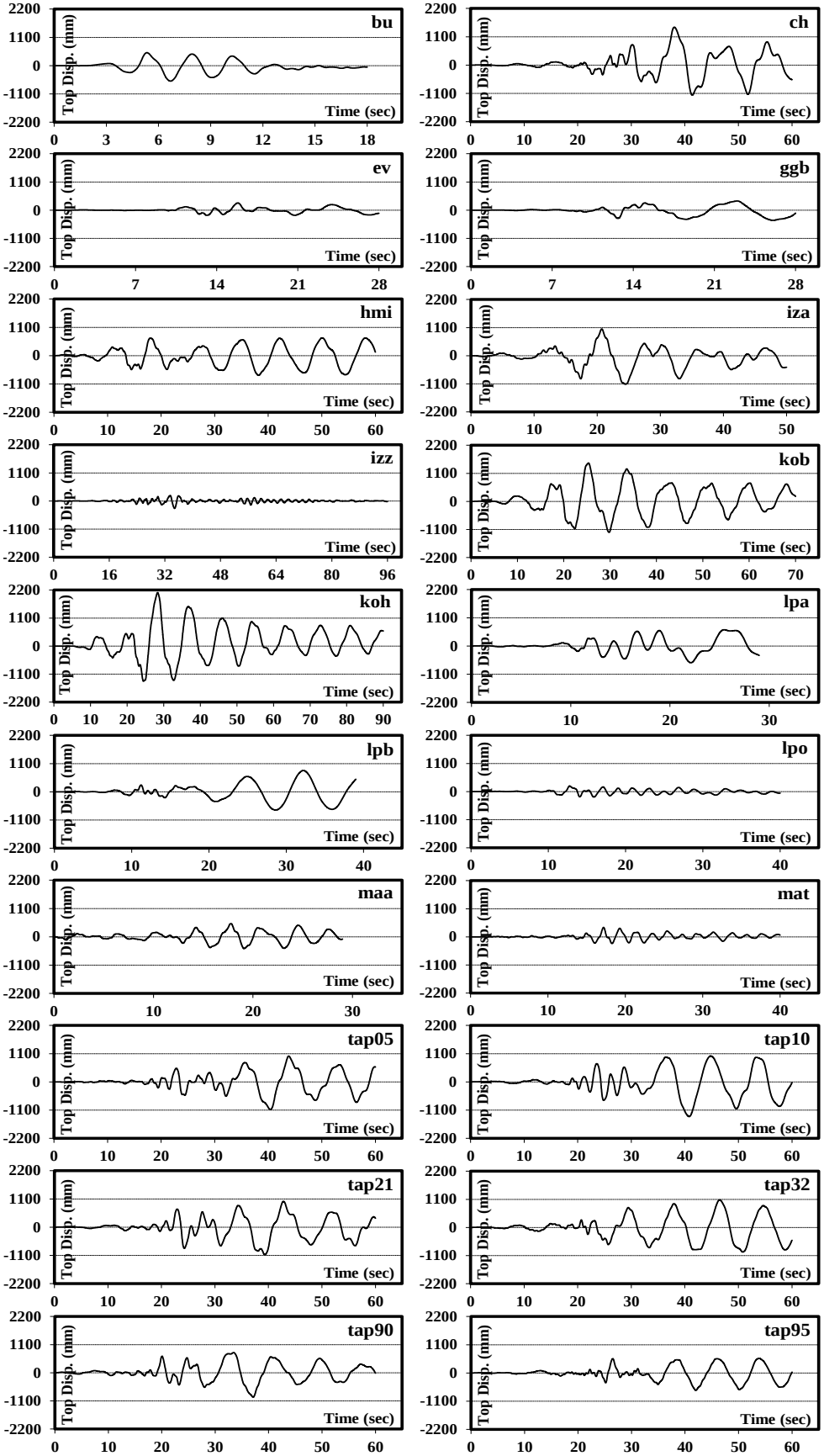

Figure A.10. Sample of top displacement time histories of the 66-story building at twice the design intensity (0.32g) under the twenty severe distant earthquakes

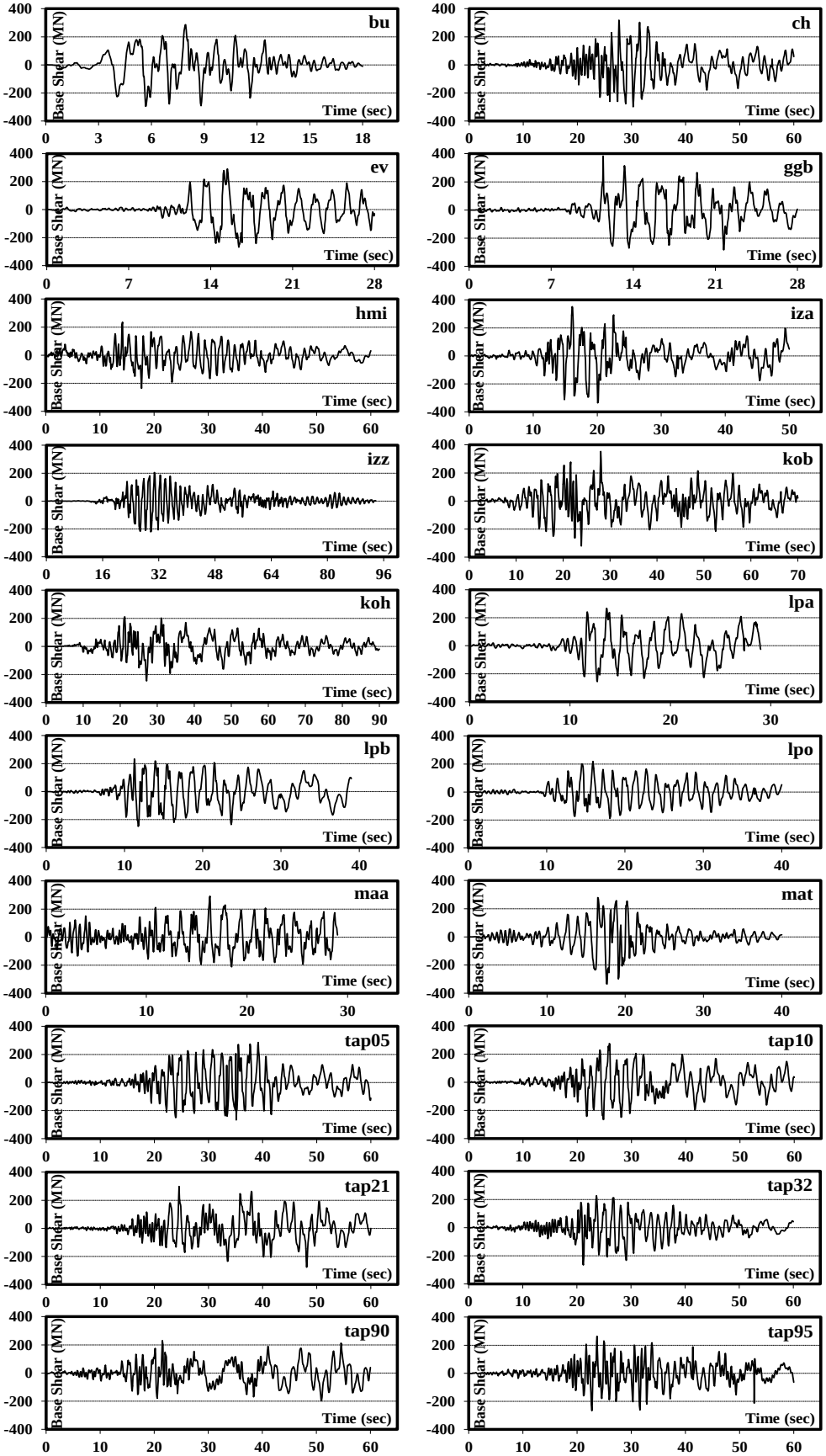

Figure A.11. Sample of base shear time histories of the 80-story building at twice the design intensity (0.32g) under the twenty severe distant earthquakes

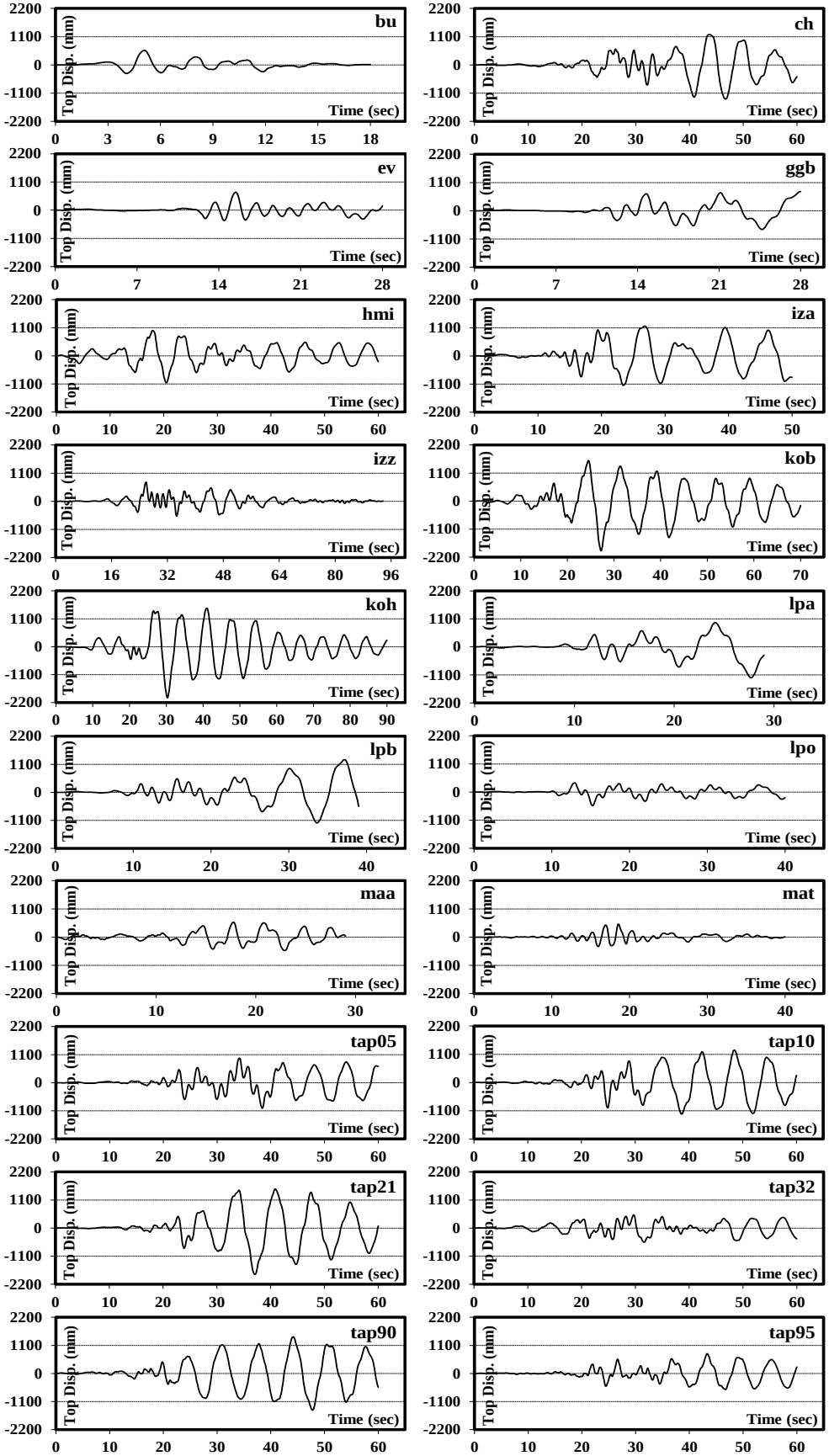

Figure A.12. Sample of top displacement time histories of the 80-story building at twice the design intensity (0.32g) under the twenty severe distant earthquakes

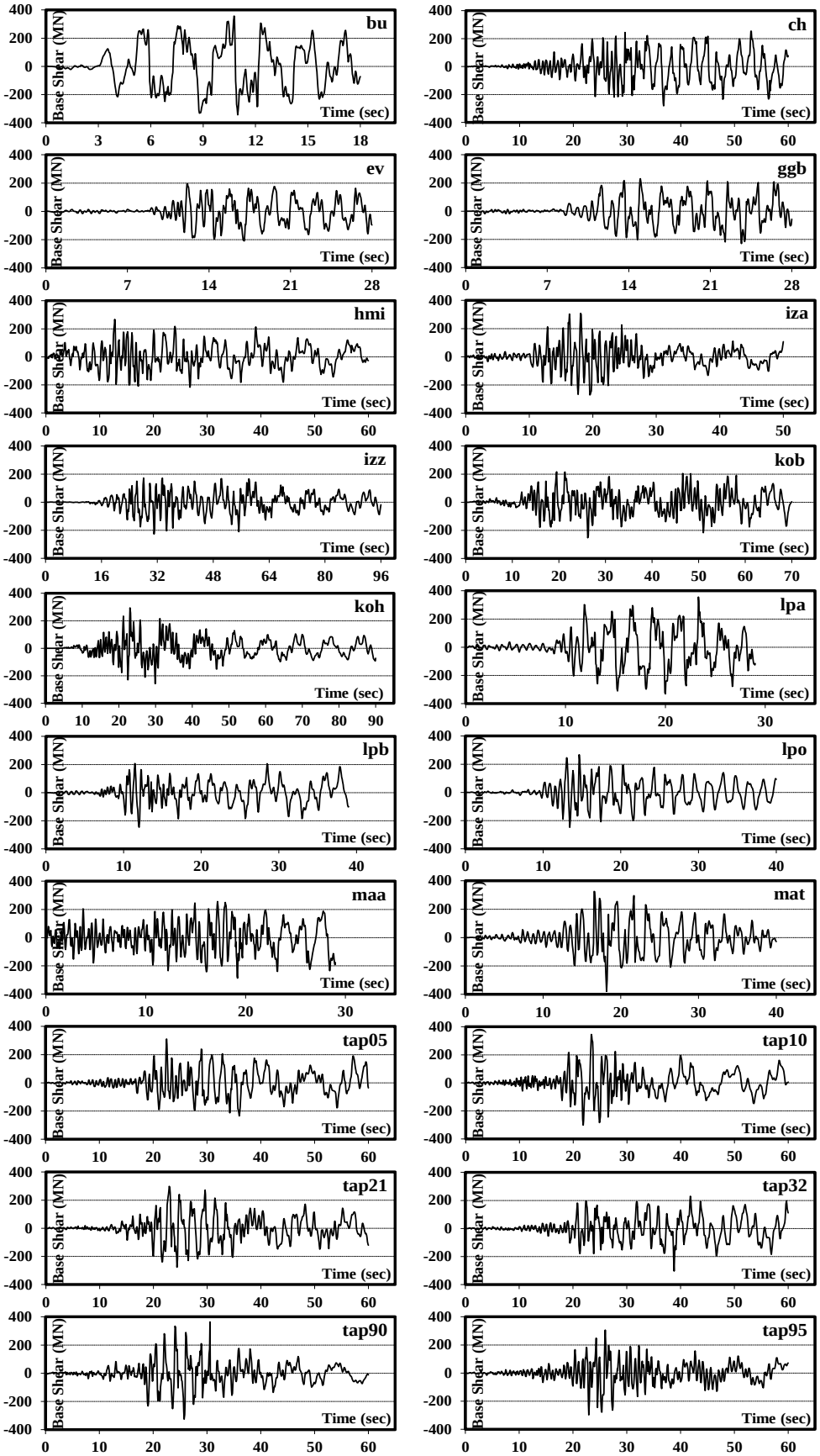

Figure A.13. Sample of base shear time histories of the 100-story building at twice the design intensity (0.32g) under the twenty severe distant earthquakes

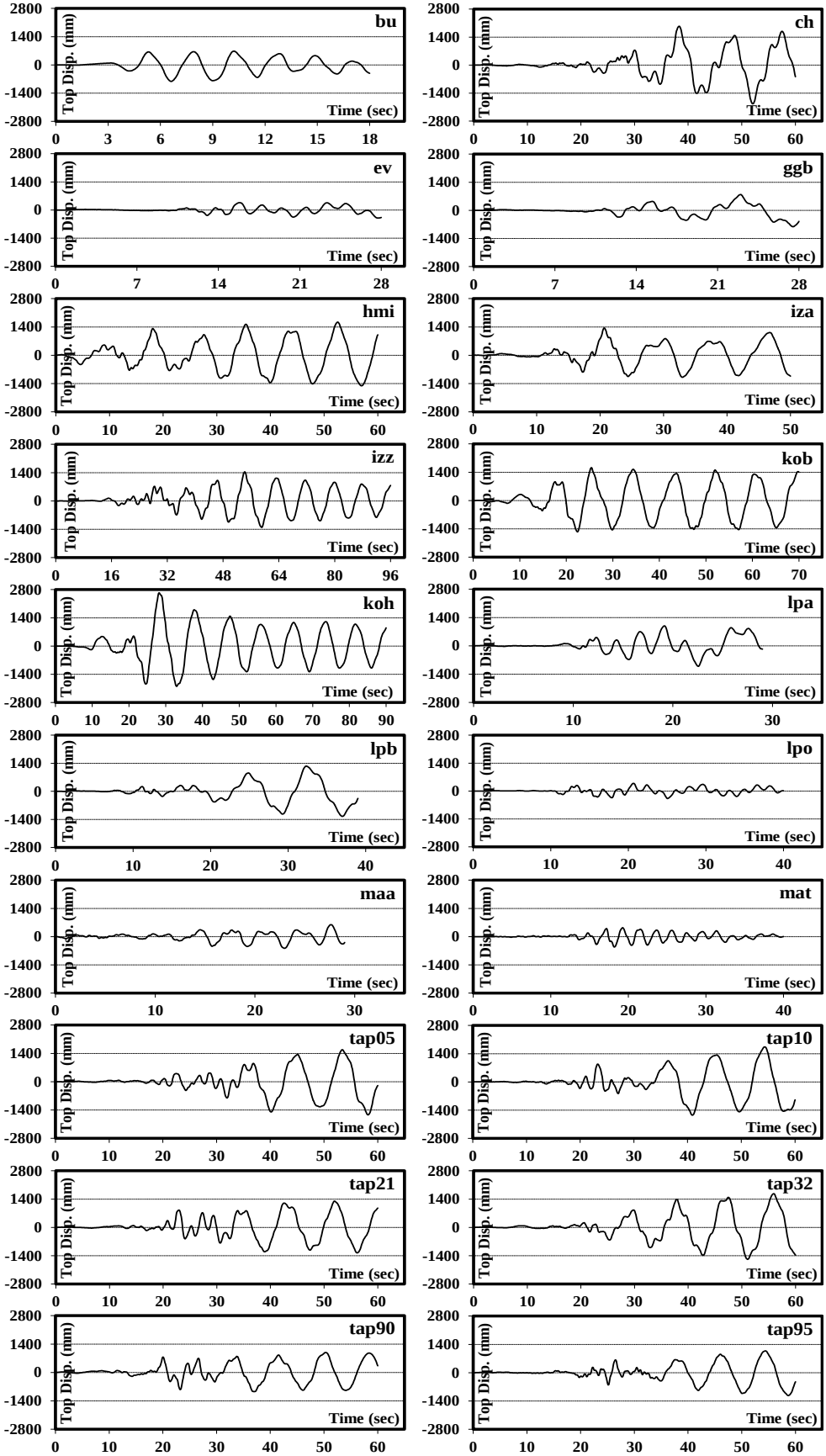

Figure A.14. Sample of top displacement time histories of the 100-story building at twice the design intensity (0.32g) under the twenty severe distant earthquakes